4

Robust Beamforming and DOA Estimation

Liu Congfeng
Electronic Countermeasure Research Institute, Xidian University, Xian Shaanxi, China

1. Introduction

1.1 Robust beamforming overview

Beamforming is a ubiquitous task in array signal processing with applications, among others, in radar, sonar, acoustics, astronomy, seismology, communications, and medical imaging. Without loss of generality, we consider herein beamforming in array processing applications. The introduction to beamforming can be found in [1]-[9] and the references herein.

The traditional approach to the design of adaptive beamformers assumes that the desired signal components are not present in training data, and the robustness of beamformer is known to depend essentially on the availability of signal-free training data. However, in many important applications such as mobile communications, passive location, microphone array speech processing, medical imaging, and radio astronomy, the signal-free training data cells are unavailable. In such scenarios, the desired signal is always present in the training snapshots, and the adaptive beamforming methods become very sensitive to any violation of underlying assumptions on the environment, sources, or sensor array. In fact, the performances of the existing adaptive array algorithms are known to degrade substantially in the presence of even slight mismatches between the actual and presumed array responses to the desired signal [10]-[12]. Similar types of degradation can take place when the array response is known precisely but the training sample size is small, namely the mismatch between the actual and the estimated covariance matrix [13]-[15]. Therefore, robust approaches to adaptive beamforming appear to be of primary importance in these cases [16][17].

Many approaches have been proposed to improve the robustness of the adaptive beamformer during the past three decades. Indeed, the literatures on the robust adaptive beamformer are quite extensive. We provide a brief review as fellows. For more recent detailed critical reviews, see [18] and [19]-[25].

1.1.1 Robust approaches for signal direction mismatch

For the specific case of the signal direction mismatch, there are several efficient methods have been developed. Representative examples of such techniques are the linearly constrained minimum variance (LCMV) beamformer [26], which is also denoted as the linearly constrained minimum power (LCMP) beamformer in other references [27] and this chapter, signal blocking-based algorithms [10][28], and Bayesian beamformer [29]. Although

all these methods provide excellent robustness against the signal direction mismatch, they are not robust against other types of mismatches caused by poor array calibration, unknown sensor mutual coupling, near-far wavefront mismodeling, signal wavefront distortions, source spreading, and coherent/incoherent local scattering, as well as other effects [17].

Chun-Yang Chen and P.P.Vaidyanathan consider a simplified uncertainty set which contains only the steering vectors with a desired uncertainty range of direction of arrival (DOA) [25], although the closed-form solution is given, and the diagonal loading level can be computed by the iteration method systematically, but how to determine the DOA uncertainty range is the critical problem.

1.1.2 Robust approaches for general mismatch

Several other approaches are known to provide the improved robustness against more general types of mismatches, for example, the algorithms that use the diagonal loading of the sample covariance matrix [14][16], the eigenspace-based beamformer [11][30][31], and the covariance matrix taper (CMT) approach [32]-[34]. For the diagonal loading method, a serious drawback is that there is no reliable way to choose the diagonal loading level, F.Vincent and O.Besson propose the method to select the optimal loading level with a view to maximizing the signal-to-noise ratio (SNR) in the presence of steering vector errors and it is shown that the loading is negative, but they can't give the exact solution, instead of the approximate solution, moreover, they can't give the expression of steering vector errors [35]. The eigenspace-based approach is essentially restricted in its performance at low SNR and when the dimension of the signal-plus-interference subspace is high, and the dimension must be known in the latter technique [31]. The CMT approach is known to provide an excellent robustness in scenarios with nonstationary interferers, however, its robustness against mismatches of the desired signal array response may be unsatisfactory, furthermore, it can also be explained as the diagonal loading [33].

1.1.3 Uncertainty set constraint approaches for general mismatch

Very recently, many approaches have been proposed for improving the robustness of the standard minimum variance distortionless response (MVDR) beamformer. Their main ideas are based on the definition of the uncertainty set and the worst-case performance optimization, but these algorithms are all classified to the diagonal loading technique.

Jian Li et al propose the robust Capon beamformer under the constraint of steering vector uncertainty set [20], then the constraint of steering vector norm is imposed and the doubly constraint robust Capon beamformer is proposed [22]. For the two beamformers, although they give the exact weight vectors, and the methods of finding the optimal loading level, but their performance improvements are not obvious. Actually, the constraint of uncertainty set is the essence of the two robust beamformers, and the two beamfomer have the same robustness characteristic. F.Vincent and O.Besson also analyze the performance of the beamformer under the uncertainty set constraint approximatively, but they can't give the exact loading level [36].

S. A. Vorobyov et al propose a robust beamformer in the presence of an arbitrary unknown signal steering vector mismatch [19], although they prove the proposed approach equivalent to the loading sample matrix inversion (LSMI) algorithm, but they can't give the direct

method to compute the optimal weight vector, and the second-order cone (SOC) programming-based approach is used to solve the original problem. Ayman Elnashar et al make use of the diagonal loading technique to implement the robust beamformer [24], but the optimal value of diagonal loading level is not solved exactly, alternatively, the diagonal loading technique is integrated into the adaptive update schemes by means of optimum variable loading technique. R. G. Lorenz and S. P. Boyd also solve the similar beamformer by the Lagrange multiplier techniques [23], but they express the weight vector and the array manifold as the direct sum of the corresponding real and imaginary components. Almir Mutapcic et al show that worst-case robust beamforming with multiplicative uncertainty in the weights can be cast as a tractable convex optimization problem [37], but they can't give the solving method, In fact, the proposed robust beamformer with uncertain weights can be converted to that in [19] equivalently.

S. Shahbazpanahi et al consider the general-rank signal model, and the robust beamformer is proposed for the distributed sources [21], therein, an elegant closed-form solution is given, but its performance improvement depends on the constraint parameter severely, and is not up to optimal.

1.1.4 Weight norm constraint approaches for general mismatch

Jian Li et al propose a Capon beamforming approach with the norm inequality constraint (NIC) to improve the robustness against array steering vector errors and noise [22], although the exact solution is given, and optimal loading level can be computed via the proposed method, but by analysis and simulation, its efficiency is not as good as expectation. Since the constraint parameter determines its robustness, but how to select the constraint parameter is not discussed.

Quadratic inequality constraints (QIC) on the weight vector of LCMP beamformer can improve robustness to pointing errors and random perturbations in sensor parameter [27]. The weights that minimize the output power subject to linear constraints and an inequality constraint on the norm of the weight vector have the same form as that of the optimum LCMP beamformer with diagonal loading of the data covariance matrix. But the optimal loading level cannot be directly expressed as a function of the constraint in a closed form, and cannot be solved exactly. Hence, its application is restricted by the optimal weight vector finding. So that some numerically algorithms are proposed to implement the QICLCMP, such as Least Mean Squares (LMS) or Recursive Least Squares (RLS) [27], but the application effect isn't good as the expectation.

This chapter is organized as follows [38]. First, the norm inequality constraint Capon beamformer (NICCB) is introduced and analyzed particularly. Second, the choice of the norm constraint parameter and the selecting bound is discussed. Third, the norm equality constraint Capon beamformer (NECCB) is proposed and is solved effectively. Finally, the simulation analyses and the conclusion are given.

1.2 Capon beamformer under norm inequality constraint (NICCB)

The Capon beamformer can experience significant performance degradation when there is a mismatch between the presumed and actual characteristics of the source or array. The goal of NICCB is to impose an additional inequality constraint on the Euclidean norm of $\mathbf{w}$ for

the purpose of improving the robustness to pointing errors and random perturbations in sensor parameters, here $\mathbf{w}$ denotes the array weight vector. This requires incorporating a norm inequality constraint on $\mathbf{w}$ of the form:

$$\|\mathbf{w}\|^2 \le \varsigma \tag{1.1}$$

where ς is the norm constraint parameter. Consequently, the NICCB problem is formulated as follows:

$$\begin{cases} \min\limits_{\mathbf{w}} \mathbf{w}^H \mathbf{R} \mathbf{w} \\ s.t. \quad \mathbf{w}^H \bar{\mathbf{s}} = 1 \\ \qquad \|\mathbf{w}\|^2 \le \varsigma \end{cases} \tag{1.2}$$

where $\mathbf{R}$ is the data covariance matrix, $\bar{\mathbf{s}}$ is the presumed signal steering vector, and $(\cdot)^H$ denotes the conjugate transposition, $\|\cdot\|$ denotes the vector l_2 norm. For the convenience of analysis, and analyzing the choice of the norm constraint parameter, the solution to NICCB [22] is introduced as follows.

1.2.1 Solution to NICCB

Let S be the set defined by the constraints in above optimization problem, namely:

$$S = \left\{ \mathbf{w} \middle| \mathbf{w}^H \bar{\mathbf{s}} = 1, \|\mathbf{w}\|^2 \le \varsigma \right\} \tag{1.3}$$

Define a function:

$$f_1(\mathbf{w}, \lambda, \mu) = \mathbf{w}^H \mathbf{R} \mathbf{w} + \lambda \left(\|\mathbf{w}\|^2 - \varsigma \right) + \mu \left(-\mathbf{w}^H \bar{\mathbf{s}} - \bar{\mathbf{s}}^H \mathbf{w} + 2 \right) \tag{1.4}$$

where λ is the real-valued Lagrange multiplier, and $\lambda \ge 0$ satisfying $\mathbf{R} + \lambda \mathbf{I} > 0$ so that $f_1(\mathbf{w}, \lambda, \mu)$ can be minimized with respect to $\mathbf{w}$. μ is the arbitrary Lagrange multiplier. Then:

$$f_1(\mathbf{w}, \lambda, \mu) \le \mathbf{w}^H \mathbf{R} \mathbf{w}, \quad \mathbf{w} \in S \tag{1.5}$$

with equality on the boundary of S.

For the standard Capon beamformer

$$\begin{cases} \min\limits_{\mathbf{w}} \mathbf{w}^H \mathbf{R} \mathbf{w} \\ s.t. \quad \mathbf{w}^H \bar{\mathbf{s}} = 1 \end{cases} \tag{1.6}$$

The optimal solution is:

$$\mathbf{w} = \frac{\mathbf{R}^{-1} \bar{\mathbf{s}}}{\bar{\mathbf{s}}^H \mathbf{R}^{-1} \bar{\mathbf{s}}} \tag{1.7}$$

where $\mathbf{R}^{-1}$ is the inversion of $\mathbf{R}$, namely $(\cdot)^{-1}$ denotes the matrix inversion. Here, we can have:

$$\|\mathbf{w}\|^2 = \mathbf{w}^H\mathbf{w} = \left(\frac{\mathbf{R}^{-1}\bar{\mathbf{s}}}{\bar{\mathbf{s}}^H\mathbf{R}^{-1}\bar{\mathbf{s}}}\right)^H \frac{\mathbf{R}^{-1}\bar{\mathbf{s}}}{\bar{\mathbf{s}}^H\mathbf{R}^{-1}\bar{\mathbf{s}}} = \frac{\bar{\mathbf{s}}^H\mathbf{R}^{-2}\bar{\mathbf{s}}}{\left(\bar{\mathbf{s}}^H\mathbf{R}^{-1}\bar{\mathbf{s}}\right)^2} \tag{1.8}$$

where $\mathbf{R}^{-2} = \left(\mathbf{R}^{-1}\right)^2 = \mathbf{R}^{-1}\cdot\mathbf{R}^{-1}$, the above result using the Hermitian property of $\mathbf{R}$.

Consider the condition:

$$\frac{\bar{\mathbf{s}}^H\mathbf{R}^{-2}\bar{\mathbf{s}}}{\left(\bar{\mathbf{s}}^H\mathbf{R}^{-1}\bar{\mathbf{s}}\right)^2} \le \varsigma \tag{1.9}$$

when the above condition is satisfied, the standard Capon beamformer solution (1.7) satisfies the norm constraint of NICCB, hence, is also the solution to NICCB. For this case, $\lambda = 0$ and the norm constraint in NICCB is inactive.

Otherwise, we have the condition:

$$\varsigma < \frac{\bar{\mathbf{s}}^H\mathbf{R}^{-2}\bar{\mathbf{s}}}{\left(\bar{\mathbf{s}}^H\mathbf{R}^{-1}\bar{\mathbf{s}}\right)^2} \tag{1.10}$$

which is an upper bound on ς so that NICCB is different from the standard Capon beamformer. To deal with this case, we can rewrite the $f_1(\mathbf{w},\lambda,\mu)$ as follows:

$$\begin{aligned} f_1(\mathbf{w},\lambda,\mu) = &\left[\mathbf{w} - \mu\left(\mathbf{R}+\lambda\mathbf{I}\right)^{-1}\bar{\mathbf{s}}\right]^H\left(\mathbf{R}+\lambda\mathbf{I}\right)\left[\mathbf{w} - \mu\left(\mathbf{R}+\lambda\mathbf{I}\right)^{-1}\bar{\mathbf{s}}\right] - \\ &-\mu^2\bar{\mathbf{s}}^H\left(\mathbf{R}+\lambda\mathbf{I}\right)^{-1}\bar{\mathbf{s}} - \lambda\varsigma + 2\mu \end{aligned} \tag{1.11}$$

Hence, the unconstrained minimizer of $f_1(\mathbf{w},\lambda,\mu)$, for fixed λ and μ, is given by:

$$\hat{\mathbf{w}}_{\lambda,\mu} = \mu\left(\mathbf{R}+\lambda\mathbf{I}\right)^{-1}\bar{\mathbf{s}} \tag{1.12}$$

Clearly, we have:

$$f_2(\lambda,\mu) \overset{\Delta}{=} f_1\left(\hat{\mathbf{w}}_{\lambda,\mu},\lambda,\mu\right) = -\mu^2\bar{\mathbf{s}}^H\left(\mathbf{R}+\lambda\mathbf{I}\right)^{-1}\bar{\mathbf{s}} - \lambda\varsigma + 2\mu \le \mathbf{w}^H\mathbf{R}\mathbf{w}, \quad \mathbf{w}\in S \tag{1.13}$$

The maximization of $f_2(\lambda,\mu)$ with respect to μ. Hence, μ is given by:

$$\hat{\mu} = \frac{1}{\bar{\mathbf{s}}^H\left(\mathbf{R}+\lambda\mathbf{I}\right)^{-1}\bar{\mathbf{s}}} \tag{1.14}$$

Insert $\hat{\mu}$ into $f_2(\lambda,\mu)$, and let:

$$f_3(\lambda) \overset{\Delta}{=} f_2(\lambda,\hat{\mu}) = -\lambda\varsigma + \frac{1}{\bar{\mathbf{s}}^H\left(\mathbf{R}+\lambda\mathbf{I}\right)^{-1}\bar{\mathbf{s}}} \tag{1.15}$$

The maximization of the above function $f_3(\lambda)$ with respect to λ gives:

$$\frac{\bar{\mathbf{s}}^H(\mathbf{R}+\lambda\mathbf{I})^{-2}\bar{\mathbf{s}}}{\left[\bar{\mathbf{s}}^H(\mathbf{R}+\lambda\mathbf{I})^{-1}\bar{\mathbf{s}}\right]^2}=\varsigma \tag{1.16}$$

Hence, the optimal Lagrange multiplier $\hat{\lambda}$ can be obtained efficiently via, for example, a Newton's method from the above equation of λ.

Note that using $\hat{\mu}$ in $\hat{\mathbf{w}}_{\lambda,\mu}$ yields:

$$\hat{\mathbf{w}}=\frac{(\mathbf{R}+\lambda\mathbf{I})^{-1}\bar{\mathbf{s}}}{\bar{\mathbf{s}}^H(\mathbf{R}+\lambda\mathbf{I})^{-1}\bar{\mathbf{s}}} \tag{1.17}$$

which satisfies the constraints of NICCB, namely:

$$\hat{\mathbf{w}}^H\bar{\mathbf{s}}=1 \tag{1.18}$$

and

$$\|\hat{\mathbf{w}}\|^2=\varsigma \tag{1.19}$$

Hence, $\hat{\mathbf{w}}$ belongs to the boundary of S. Therefore, $\hat{\mathbf{w}}$ is our sought solution to the NICCB optimization problem, which has the same form as the Capon beamformer with a diagonal loading term $\lambda\mathbf{I}$ added to $\mathbf{R}$, namely, NICCB also belongs to the class of diagonal loading approaches.

From the above analysis, we can see that if the Lagrange multiplier λ is obtained, the optimal weight vector for NICCB will be solved. In order to obtain the Lagrange multiplier λ, we must solve the following equation via Newton's method, and let:

$$h(\lambda)=\frac{\bar{\mathbf{s}}^H(\mathbf{R}+\lambda\mathbf{I})^{-2}\bar{\mathbf{s}}}{\left[\bar{\mathbf{s}}^H(\mathbf{R}+\lambda\mathbf{I})^{-1}\bar{\mathbf{s}}\right]^2} \tag{1.20}$$

Hence, the key problem of NICCB is finding the optimal Lagrange multiplier by above equation (1.20). In this chapter, we will give the complete investigation on NICCB, and the existence of its solution is analyzed as follows.

1.2.2 Solution to the optimal Lagrange multiplier

In order to solve the equation (1.20), we perform an eigenvalue decomposition (EVD) of the sample covariance matrix as follows:

$$\mathbf{R}=\mathbf{U}\cdot\mathbf{\Gamma}\cdot\mathbf{U}^H=\sum_{i=1}^{M}\lambda_i\mathbf{u}_i\mathbf{u}_i^H \tag{1.21}$$

where $\mathbf{\Gamma}=diag(\lambda_1,\lambda_2,\cdots,\lambda_M)$ is diagonal matrix, $\mathbf{U}=(\mathbf{u}_1,\mathbf{u}_2,\cdots,\mathbf{u}_M)$ is an Hermitian matrix, λ_i $(i=1,2\cdots M)$ and $\mathbf{u}_i$ $(i=1,2\cdots M)$ are the eigenvalues and eigenvectors of $\mathbf{R}$,

respectively, M is the total number of degrees-of-freedom. For the convenience of analysis, we assume that the eigenvalues / eigenvectors of $\mathbf{R}$ are sorted in descending order, i.e. ,

$$\lambda_1 \geq \lambda_2 \geq \cdots \geq \lambda_M \tag{1.22}$$

We can have:

$$h(\lambda) = \frac{\sum_{i=1}^{M} \frac{\bar{\mathbf{s}}^H \mathbf{u}_i \mathbf{u}_i^H \bar{\mathbf{s}}}{(\lambda_i + \lambda)^2}}{\left[\sum_{i=1}^{M} \frac{\bar{\mathbf{s}}^H \mathbf{u}_i \mathbf{u}_i^H \bar{\mathbf{s}}}{\lambda_i + \lambda}\right]^2} = \frac{\sum_{i=1}^{M} \frac{\left\|\bar{\mathbf{s}}^H \mathbf{u}_i\right\|^2}{(\lambda_i + \lambda)^2}}{\left[\sum_{i=1}^{M} \frac{\left\|\bar{\mathbf{s}}^H \mathbf{u}_i\right\|^2}{\lambda_i + \lambda}\right]^2} \tag{1.23}$$

Therefore, $h(\lambda)$ is monotonically increasing function of $\lambda \geq 0$ [22] , then:

$$h(\lambda) = \frac{\sum_{i=1}^{M} \frac{\left\|\bar{\mathbf{s}}^H \mathbf{u}_i\right\|^2}{(\lambda_i + \lambda)^2}}{\left[\sum_{i=1}^{M} \frac{\left\|\bar{\mathbf{s}}^H \mathbf{u}_i\right\|^2}{\lambda_i + \lambda}\right]^2} \leq \frac{\sum_{i=1}^{M} \frac{\left\|\bar{\mathbf{s}}^H \mathbf{u}_i\right\|^2}{(\lambda_M + \lambda)^2}}{\left[\sum_{i=1}^{M} \frac{\left\|\bar{\mathbf{s}}^H \mathbf{u}_i\right\|^2}{\lambda_1 + \lambda}\right]^2} = \left(\frac{\lambda_1 + \lambda}{\lambda_M + \lambda}\right)^2 \frac{1}{\sum_{i=1}^{M} \left\|\bar{\mathbf{s}}^H \mathbf{u}_i\right\|^2} \tag{1.24}$$

and

$$h(\lambda) = \frac{\sum_{i=1}^{M} \frac{\left\|\bar{\mathbf{s}}^H \mathbf{u}_i\right\|^2}{(\lambda_i + \lambda)^2}}{\left[\sum_{i=1}^{M} \frac{\left\|\bar{\mathbf{s}}^H \mathbf{u}_i\right\|^2}{\lambda_i + \lambda}\right]^2} \geq \frac{\sum_{i=1}^{M} \frac{\left\|\bar{\mathbf{s}}^H \mathbf{u}_i\right\|^2}{(\lambda_1 + \lambda)^2}}{\left[\sum_{i=1}^{M} \frac{\left\|\bar{\mathbf{s}}^H \mathbf{u}_i\right\|^2}{\lambda_M + \lambda}\right]^2} = \left(\frac{\lambda_M + \lambda}{\lambda_1 + \lambda}\right)^2 \frac{1}{\sum_{i=1}^{M} \left\|\bar{\mathbf{s}}^H \mathbf{u}_i\right\|^2} \tag{1.25}$$

and let:

$$\gamma = \sum_{i=1}^{M} \left\|\bar{\mathbf{s}}^H \mathbf{u}_i\right\|^2 \tag{1.26}$$

Alternately, the above inequality relationship can be expressed as:

$$\sqrt{\gamma\varsigma} \leq \frac{\lambda_1 + \lambda}{\lambda_M + \lambda} \tag{1.27}$$

and

$$\sqrt{\gamma\varsigma} \geq \frac{\lambda_M + \lambda}{\lambda_1 + \lambda} \tag{1.28}$$

Next, we analyze the bound of the Lagrange multiplier λ and its existence.

1. If $\sqrt{\gamma\varsigma} > 1$, using (1.27) and (1.28), we can have:

$$\begin{cases} \sqrt{\gamma\varsigma}\left(\lambda_M + \lambda\right) \le \lambda_1 + \lambda \\ \sqrt{\gamma\varsigma}\left(\lambda_1 + \lambda\right) \ge \lambda_M + \lambda \end{cases} \Rightarrow \begin{cases} \lambda \le \dfrac{\lambda_1 - \sqrt{\gamma\varsigma}\lambda_M}{\sqrt{\gamma\varsigma} - 1} \\ \lambda \ge \dfrac{\lambda_M - \sqrt{\gamma\varsigma}\lambda_1}{\sqrt{\gamma\varsigma} - 1} \end{cases} \tag{1.29}$$

Since $\sqrt{\gamma\varsigma} > 1$, but $\lambda_M - \sqrt{\gamma\varsigma}\lambda_1 < 0$, and $\lambda \ge 0$, so that $\lambda_1 - \sqrt{\gamma\varsigma}\lambda_M > 0 \Leftrightarrow \sqrt{\gamma\varsigma} < \lambda_1/\lambda_M$. Therefore, the bound of the Lagrange multiplier λ under $1 < \sqrt{\gamma\varsigma} < \lambda_1/\lambda_M$ is given as follows:

$$\lambda_{\min}^{(1)} \overset{\Delta}{=} 0 \le \lambda \le \frac{\lambda_1 - \sqrt{\gamma\varsigma}\lambda_M}{\sqrt{\gamma\varsigma} - 1} \overset{\Delta}{=} \lambda_{\max}^{(1)} \tag{1.30}$$

Then, we have:

$$h\left(\lambda_{\min}^{(1)}\right) = h(0) = \frac{\bar{\mathbf{s}}^H \mathbf{R}^{-2} \bar{\mathbf{s}}}{\left[\bar{\mathbf{s}}^H \mathbf{R}^{-1} \bar{\mathbf{s}}\right]^2} > \varsigma \tag{1.31}$$

and

$$h\left(\lambda_{\max}^{(1)}\right) = h(\lambda)\Big|_{\lambda_{\max}^{(1)}} \le \left(\frac{\lambda_1 + \lambda}{\lambda_M + \lambda}\right)^2 \frac{1}{\gamma}\Bigg|_{\lambda_{\max}^{(1)}} = \varsigma \tag{1.32}$$

Hence, when $1 < \sqrt{\gamma\varsigma} < \lambda_1/\lambda_M$, there is unique solution $\lambda \in \left[\lambda_{\min}^{(1)},\ \lambda_{\max}^{(1)}\right]$ satisfies $h(\lambda) = \varsigma$.

2. If $\sqrt{\gamma\varsigma} < 1$, using (1.27) and (1.28), we can have:

$$\begin{cases} \sqrt{\gamma\varsigma}\left(\lambda_M + \lambda\right) \le \lambda_1 + \lambda \\ \sqrt{\gamma\varsigma}\left(\lambda_1 + \lambda\right) \ge \lambda_M + \lambda \end{cases} \Rightarrow \begin{cases} \lambda \ge \dfrac{\sqrt{\gamma\varsigma}\lambda_M - \lambda_1}{1 - \sqrt{\gamma\varsigma}} \\ \lambda \le \dfrac{\sqrt{\gamma\varsigma}\lambda_1 - \lambda_M}{1 - \sqrt{\gamma\varsigma}} \end{cases} \tag{1.33}$$

Since $\sqrt{\gamma\varsigma} < 1$, but $\sqrt{\gamma\varsigma}\lambda_M - \lambda_1 < 0$, and $\lambda \ge 0$, so that $\sqrt{\gamma\varsigma}\lambda_1 - \lambda_M > 0 \Leftrightarrow \sqrt{\gamma\varsigma} > \lambda_M/\lambda_1$. Therefore, the bound of the Lagrange multiplier λ under $\lambda_M/\lambda_1 < \sqrt{\gamma\varsigma} < 1$ is given as follows:

$$\lambda_{\min}^{(2)} \overset{\Delta}{=} 0 \le \lambda \le \frac{\sqrt{\gamma\varsigma}\lambda_1 - \lambda_M}{1 - \sqrt{\gamma\varsigma}} \overset{\Delta}{=} \lambda_{\max}^{(2)} \tag{1.34}$$

Then, we have:

$$h\left(\lambda_{\min}^{(2)}\right)=h(0)=\frac{\bar{\mathbf{s}}^H\mathbf{R}^{-2}\bar{\mathbf{s}}}{\left[\bar{\mathbf{s}}^H\mathbf{R}^{-1}\bar{\mathbf{s}}\right]^2}>\varsigma \tag{1.35}$$

and

$$h\left(\lambda_{\max}^{(2)}\right)=h(\lambda)\Big|_{\lambda_{\max}^{(2)}}\geq\left(\frac{\lambda_M+\lambda}{\lambda_1+\lambda}\right)^2\frac{1}{\gamma}\Bigg|_{\lambda_{\max}^{(2)}}=\varsigma \tag{1.36}$$

Hence, when $\lambda_M/\lambda_1<\sqrt{\gamma\varsigma}<1$, there isn't a solution $\lambda\in\left[\lambda_{\min}^{(2)},\lambda_{\max}^{(2)}\right]$ satisfies $h(\lambda)=\varsigma$.

In a word, we can conclude that when $1<\sqrt{\gamma\varsigma}<\lambda_1/\lambda_M$, there is a unique solution $\lambda\in\left[\lambda_{\min}^{(1)},\lambda_{\max}^{(1)}\right]$ satisfies $h(\lambda)=\varsigma$.

1.3 Norm inequality constraint parameter selection

From above analysis, we can see that it is important to select the norm inequality constraint parameter ς for NICCB. If the norm inequality constraint parameter ς is large, it is inactive. On the contrary, if the norm inequality constraint parameter ς is small, there isn't a solution to satisfy NICCB.

We have analyzed that when $1<\sqrt{\gamma\varsigma}<\lambda_1/\lambda_M$, there is a unique solution $\lambda\in\left[\lambda_{\min}^{(1)},\lambda_{\max}^{(1)}\right]$ satisfies $h(\lambda)=\varsigma$. Hence, we can have the selecting bound of the norm inequality constraint parameter ς as follows:

$$1<\sqrt{\gamma\varsigma}<\frac{\lambda_1}{\lambda_M} \tag{1.37}$$

Namely:

$$\frac{1}{\gamma}<\varsigma<\frac{1}{\gamma}\cdot\left(\frac{\lambda_1}{\lambda_M}\right)^2 \tag{1.38}$$

Add the condition of $\varsigma<\dfrac{\bar{\mathbf{s}}^H\mathbf{R}^{-2}\bar{\mathbf{s}}}{\left(\bar{\mathbf{s}}^H\mathbf{R}^{-1}\bar{\mathbf{s}}\right)^2}\overset{\Delta}{=}\varsigma_0$, we can obtain:

$$\varsigma_{\min}\overset{\Delta}{=}\frac{1}{\gamma}<\varsigma<\min\left\{\varsigma_0,\ \frac{1}{\gamma}\left(\frac{\lambda_1}{\lambda_M}\right)^2\right\}\overset{\Delta}{=}\varsigma_{\max} \tag{1.39}$$

If the norm inequality constraint parameter ς is out of the above bound, there is no solution to NICCB. Hence, the norm inequality constraint parameter ς should be chosen in the interval defined by the above inequalities.

1.4 Capon beamformer under norm equality constraint (NECCB)

From above analyses, we can see that the norm inequality constraint can enhance the robustness of NICCB. Since the inequality relationship has a wide range, the norm of the

weight vector will vary in the relevant wide range. If the fluctuation of weight vector norm is acutely, the performance improvement will be weakened greatly. Because the norm equality constraint (NEC) is stronger than the norm inequality constraint (QIC), NECCB will have more ascendant robust performance than NICCB. Hence, NECCB is proposed and is solved effectively in this chapter.

NECCB is to impose an additional equality constraint on the Euclidean norm of $\mathbf{w}$. The NECCB problem is formulated as follows:

$$\begin{cases} \min\limits_{\mathbf{w}} \mathbf{w}^H \mathbf{R} \mathbf{w} \\ s.t. \quad \mathbf{w}^H \bar{\mathbf{s}} = 1 \\ \qquad \|\mathbf{w}\|^2 = \varsigma \end{cases} \tag{1.40}$$

Compare NECCB with NICCB, we can educe the conclusion as follows: (1) The solution to NICCB is obtained on the boundary of its constraint, similarly, for NECCB, the solution is also obtained on its constraint boundary. (2) The solving methods of the two beamformers (or the optimization problem) is different, such as the forenamed solution to NICCB, the Lagrange multiplier of NICCB is taken as positive real-value only, but for NECCB, the Lagrange multiplier is taken as arbitrary real-value, namely, it will be not only the positive real-value, but also the negative real-value. Hence, if we analyze from the point of view of the solving optimization problem, NECCB has two solutions to the optimal Lagrange multiplier, one is positive, and another is negative. Actually, the positive one is the solution to NICCB. For the sake of distinguishing the otherness, the negative solution is interested to NECCB. In order to solve NECCB, we must make use of the discussed results of NICCB, since the manipulation of some inequality, such as the inequality lessening and enlarging is only right for the positive real-value when we solve NICCB.

Similar to NICCB, the solution to NECCB can also be solved by the Lagrange multiplier methodology. And the optimal weight vector of NECCB has the same form as NICCB. The difference between NECCB and NICCB is only the Lagrange multiplier $\breve{\lambda}$, for NICCB, $\lambda \geq 0$, here $\breve{\lambda}$ is arbitrary real-value.

Although the solution to NECCB has the same form as NICCB, but the bound of the Lagrange multiplier is different. In order to use the analyzed results of NICCB for NECCB, replace the Lagrange multiplier by its absolute value, namely the bound of the Lagrange multiplier $\breve{\lambda}$ for NECCB is given by:

$$\sqrt{\gamma\varsigma} \leq \frac{\lambda_1 + \left|\breve{\lambda}\right|}{\lambda_M + \left|\breve{\lambda}\right|} \tag{1.41}$$

and

$$\sqrt{\gamma\varsigma} \geq \frac{\lambda_M + \left|\breve{\lambda}\right|}{\lambda_1 + \left|\breve{\lambda}\right|} \tag{1.42}$$

1. If $\sqrt{\gamma\varsigma} > 1$, then:

$$\frac{\lambda_M - \sqrt{\gamma\varsigma}\lambda_1}{\sqrt{\gamma\varsigma} - 1} \le \left|\breve{\lambda}\right| \le \frac{\lambda_1 - \sqrt{\gamma\varsigma}\lambda_M}{\sqrt{\gamma\varsigma} - 1} \tag{1.43}$$

If $\lambda_1 - \sqrt{\gamma\varsigma}\lambda_M > 0$, then $\sqrt{\gamma\varsigma} < \lambda_1/\lambda_M$, since $\lambda_M - \sqrt{\gamma\varsigma}\lambda_1 < 0$, but $\left|\breve{\lambda}\right| > 0$. Therefore, if $1 < \sqrt{\gamma\varsigma} < \lambda_1/\lambda_M$, we can have:

$$\breve{\lambda}_{\min}^{(1)} \stackrel{\Delta}{=} -\frac{\lambda_1 - \sqrt{\gamma\varsigma}\lambda_M}{\sqrt{\gamma\varsigma} - 1} \le \breve{\lambda} \le \frac{\lambda_1 - \sqrt{\gamma\varsigma}\lambda_M}{\sqrt{\gamma\varsigma} - 1} \stackrel{\Delta}{=} \breve{\lambda}_{\max}^{(1)} \tag{1.44}$$

Since $\breve{\lambda}_{\max}^{(1)} > 0$, and $\breve{\lambda}_{\min}^{(1)} = -\breve{\lambda}_{\max}^{(1)} < 0$. Hence, when $1 < \sqrt{\gamma\varsigma} < \lambda_1/\lambda_M$, the solution to NECCB in the bound of $\left[0,\ \breve{\lambda}_{\max}^{(1)}\right]$ is the same as NICCB, but the solution in the bound of $\left[\breve{\lambda}_{\min}^{(1)},\ 0\right]$ is the true solution to NECCB.

2. If $\sqrt{\gamma\varsigma} < 1$, then:

$$\frac{\sqrt{\gamma\varsigma}\lambda_M - \lambda_1}{1 - \sqrt{\gamma\varsigma}} \le \left|\breve{\lambda}\right| \le \frac{\sqrt{\gamma\varsigma}\lambda_1 - \lambda_M}{1 - \sqrt{\gamma\varsigma}} \tag{1.45}$$

If $\sqrt{\gamma\varsigma}\lambda_1 - \lambda_M > 0$, then $\sqrt{\gamma\varsigma} > \lambda_M/\lambda_1$, since $\sqrt{\gamma\varsigma}\lambda_M - \lambda_1 < 0$, but $\left|\breve{\lambda}\right| > 0$. Therefore, if $\lambda_M/\lambda_1 < \sqrt{\gamma\varsigma} < 1$, we can have:

$$\lambda_{\min}^{(2)} \stackrel{\Delta}{=} -\frac{\sqrt{\gamma\varsigma}\lambda_1 - \lambda_M}{1 - \sqrt{\gamma\varsigma}} \le \breve{\lambda} \le \frac{\sqrt{\gamma\varsigma}\lambda_1 - \lambda_M}{1 - \sqrt{\gamma\varsigma}} \stackrel{\Delta}{=} \lambda_{\max}^{(2)} \tag{1.46}$$

Since $\breve{\lambda}_{\max}^{(2)} > 0$, and $\breve{\lambda}_{\min}^{(2)} = -\breve{\lambda}_{\max}^{(2)} < 0$, with the above analysis of NICCB, we can obtain that when $\lambda_M/\lambda_1 < \sqrt{\gamma\varsigma} < 1$ there isn't a solution in the bound of $\left[0,\ \breve{\lambda}_{\max}^{(2)}\right]$ to NECCB, but the solution in the bound of $\left[\breve{\lambda}_{\min}^{(2)},\ 0\right]$ is the true solution to NECCB.

From above analysis, we can conclude as follows:

1. When $1 < \sqrt{\gamma\varsigma} < \lambda_1/\lambda_M$, the solution in the bound of $\left[\breve{\lambda}_{\min}^{(1)},\ 0\right]$ is the true solution to NECCN, and the norm equality constraint parameter ς should be chosen in the interval defined by $1/\gamma < \varsigma < \min\left\{\left(\lambda_1/\lambda_M\right)^2/\gamma,\ \varsigma_0\right\}$.
2. When $\lambda_M/\lambda_1 < \sqrt{\gamma\varsigma} < 1$, the solution in the bound of $\left[\breve{\lambda}_{\min}^{(2)},\ 0\right]$ is the true solution to NECCB, and the norm equality constraint parameter ς should be chosen in the bound of $\left(\lambda_M/\lambda_1\right)^2/\gamma < \varsigma < \min\left\{1/\gamma,\ \varsigma_0\right\}$.
3. NECCB has the form of diagonal loading with negative loading level, but NICCB has the form of diagonal loading with positive loading level.

1.5 Simulation analysis

In order to validate the correctness and the efficiency of the proposed algorithms, we analyze as follows. In our simulations, we assume a uniform linear array with N=10 omnidirectional sensors spaced half a wavelength apart. Through all examples, we assume that there is one desired source, namely, there is a signal from direction 0^o, the Signal Noise Ratio (SNR) is -5dB. Therein, the presumed signal direction is equal to 5^o (i.e., there is a 5^o direction mismatch).

For the comparison, the benchmark standard Capon beamforming algorithm that corresponds to the ideal case when the covariance matrix is estimated by the maximun likelihood estimator (MLE) and the actual steering vector is used, this algorithm does not correspond to any real situation but is included in our simulations for the sake of comparison only, and is denoted by Ideal-SCB in the figure. The other algorithms include: standard Capon beamformer (SCB), NICCB, NECCB. For NICCB and NECCB, the constraint parameter is selected as the median of the allowable bound.

1.5.1 Effectivity analyzing

In order to show the effectivity of the proposed algorithms, we first compare the pattern of the mentioned Capon beamforming algorithms. The Capon beamformer pattern is given in Fig. 1. Since the signal direction mismatch, the mainlobe of SCB departs from the signal direction. The performance of NICCB is slightly better than SCB, and NECCB is the best of all, the direction mismatch is overcame commendably and NECCB also has lower sidelobe level. Here, NICCB uses the positive optimal loading level, NECCB uses the negative optimal loading level. From the comparison, we can see that NECCB has the better performance than NICCB.

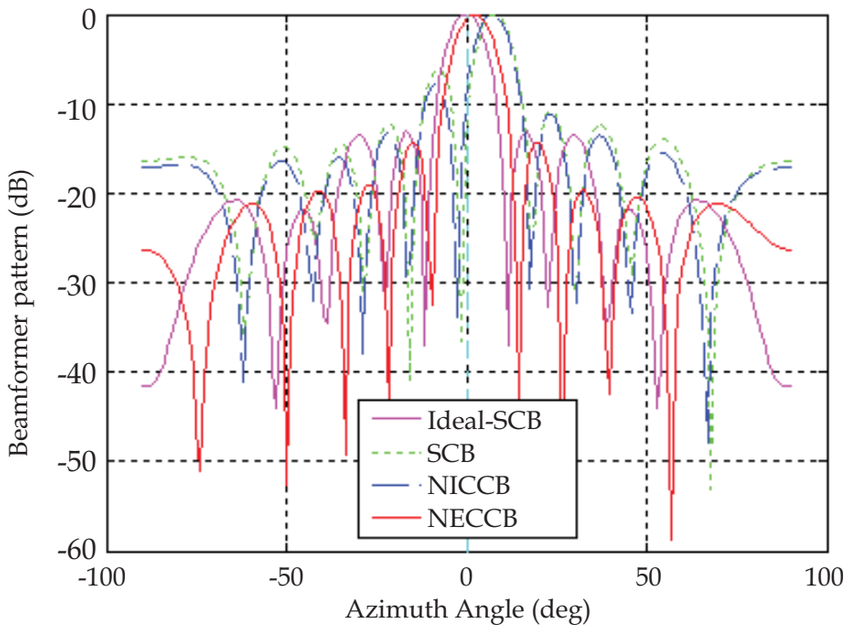

Fig. 1. Capon beamformer pattern comparison

The variation of the beamformer SNR versus samples number is given in Fig. 2. We can see that with the change of the samples number, the SNRs varies accordingly. The SNR of NICCB is almost closed to the SNR of SCB, and is lower than the SNR of Ideal-SCB, but NECCB is the best of all, especially for the small number, it has preferable performance. Hence, the norm constraint can improve the SNR, and NECCB has the highest SNR among the listed algorithms.

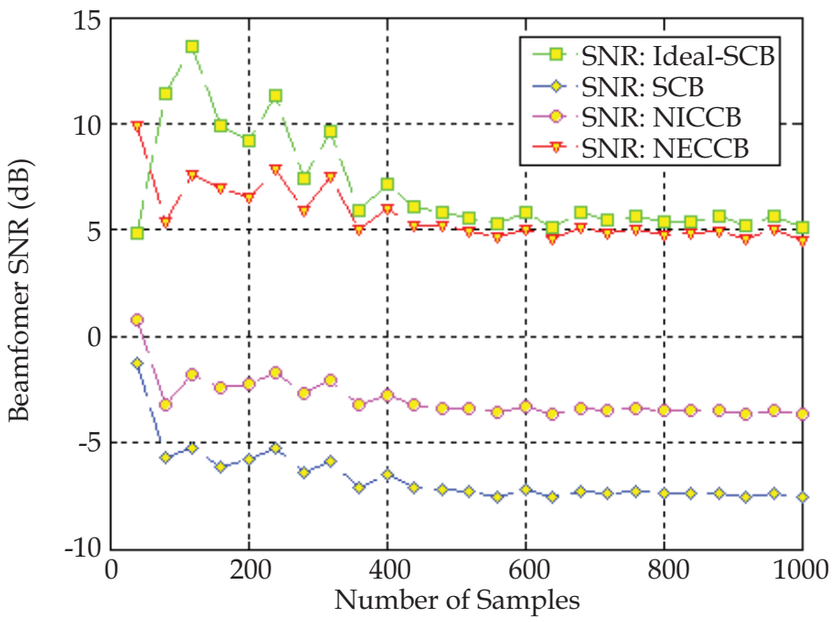

Fig. 2. Output SNR versus samples number

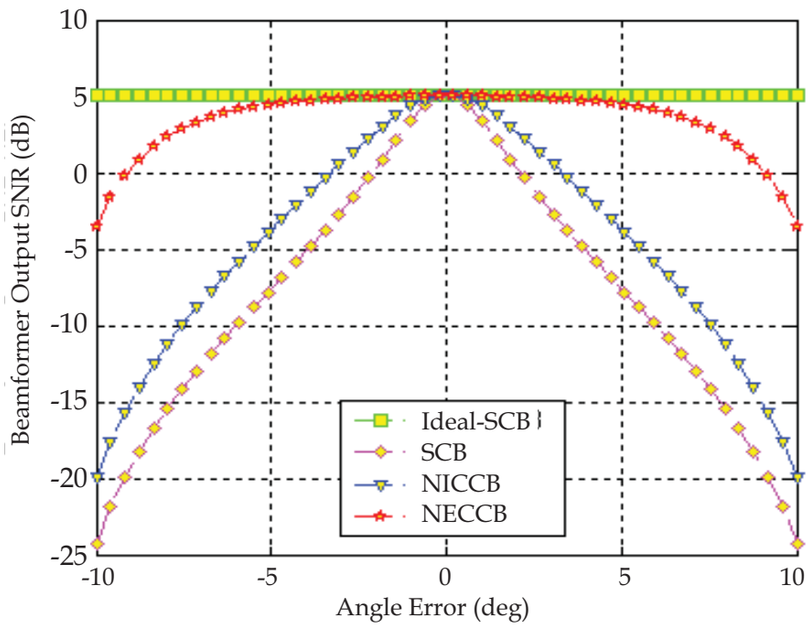

Fig. 3. Output SNR versus angle mismatch

The variation of the Capon beamformer output signal-to-noise-ratio (SNR) versus signal direction mismatch is given in Fig. 3. We can see that with the change of the signal direction mismatch, the SNR varies accordingly, when the angle error is in the range of [-7°, 7°], NECCB will has higher SNR than SCB, NICCB. The NECCB has the higher SNR can be explained by the Fig. 1 of the beam pattern comparison, NECCB not only has the good pointing performance, but also has the lower sidelobe level. Namely, for the same desired signal output, the output noise of NECCB is lower. The simulation results can also be explained as follows, for the used scene, the Signal Noise Ratio is -5dB, and for NECCB, the optimal Lagrange is negative, namely the optimal loading level is negative, but for others, the loading level is zero or positive. Therefore, for the NECCB beamformer, the output noise power is decreased, but for other beamformers, the output noise power is increased. Hence, the NECCB has higher output SNR than others. For the sake of saving space, the corresponding beam pattern comparison isn't given, but in the simulation, NECCB pattern also points to the actual signal direction exactly. Hence, NECCB has the better robustness in the signal direction mismatch case.

From above analysis, we can see that NECCB has the best robustness against the signal direction mismatch.

1.5.2 Correctness analyzing

Since NICCB and NECCB have the same form as that of SCB with diagonal loading. But their key problems are how to find their own optimal loading level or Lagrange multiplier, In order to show the impact of loading level on the Capon beamformer under norm constraint (NCCB) and attest the correctness of the proposed algorithms, the simulation results are given as follows.

The variation of the output SNR versus diagonal loading level is given in Fig. 4. We can see that with the change of the loading level in the bound of $\left[\breve{\lambda}_{\min}^{(1)}, \breve{\lambda}_{\max}^{(1)}\right]$, the SNR of NCCB varies accordingly. When the loading level is positive, NCCB is NICCB, whereas, when the loading level is negative, NCCB is NECCB. By comparison, we can see that NECCB has higher SNR than NICCB, but for the optimal loading, namely when the loading level is equal to -6.09, NECCB has the best pointing performance, and its SNR is the highest one, where the optimal loading level -6.09 is calculated using the equation $h(\lambda) = \varsigma$ with $1 < \sqrt{\gamma\varsigma} < \lambda_1/\lambda_M$ in the bound of $\left[\breve{\lambda}_{\min}^{(1)}, \ 0\right]$. Hence, the loading level has a great impact on the SNR of the Capon beamformer, and determines the performance improvement.

The variation of the weight vector norm versus diagonal loading level is given in Fig. 5. We can see that with the change of the loading level in the bound of $\left[\breve{\lambda}_{\min}^{(1)}, \breve{\lambda}_{\max}^{(1)}\right]$, the weight vector norm of NCCB varies accordingly. For most loading levels, the weight vector norm varies slightly, but when the loading level is small in negative domain, the weight vector norm is a little high, and the highest point is corresponding to the lowest point in Fig. 4. Therefore, the loading level has a great impact on the weight vector norm, especially for the negative loading.

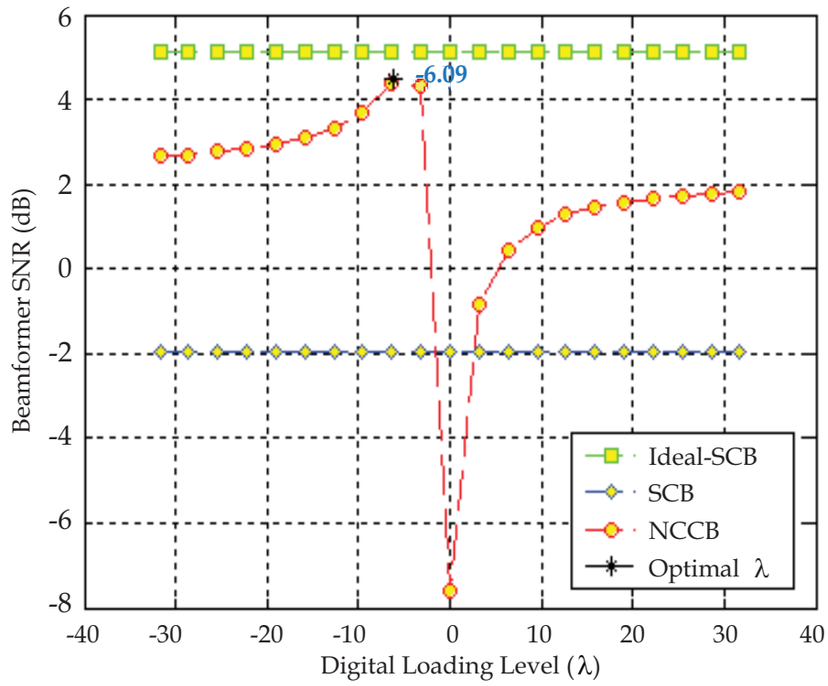

Fig. 4. Output SNR versus loading level

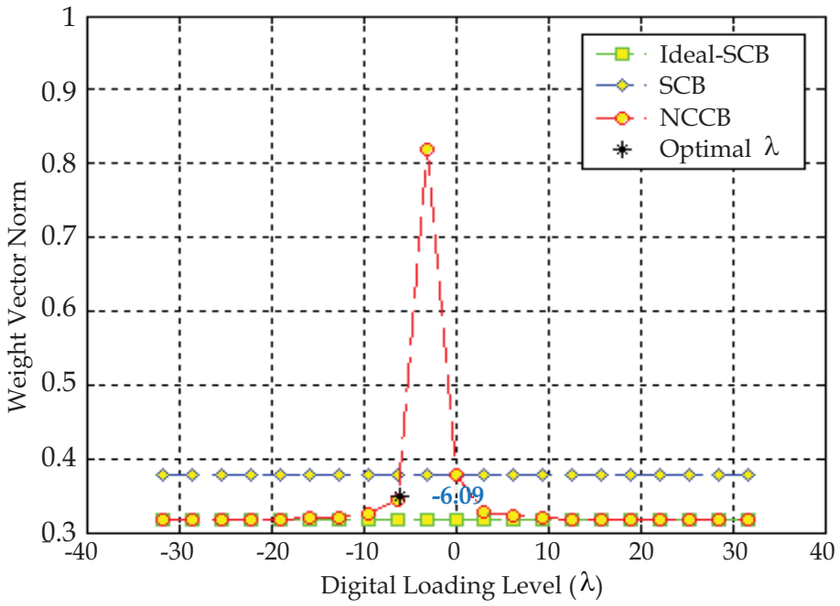

Fig. 5. Weight vector norm versus loading level

From the above simulation results, we can see that the loading level has a great impact on the performance of the Capon beamformer, and NECCB has the best pointing performance, namely, the optimal negative loading is the best. This is also consistent to the theory analysis, for the robust beamformer with diagonal loading, the improvement is determined by the optimal loading level, when the loading level is optimal, the performance

improvement will be the optimal, but for other values, the improvement will be little, or even worse.

1.5.3 Constraint parameter selection analyzing

For NCCB, there are two key problems, one is how to find the optimal loading level, and the other is how to select the norm constraint parameter. Although we have solved the two problems in theory, but there is another key problem, namely, how to select the optimal norm constraint parameter. Therefore, the impact of norm constraint parameter on NCCB is analyzed here particularly.

The variation of the output SNR versus norm constraint parameter is given in Fig. 6. We can see that with the change of the norm constraint parameter in the allowable bound of $(\varsigma_{\min}, \varsigma_{\max})$, the SNR of the Capon beamformer varies accordingly. NICCB has a little higher SNR than that of SCB, NECCB has the highest SNR. And with the norm constraint parameter increasing, the SNR of NECCB increases correspondingly, but the SNR of NICCB is inclined to the SNR of SCB. When the norm constraint parameter is equal to the maximum, the constraint is inactive, and the three SNRs tend to the same value. Hence, the SNR is determined by the choice of the norm constraint parameter, especially for NECCB.

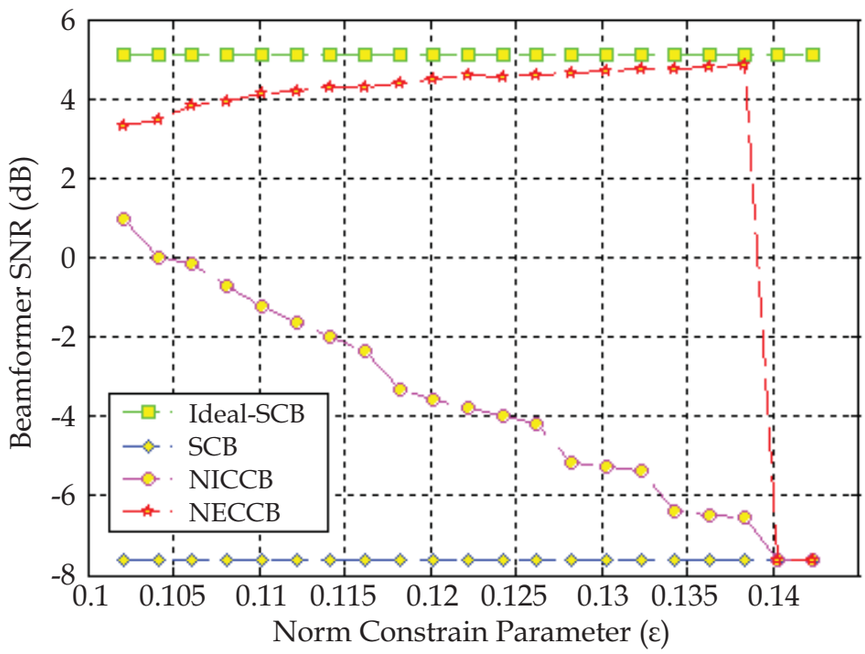

Fig. 6. Output SNR versus constraint parameter

The variation of the weight vector norm versus norm constraint parameter is given in Fig. 7. When the norm constraint parameter is selected in the allowable bound of $(\varsigma_{\min}, \varsigma_{\max})$, the weight vector norms of NICCB and NECCB vary adaptively, and are equal to the square root of the constraint parameter approximatively, this is consistent with the theory, namely the solution is obtained on the constraint boundary. The slight difference is caused by the approximative computation.

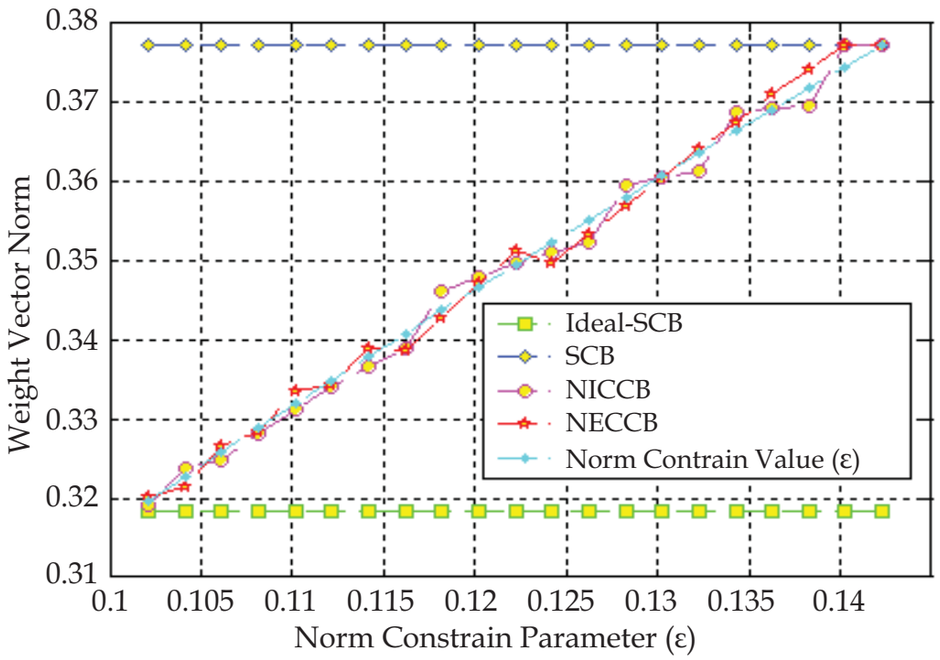

Fig. 7. Weight norm versus constraint parameter

From above simulation results, we can see that if the norm constraint parameter is selected in the allowable bound, the norm constraint parameter has a great impact on the performance of NICCB and NECCB, especially for NECCB. But NECCB with the larger constraint parameter has the better pointing performance, namely, when the constraint parameter is selected as more larger in its allowable bound, the optimal negative loading has the optimal improvement.

1.6 Conclusion

From the above analysis, we can conclude as follows. (I) The proposed algorithm is correct and effective. (II) The norm constraint can improve the robustness of the Capon beamformer. Especially, the equality constraint has the preferable improvement to overcome the steering vector mismatch, and also has good robustness for the samples number. (III) When the norm constraint parameter is selected in the allowable bound, NECCB has the best performance, namely the optimal negative loading has the optimal improvement, this is because that the norm equality constraint is stronger than the norm inequality constraint.

2. Improved pattern synthesis method with linearly constraint minimum variance criterion

Antenna pattern synthesis becomes the fundamental research contents with the wide application of the array antenna in communication, radar and other areas, and catches the attentions widely. The array antenna pattern synthesis is the task which solves the weight values of the every element to force the antenna pattern inclining to the anticipant shape. Dolph has first given the method of getting the weight function for uniform linear array to

achieve the Chebychev pattern [39], therefore the optimal solution can be achieved in the sense of giving the mainlobe width and the maximum lowest sidelobe level. However, how to implement the pattern synthesis for the arbitrary array antenna efficiently is a challenging research task in array signal processing society.

Currently, the methods of pattern synthesis can be classified as the two types, one is the traditional vector weight methods [40-42], the other one is the matrix weight methods [43], therein, the intelligent computer methods are used to improve the calculating efficiency of the optimal weight vector, such as the genetic evolution algorithms [44] and the particle swarm optimization algorithms [45]. However, for any pattern synthesis method, the iterative operation can't be avoided, and the iterative number determines the operation load directly, the operation load, or titled as the compute efficiency is the key metric to evaluate the validity of the pattern synthesis.

Guo Q et al propose the pattern synthesis method for the arbitrary array antenna with the linearly constraint minimun variance criterion (LCMV-PS) [45], compared with the traditional vector weight methods, this algorithm has the small iterative number and the preferable convergence. However, by analysis and simulation, it is found that the iterative coefficient determines its performance, namely, the iterative coefficient not only determines the pattern shape, but also determines the iterative number, or titled as the compute load. Therefore, how to select the iterative formula and its iterative coefficient is the key problem to reduce the compute load and enhanced the applicability.

In this chapter, for the LCMV-PS method proposed in [45], by analyzing its implementation and jammer power iterative formula, the improved fast robust LCMV-PS method is proposed [46]. This algorithm takes into account the effect of the relative amplitude between synthesis pattern and its reference upon the pattern synthesis adequately, via adding a proportion constant to the iterative formula, the effect of their relative amplitude upon the changing ratio of the jammer power is strengthened, not only the iterative efficiency of the jammer power is improved, namely the iterative number is reduced, and the pattern synthesis efficiency is improved, but also the selecting bound of the iterative coefficient is extended, namely the effect of the iterative coefficient upon the pattern synthesis is weakened, and the application area and applicability of the pattern synthesis method is enhanced greatly. The last simulation attests its correctness and effectiveness.

2.1 Pattern synthesis method with LCMV criterion

The problem of array pattern synthesis can be simplified as follows, namely for the given element number M and element position $\{\mathbf{x}_i\}_{i=1}^{M}$, solving the complex weight vector $\mathbf{w}$, and force the array pattern $P(\theta)$ with the definite width and maximum value in the desired direction, at the same time, make the sidelobe level according to the requirement.

The target of the pattern synthesis method for arbitrary arrays based on LCMV criterion (LCMV-PS) is making all the sidelobe peak level equal to the minimum that the array can achieve as possible. Furthermore, this method constructs many illusive jammers in the sidelobe region, and the jammer power will be justed by the synthesis pattern amplitude in its relative direction, namely, if the synthesis pattern amplitude is high in this direction, the illusive jammer power will be increased. Therefore, the LCMV-PS method can be simple described as follows:

1. Specify the mainlobe region $[\theta_{ML1},\theta_{ML2}]$ and sidelobe envelope $D(\theta_i)$.
   Set the initial value of jammer power $f_0(\theta_i)$, if θ_i is in the sidelobe region, $f_0(\theta_i)=1$, otherwise if in the mainlobe region, $f_0(\theta_i)=0$, $i=1,\cdots N$, where N is the number of the uniformly distributed jammers with one degree spacing, namely, $\theta_1,\theta_2,\cdots,\theta_N$ are the degree values with the one degree spacing in the array pattern overlay region. And $D(\theta_i)$ is the given reference sidelobe envelope of the synthesis pattern.
2. Calculate jammer powers for the k-th iteration $f_k(\theta_1),f_k(\theta_2),\cdots,f_k(\theta_N)$.
   If k=0, then the jammer powers are the initial values $f_0(\theta_1),f_0(\theta_2),\cdots,f_0(\theta_N)$.
   If $k\geq 1$, there is the iterative formula as follows:

$$f_k(\theta)=\begin{cases} 0 & \theta\in[\theta_{ML1},\theta_{ML2}] \\ \max\left\{f_{k-1}(\theta)+Kf_{k-1}(\theta)\dfrac{P_{k-1}(\theta)-Pr_{k-1}}{Pr_{k-1}},\quad 0\right\} & \theta\notin[\theta_{ML1},\theta_{ML2}] \end{cases} \tag{2.1}$$

where $f_{k-1}(\theta)$ is the jammer powers of the k-1-th iteration, K is the iterative coefficient. $P_{k-1}(\theta)=\left|\mathbf{w}^H\mathbf{a}(\theta)\right|$ is the pattern of the k-1-th iteration, therein $\mathbf{w}$ is the relative weight vector, $\mathbf{a}(\cdot)$ is the steering vector, and $(\cdot)^H$ denotes the conjugate transposition. Pr_{k-1} is the sidelobe reference amplitude, if the arbitrary sidelobe shape is required in the pattern synthesis, it is only to substitute $Pr_{k-1}(\theta)=Pr_{k-1}\cdot D(\theta)$ for Pr_{k-1} in the above formula, and $D(\theta)$ is the given sidelobe envelope.

3. Calculate the data covariance matrix $\mathbf{R}_x$, namely:

$$\mathbf{R}_x=\mathbf{A}\cdot diag\left[f_k(\theta_1),f_k(\theta_2),\cdots,f_k(\theta_N)\right]\cdot\mathbf{A}^H+\sigma\mathbf{I} \tag{2.2}$$

where $\mathbf{A}=\left[\mathbf{a}(\theta_1),\mathbf{a}(\theta_2),\cdots,\mathbf{a}(\theta_N)\right]$ is the array manifold matrix. σ is a given small quantity, and $\mathbf{I}$ is the identity matrix, $\sigma\mathbf{I}$ is added to prevent the covariance matrix from being ill-conditioned.

4. Calculate the weight vector $\mathbf{w}$ according with the following LCMV beamforming algorithm, then synthesize the pattern. If it is satisfactory, stop; otherwise, go to step (2) and continue. Therein, $\mathbf{w}$ is solved by the below LCMV optimization problem, namely:

$$\begin{cases} \min\limits_{\mathbf{w}}\mathbf{w}^H\mathbf{R}_\mathbf{x}\mathbf{w} \\ s.t.\quad \mathbf{C}^H\mathbf{w}=\mathbf{f} \end{cases} \tag{2.3}$$

where $\mathbf{C}$ is the M×m constraint matrix, and $\mathbf{f}$ is the m×1 constraint value vector. Its optimal solution is:

$$\mathbf{w}=\mathbf{R}_\mathbf{x}^{-1}\mathbf{C}\left(\mathbf{C}^H\mathbf{R}_\mathbf{x}^{-1}\mathbf{C}\right)^{-1}\mathbf{f} \tag{2.4}$$

In the constraint condition of the optimization problem, the constraint of the mainlobe can be imposed, the constraint of the sidelobe can also be added, in other words, the constraint condition and parameter can be selected according to the pattern synthesis requirement.

2.2 Improvement of the jammer power iteration formula

From the step of the LCMV-PS method, we can see that the key is the jammer power iteration in step (2), since it not only determines the synthesis pattern shape, but also determines the final iterative number.

By the particular analysis of the LCMV-PS implementing steps, it is not difficulty to find that although the relative difference of the synthesis pattern and the reference pattern $\left(P_{k-1}(\theta)-Pr_{k-1}\right)/Pr_{k-1}$ is used as the ratio factor for the gain change, and to control the change direction and quality of the jammer powers, actually, the expression of the iterative formula $f_{k-1}(\theta)+Kf_{k-1}(\theta)\left(\left(P_{k-1}(\theta)-Pr_{k-1}\right)/Pr_{k-1}\right)$ can be transformed as:

$$f_{k-1}(\theta)+Kf_{k-1}(\theta)\frac{P_{k-1}(\theta)-Pr_{k-1}}{Pr_{k-1}}=f_{k-1}(\theta)\left(K\cdot\frac{P_{k-1}(\theta)}{Pr_{k-1}}+(1-K)\right) \tag{2.5}$$

This expression indicates that the jammer powers between the adjacent iterations are different by a proportional factor, when the iterative coefficient K is given, the jammer power ratio of the adjacent iterations is determined by the relative amplitude of the synthesis pattern and the reference pattern $P_{k-1}(\theta)/Pr_{k-1}$. Therefore, for the given K, the change of the jammer powers in the iteration process is determined by $P_{k-1}(\theta)/Pr_{k-1}$, and the relationship is a linear function.

From the pattern synthesis process of the LCMV-PS method, when the synthesis pattern is higher than the reference pattern, the jammer powers should increase, and is in direct proportion to the difference of the two patterns. When the synthesis pattern is more higher than the reference pattern, the jammer powers should increase more larger. But when the synthesis pattern is close to the reference pattern, the change of the jammer power should be small, namely the adjustment should be precise at this time. Although the original iterative formula is consistent to the analyzing idea, and the change ratio of the iterative jammer powers is $K\cdot\left(P_{k-1}(\theta)/Pr_{k-1}\right)+(1-K)$, namely is in direct proportion to $P_{k-1}(\theta)/Pr_{k-1}$. Therefore, for the original method, K is the main parameter to determine the iterative effect and efficiency, and by the simulation, it is found that the synthesis pattern will be good when the parameter K is selected in a small region, such as the reference value K=0.1 in [42]. Actually, for the difference element number or array parameter, the optimal value of K will vary correspondingly. Hence, for the original method, how to select the optimal parameter K is the key matter, it not only determines the effect of the synthesis pattern, but also determines the efficiency of the jammer power iteration, namely the iterative number.

Since in the iterative process, it is the factor $K\cdot\left(P_{k-1}(\theta)/Pr_{k-1}\right)+(1-K)$ determining the change quantity and direction of the jammer powers iteration, for the given K, the second item is constant, but the first item is the linear function of $P_{k-1}(\theta)/Pr_{k-1}$, and its proportional coefficient is K, namely the slope K determines the change quantity of the jammer power with $P_{k-1}(\theta)/Pr_{k-1}$. With the slope of the linear function increasing, namely for the given parameter K_p>1, the change ratio of $K\cdot K_p\cdot\left(P_{k-1}(\theta)/Pr_{k-1}\right)+(1-K)$ with $P_{k-1}(\theta)/Pr_{k-1}$ will be larger, namely the efficiency of the jammer power iteration will be improved. At the same time, for the given parameter K_p, when the effect of the jammer power iteration is better, the selection of K will be loosened, namely K can be selected in a wider region. Therefore, if the constant factor K_p (K_p>1) can be added as this method, the

efficiency of the jammer power iteration will be improved, and the bound for selecting the iterative coefficient K will be enlarged, namely the selection of K will be simplified greatly.

Hence, in order to improve the iterative efficiency of the LCMV-PS method and simplify the selection of the iterative coefficient K, the iterative formula of the jammer power can be improved as follows, namely

$$f_k(\theta)=\begin{cases} 0 & \theta\in[\theta_{ML1},\theta_{ML2}] \\ \max\left\{ f_{k-1}(\theta)+K\cdot f_{k-1}(\theta)\cdot\dfrac{K_p\cdot P_{k-1}(\theta)-Pr_{k-1}}{Pr_{k-1}},\ 0\right\} & \theta\notin[\theta_{ML1},\theta_{ML2}] \end{cases} \tag{2.6}$$

where K_p is used to adjust the effect of the relative amplitude $P_{k-1}(\theta)/Pr_{k-1}$ of the synthesis pattern and reference pattern upon the change ratio of the jammer power, namely is used to adjust the iterative efficiency of the pattern synthesis method, and other parameters have the same sense as forenamed. If K_p>1, the iterative efficiency will be advanced, whereas the iterative efficiency will be reduced. It is important that the effect of the iterative coefficient K upon the pattern synthesis is reduced greatly by adding the parameter K_p, therefore, the selection of parameter K will be simplified greatly.

Compared with the LCMV-PS method proposed in [42], the iterative formula of the jammer power is added by a constant K_p to adjust the iterative efficiency in this chapter, if K_p>>1, the efficiency of the proposed method will be improved greatly, therefore, the iterative number will be reduced, so that the operation load will be reduced greatly by the proposed method. At the same time, the bound for selecting K will also be enlarged greatly, and the application area and applicability of the pattern synthesis method is enhanced.

2.3 Simulations

Since the proposed method has the higher iterative efficiency and stronger applicability as compared with the LCMV-PS method proposed in [42], the simulation keystone is to compare the iterative efficiency of the two methods, and the effect of the iterative coefficient upon the two methods. The simulations are as follows.

2.3.1 Efficiency analyzing

In order to validate the efficiency of the proposed method, the single beam and multi-beam pattern synthesis examples of the uniform and non-uniform linear array are given respectively, and the single beam pattern synthesis examples of uniform and non-uniform planar array are also given respectively. For the convenience of comparison, the proposed improved LCMV-PS method is denoted as I-LCMV-PS, the LCMV-PS in [42] is denoted as LCMV-PS, the reference pattern is denoted as Reference.

The single beam synthesis pattern of the uniform linear array is given in Fig. 8. Therein, the element number is 32, the elements inter-space is half wavelength ($\lambda/2$), the mainlobe is point to 0^o, the mainlobe width is 22^o, the iterative parameter of jammer power K=0.5, and K_p=100. When the optimal weight vector is solved under the LCMV criterion, the mainlobe direction constraint is used only. Therein the iterative number of I-LCMV-PS is 5, but the iterative number of LCMV-PS is 20.

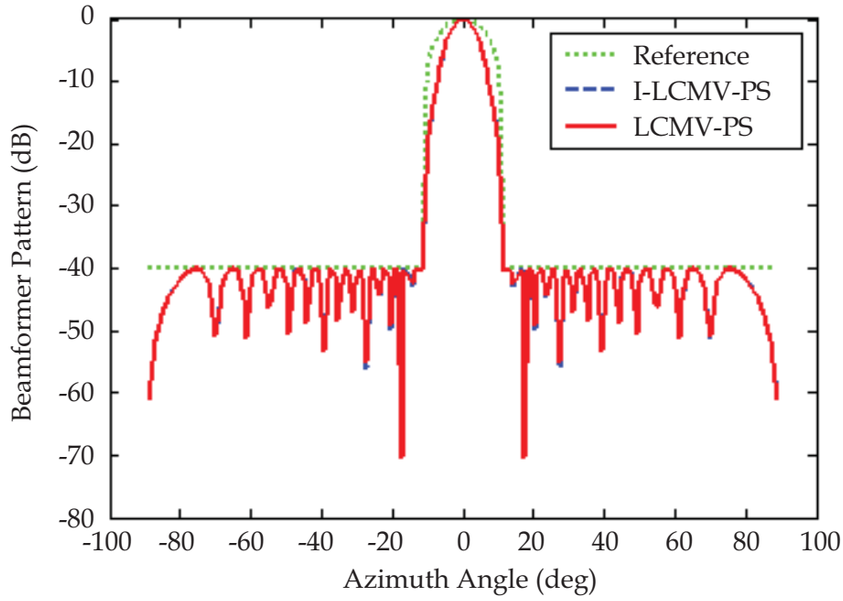

Fig. 8. Single beam synthesis pattern of uniform linear array

The single beam synthesis pattern of the non-uniform linear array is given in Fig. 9. Therein, the element number is 32, the element space vector is $(\lambda/2)\times$[0.29595, 1.5655, 2.7845, 3.9334, 4.999, 5.9753, 6.8645, 7.6764, 8.428, 9.1413, 9.842, 10.557, 11.311, 12.127, 13.021, 14.002, 15.073, 16.226, 17.449, 18.72, 20.017, 21.312, 22.579, 23.795, 24.939, 26, 26.971, 27.856, 28.664, 29.413, 30.125, 30.825], the mainlobe is also point to 0^o, the mainlobe width is also 22^o, and K=0.5, K_p=100. When the optimal weight vector is solved under the LCMV criterion, the mainlobe direction constraint is used only. The iterative number of the two methods are 5 and 20, respectively.

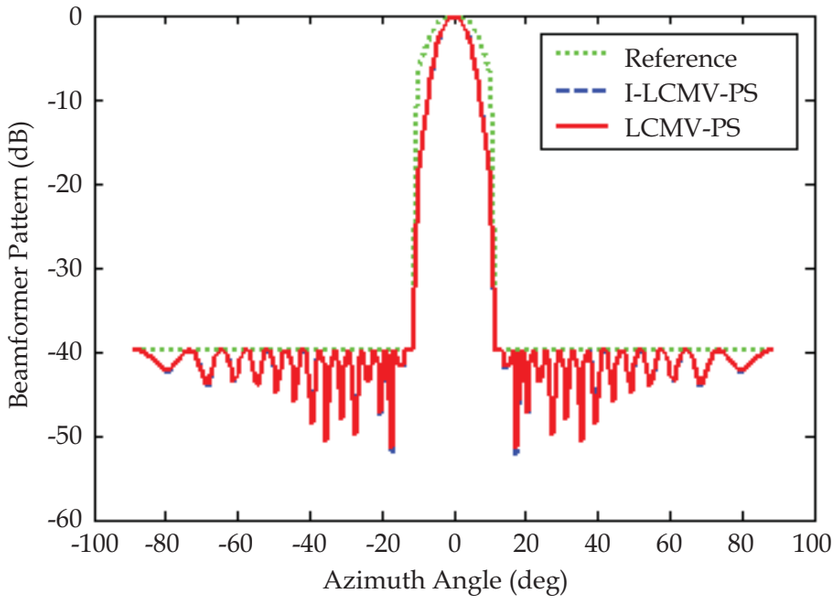

Fig. 9. Single beam synthesis pattern of non-uniform linear array

In order to attest the applicability of the improved algorithm to the planar array, and its effectivity of multi-beam synthesis, namely the arbitrary array and arbitrary pattern synthesis, the particular simulation examples are given as Fig. 11.~Fig. 16.

The multi-beam synthesis patterns of the uniform and non-uniform linear array are given in Fig. 11. and Fig. 12. The parameters are same as Fig. 8. and Fig. 9., the two beams point to 45° and -45° respectively. Therein the iterative number of I-LCMV-PS is 6, but the iterative number of LCMV-PS is 25.

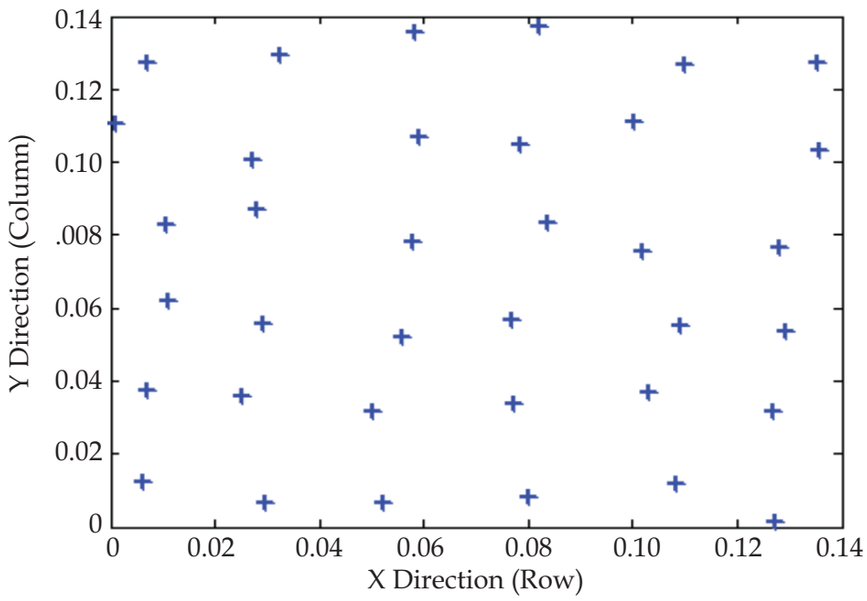

Fig. 10. Element position of the non-uniform planar array

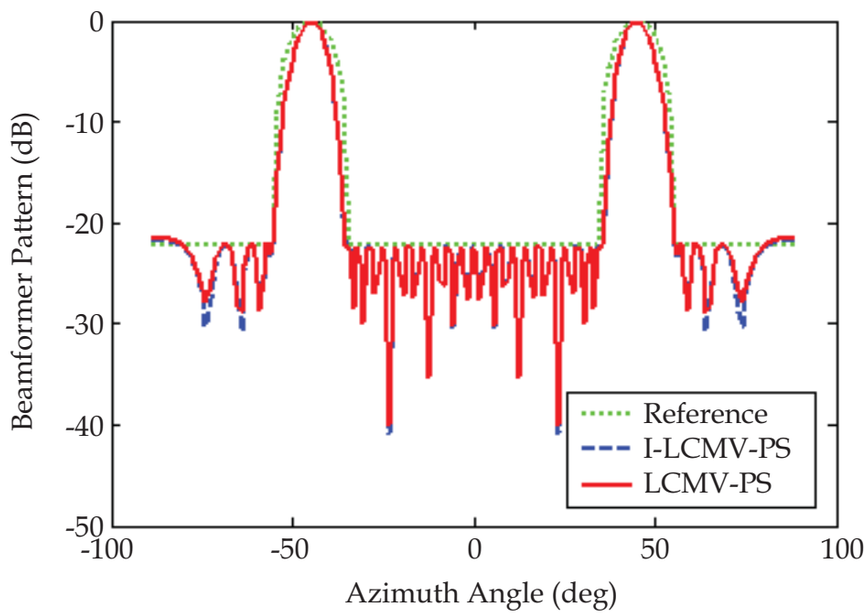

Fig. 11. Multi-beam synthesis pattern of uniform linear array

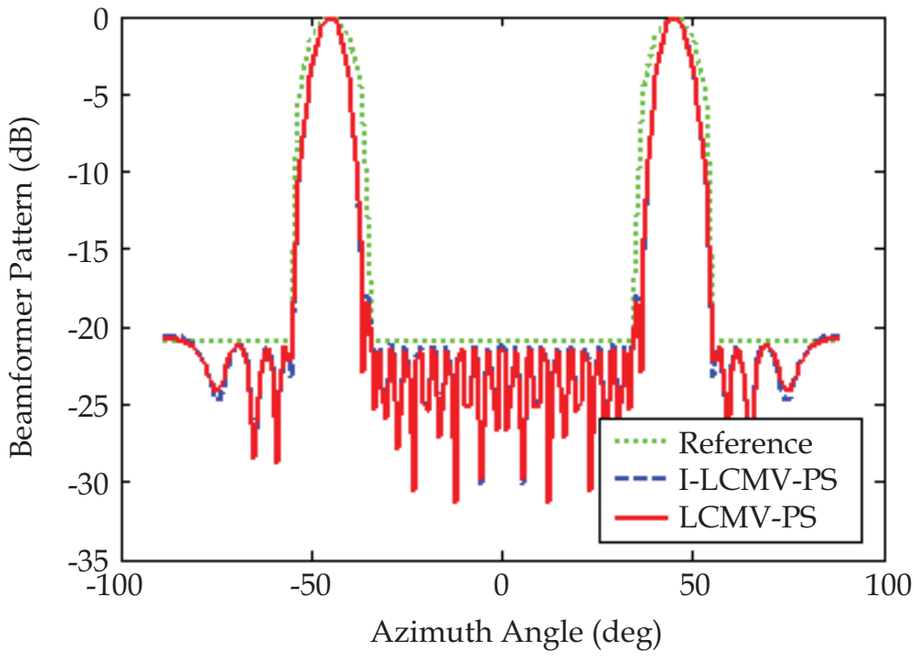

Fig. 12. Multi-beam synthesis pattern of non-uniform linear array

The single beam synthesis patterns of the uniform and non-uniform planar array with I-LCMV-PS are given in Fig. 13.~ Fig. 16. Therein, they have the same element number 36, the uniform planar array is phalanx, and element space is half wavelength, but the element position of the non-uniform planar array is given as Fig. 10. The mainlobe of the two array point to (0^o,0^o), and the beam-widths in the azimuth and elevation direction are all 30^o. In the simulation, the iterative number of I-LCMV-PS is 8, and the Fig. 14. and Fig. 16. is the side view figure of Fig. 13. and Fig. 15. respectively.

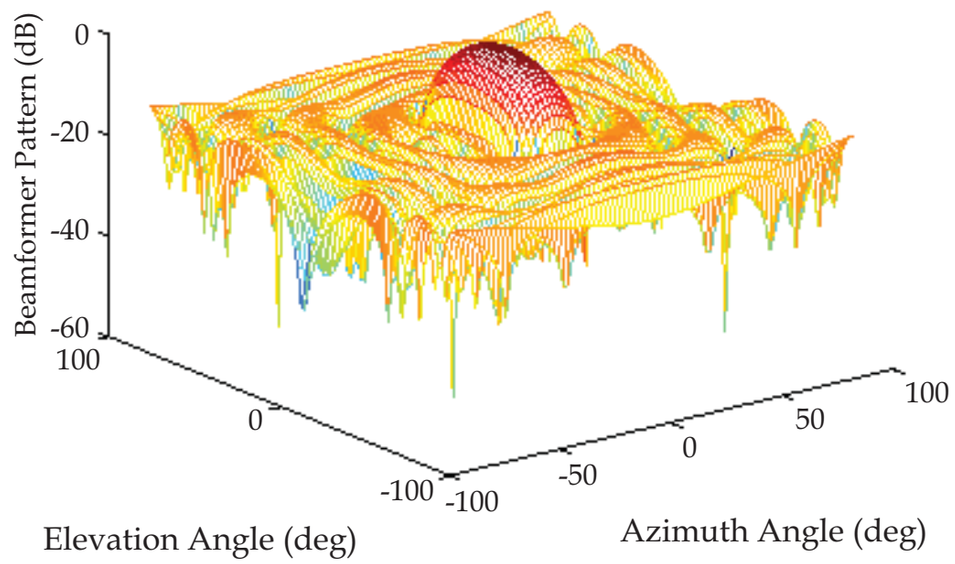

Fig. 13. Single beam synthesis pattern of uniform planar array (1)

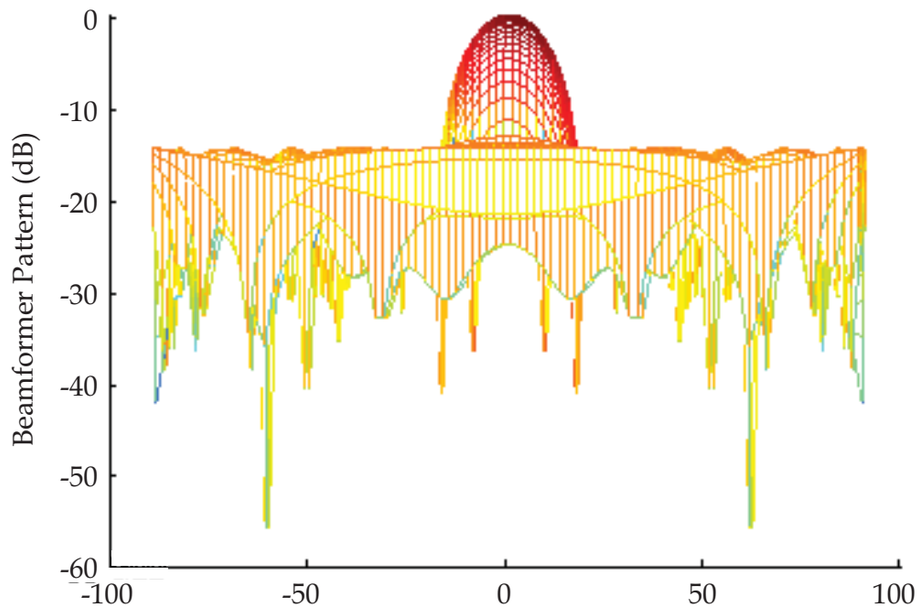

Fig. 14. Single beam synthesis pattern of uniform planar array (2)

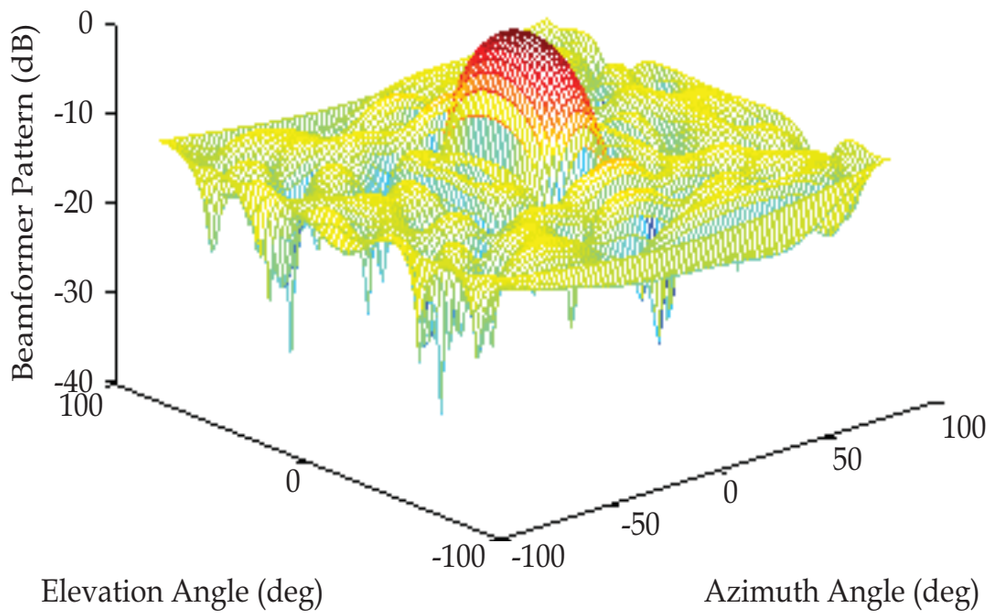

Fig. 15. Single beam synthesis pattern of non-uniform planar array (1)

From the above simulations, we can see that the two methods have the preferable synthesis pattern, but I-LCMV-PS has small iterative number, namely it has the higher pattern synthesis efficiency.

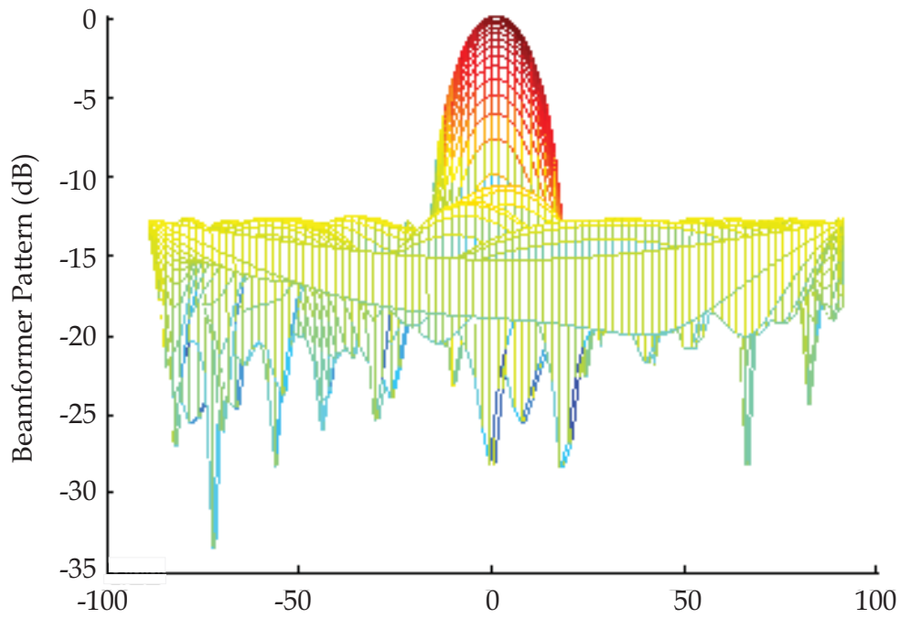

Fig. 16. Single beam synthesis pattern of non-uniform planar array (2)

2.3.2 Convergence analyzing

In order to compare the convergence characteristic, limit by the chapter length, here the example of the uniform linear array is given, about the examples of the non-uniform linear array and the planar array are similar to the uniform linear array.

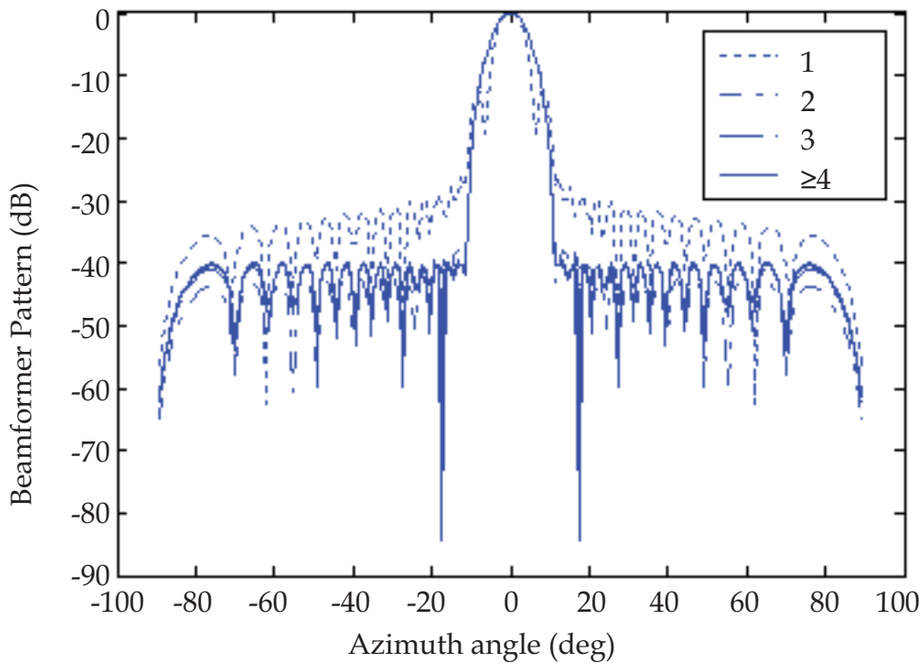

Fig. 17. Synthesis pattern versus iterative number of I-LCMV-PS

Fig. 10. and Fig. 11. give the convergence of the synthesis pattern for the uniform linear array with I-LCMV-PS and LCMV-PS respectively. Therein, the parameters are as same as 2.3.1. From Fig. 10., we can see that when the iterative number is larger than 4, I-LCMV-PS can achieve the preferable pattern synthesis effect, but for LCMV-PS, the iterative number must be larger than 20, because I-LCMV-PS has the higher efficiency of the jammer power iteration.

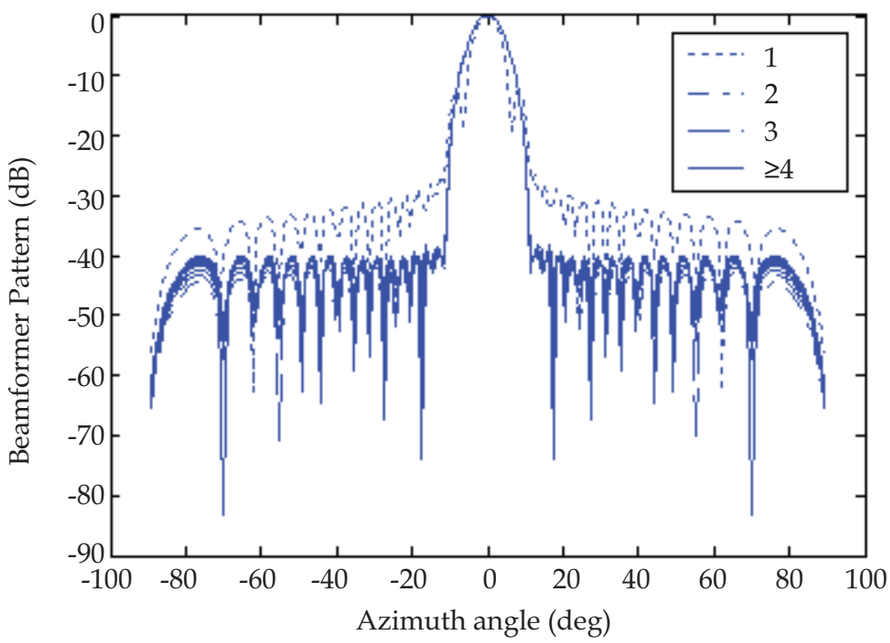

Fig. 18. Synthesis pattern versus iterative number of LCMV-PS

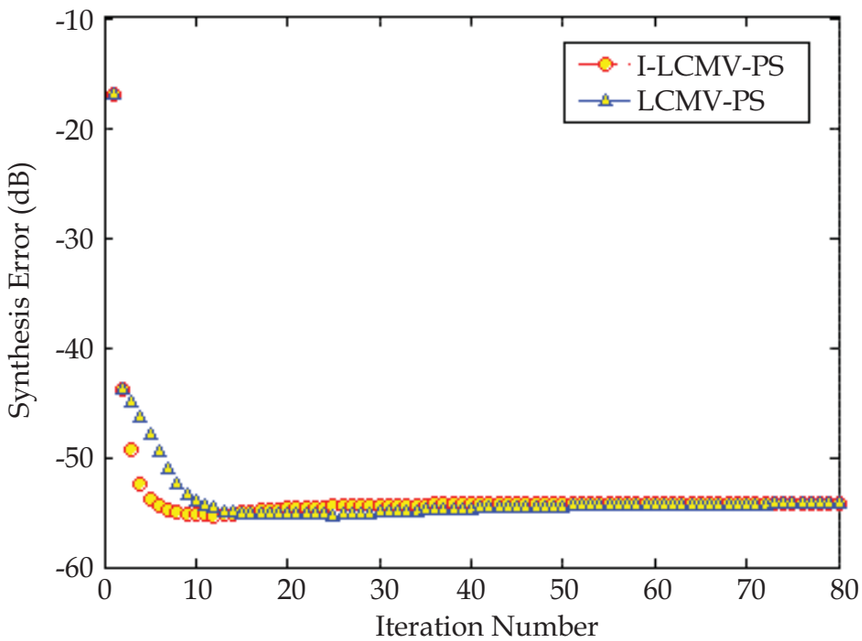

Fig. 19. Pattern synthesis error versus iteration number

In order to attest the convergence and synthesis precision of the improved algorithm, Fig. 19. gives the pattern synthesis error versus the iterative number. Therein, the pattern synthesis error is calculated as follows:

$$E_{sum} = \sum_{i=1}^{N} \left| P_k(\theta_i) - Pr(\theta_i) \right| \tag{2.7}$$

where $Pr(\theta)$ is the reference pattern, $P_k(\theta)$ is the synthesis pattern after k-th iteration. From the error curve, we can see that the improved algorithm has the fast convergence performance, and fall rapidly from beginning, at last, the two curves converge at the same value, namely the convergence is consistent with the Fig. 17. and Fig. 18. Therefore, the proposed algorithm has the good convergence and synthesis precision.

In order to analyze the effect of the iterative coefficient upon the pattern synthesis, Fig. 20. and Fig. 21. give the synthesis pattern versus iterative coefficient for the uniform linear array with I-LCMV-PS and LCMV-PS respectively. Therein, the parameters are as same as 2.3.1. From Fig. 20., we can see that when K_p=100, the selection of iterative coefficient K has very little effect upon the pattern synthesis, in simulation, when 0.005<K<2000, the preferable performance can be achieved, the 2000 is the upper bound in simulation, if the parameter is larger than this value, the good performance can also be achieved. Actually, if K_p larger, the selecting bound for K wll be wider, it is consistent with the theory analysis. But from Fig. 21., we can also see that the efficiency of the pattern synthesis is determined by K, in the simulation, we find that when 0.1<K<1.6, the preferable effect is achieved. By the comparison, we can see that the improved LCMV-PS method has the lower dependence upon the iterative coefficient, and enables the selecting bound for the iterative coefficient K enlarged greatly, and enhanced its application area and applicability.

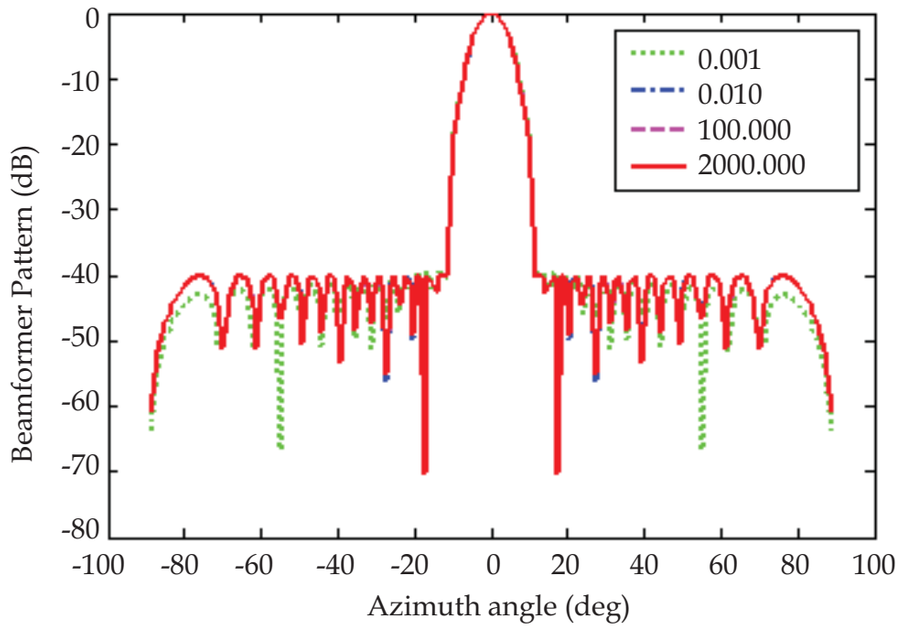

Fig. 20. Synthesis pattern versus iterative coefficient of I-LCMV-PS

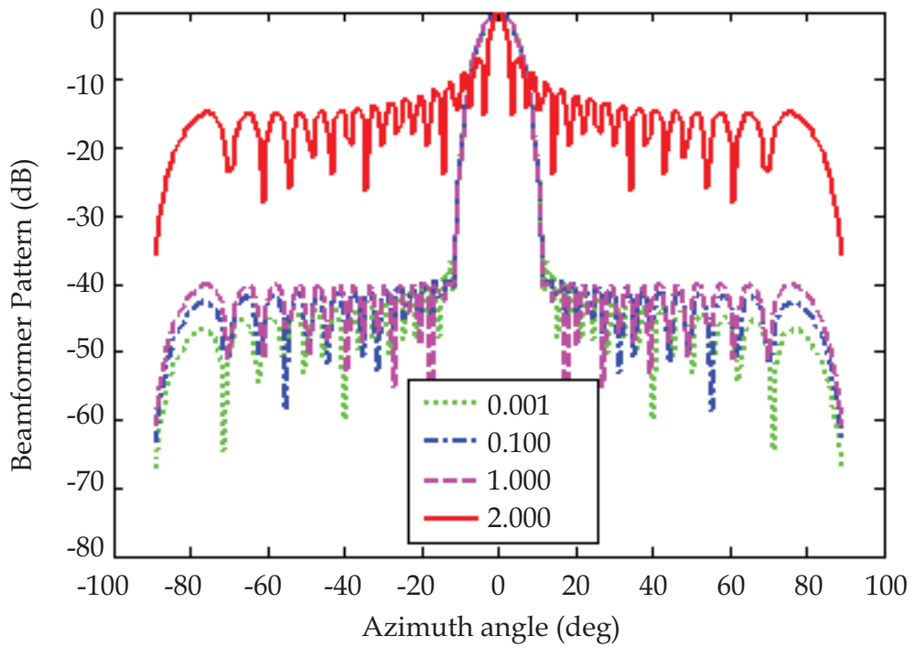

Fig. 21. Synthesis pattern versus iterative coefficient of LCMV-PS

2.4 Conclusion

From the above analysis and simulation, we can conclude as follows: (I) The proposed jammer power iterative formula is correct and effective. (II) By the improvement for the iterative formula of the original method, the iterative efficiency is increased greatly, and the iterative number is reduced greatly, therefore the operation load of the pattern synthesis is reduced efficiently. (III)The improved jammer power iterative formula enlarges the selecting bound for the iterative coefficient, and reduces the effect of the parameter upon the pattern synthesis, and enhances the application area and applicability of the proposed pattern synthesis method.

3. Unitary Root-MUSIC

The problem of estimating the direction-of-arrival (DOA) of narrowband sources from sensor array data has received considerable attention. The eigen-based methods for DOA estimation represent a class techniques that offer a much better resolution performance than that of conventional beamformers. In eigen-based methods, signal and noise subspaces are identified first via a $M \times M$ generalized EVD (GEVD) of the array data/noise correlation matrix pencil, where M equals the number of array elements. A search is then conducted over a null spectrum associated with the noise subspace, to locate the minima, from which the source DOA's can be determined. In the case where a uniform linear array (ULA) is employed, the null-spectrum searching can be converted into a polynomial rooting problem. Two well known examples are the Root-MUSIC[47] and Root-Minimum-Norm[48] method. They belong to the so-called weighted root-form eigen-based methods. Compared to their spectrum-searching or spectral-form counterparts, root-form methods exhibit a higher resolution capability in dealing with closely spaced sources.Rao and Hari[49] argue that a

zero of the null spectrum, having a large radial error, will cause the corresponding spectral minima to be less defined,but does not affect the DOA estimates. As for the mean-squared errors of the DOA estimates,Li and Vaccaro[50] show that both spectral and root-form methods yield the same expression. It should be borne in mind, however, that the result holds only when each of the sources has a minimum corresponding to it in the null spectrum.

A major issue regarding eigen-based methods is the heavy computational load associated with the GEVD. This is more significant when *M* is large. To remedy this the concept of beamspace transformation was proposed[51] as a means of reducing the dimension of the array data. Ta.S.L proposed a novel iterative implementation of beamspace root-form methods without the need for large-order polynomial rooting[52]. Marius.P, Alex.B.G and Martin.H proposed the unitary root MUSIC algorithm reduces the computational complexity because it exploits the eigendecomposition of a real-valued covariance matrix[53].

In this chapter [54], combining the algorithms of Root-MUSIC and Unitary-root MUSIC, the Root-MUSIC algorithm with real-valued eigendecomposition is given.

3.1 Array signal model

Assume a uniform linear array (ULA) is composed of M sensors, and let it receive q ($q < M$) narrowband signals impinging with unknown directions of arrival ((DOA) $\theta_1, \theta_2, \ldots, \theta_q$. Assume that there are N snapshots $\mathbf{x}(1), \mathbf{x}(2), \ldots, \mathbf{x}(N)$ available. The tth measured snapshot of the array is generally modeled as:

$$\mathbf{x}(t) = \mathbf{A}\mathbf{s}(t) + \mathbf{n}(t) \tag{3.1}$$

where $\mathbf{A} = \left[\mathbf{a}(\theta_1), \ \cdots, \ \mathbf{a}(\theta_q)\right]$ is the $M \times q$ composite steering matrix, the columns of which represent a basis for the signal subspace, $\mathbf{a}(\theta)$ represents the array's $M \times 1$ complex manifold:

$$\mathbf{a}(\theta) = \left[1, \ e^{j(2\pi/\lambda)d\sin\theta}, \ \cdots, \ e^{j(2\pi/\lambda)d(M-1)\sin\theta}\right]^T \tag{3.2}$$

In addition

$\mathbf{s}(t)$ denotes the $q \times 1$ vector of source waveforms;
$\mathbf{n}(t)$ denotes the $M \times 1$ vector of white sensor noise;
λ is the wavelength;
d is the interelement space;
$(\cdot)^T$ denotes transpose.

It is generally assumed that signals are uncorrelated with the noise $\mathbf{n}(t)$. The sensor noise is assumed to be a zero-mean spatially and temporally uncorrelated Gaussian process with the uunknown diagonal covariance matrix given by

$$\mathbf{R}_n = E\left\{\mathbf{n}(t)\mathbf{n}(t)^H\right\} = diag\left\{\sigma^2, \ \sigma^2, \ \cdots, \ \sigma^2,\right\} = \sigma^2\mathbf{I} \tag{3.3}$$

where $E\{\cdot\}$ is the expectation operator,and $(\cdot)^H$ stands for the Hermitian transpose, $\mathbf{I}$ is the identity matrix, σ^2 is the noise variance.

Data model (1) allows us to write the covariance matrix of the array measurements as:

$$\mathbf{R} = E\left\{\mathbf{x}(t)\mathbf{x}(t)^H\right\} = \mathbf{ASA}^H + \sigma^2\mathbf{I} \tag{3.4}$$

where $\mathbf{S} = E\left\{\mathbf{s}(t)\mathbf{s}(t)^H\right\}$ is the $q \times q$ source waveform covariance matrix.

3.2 Root-MUSIC

Root-MUSIC is the polynomial rooting form of MUSIC, namely, the spectrum peak searching is replaced by polynomial rooting in MUSIC implementation.

In Root-MUSIC, the polynomial should be defined as follows

$$f_i(z) = \mathbf{u}_i^H\mathbf{a}(z) \qquad i = q+1,\cdots,M \tag{3.5}$$

where, $\mathbf{u}_i$ is the eigenvector corresponding to the *M*-*q* minimum eigen-value of the data covariance matrix, and

$$\mathbf{a}(z) = \begin{bmatrix} 1 & z & \cdots, & z^{M-1} \end{bmatrix}^T \tag{3.6}$$

From the above definition, we can include that the polynomial roots lie on the unit circle properly when $z = \exp(j\omega)$, and $\mathbf{a}(e^{j\omega})$ is the steering vector of space frequency ω. From the eigen-space algorithms, $\mathbf{a}(e^{j\omega_m}) = \mathbf{a}_m$ is the signal steering vector, and it is orthogonal to the space of the noise. Therefore, the polynomial definition can be modified as the following form

$$f(z) = \mathbf{a}^H(z)\mathbf{U}_N\mathbf{U}_N^H\mathbf{a}(z) \tag{3.7}$$

where $\mathbf{U}_N$ is the noise space, namely, let the eigendecomposition of the matrix $\mathbf{R}$ be defined in a standard way

$$\mathbf{R} = \mathbf{U}\ \mathbf{\Lambda}\ \mathbf{U}^H = \mathbf{U}_S\mathbf{\Lambda}_S\mathbf{U}_S^H + \sigma^2\mathbf{U}_N\mathbf{U}_N^H \tag{3.8}$$

where

$\mathbf{U}_S = \begin{bmatrix} \mathbf{u}_1 & \cdots & \mathbf{u}_q \end{bmatrix}$, $\mathbf{U}_N = \begin{bmatrix} \mathbf{u}_{q+1}, & \cdots & \mathbf{u}_M \end{bmatrix}$, $\mathbf{\Lambda}_S = \mathrm{diag}\left\{\lambda_1, \quad \cdots, \quad \lambda_q\right\}$

and the subscripts S and N stand for signal- and noise-subspace, respectively.

Therefore, the source DOA information can be obtained when the above roots are solved. At the same time, we found the item of z^* in the polynomial, and the solving process will become complex and difficult. In order to simplify problem, the above polynomial can be modified as

$$f(z) = z^{M-1}\mathbf{a}^T\left(z^{-1}\right)\mathbf{U}_N\mathbf{U}_N^H\mathbf{a}(z) \tag{3.9}$$

Here, the polynomial order is 2(*M*-1), and has (*M*-1) pairs roots, the every pair roots have the mutual conjugate relationship. In the (M-1) pairs roots, there are q roots $z_1,\cdots,z_q$ are distributed on the unit circle, and

$$z_i = \exp(j\omega_i), \qquad 1 \le i \le q \tag{3.10}$$

For the ULA, the corresponding DOA of signal can be calculated as

$$\theta_i = \arcsin\left(\frac{\lambda}{2\pi d}\arg(z_i)\right), \qquad i = 1,\cdots,q \tag{3.11}$$

where λ is the signal wavelength, d is the array space.

A simple alternative method is proposed in Ref.[55]. From above analysis, we can see that the signal space is orthogonal to the noise space, therefore

$$z_i = \exp\left(j2\pi\frac{d}{\lambda}\sin\theta_i\right), \qquad i = 1,\cdots,q \tag{3.12}$$

should be q roots of all M-q polynomials in Eq. (3.9), namely

$$f_i(z_j) = 0, \qquad j = 1,\cdots,q, \qquad i = q+1,\cdots,M \tag{3.13}$$

Eq.(3.9) represents M-q polynomials of M-1 order. From Eq.(3-13), they should have a q-order maximum common factor, which can be denoted as $f(z)$. The DOAs of all the sources can be obtained by rooting $f(z)$. From the eigenvectors of the noise space, $f(z)$ can be obtained as follows

There exists a vector $\mathbf{b} = \begin{bmatrix} b_1 & \cdots & b_{M-q} \end{bmatrix}^T$ which satisfies

$$\mathbf{U}_N^H\mathbf{b} = \begin{bmatrix} \mathbf{U}_{N1}^H \\ \mathbf{U}_{N2}^H \end{bmatrix}\mathbf{b} = \begin{bmatrix} c_1 & \cdots & c_q & 1 & 0 & \cdots & 0 \end{bmatrix}_{1\times M}^T \tag{3.14}$$

where $\mathbf{U}_{N1}$ is q×(M-q) sub-matrix and $\mathbf{U}_{N2}$ is (M-q)×(M-q) sub-matrix of $\mathbf{U}_N$. This can be understood by noticing that the product of $\mathbf{U}_N$ and $\mathbf{b}$ represents a linear combination of noise vectors represented in the M-q dimensional noise space. The product $\mathbf{U}_{N2}$ and $\mathbf{b}$ defines a system of M-q equations with M-q unknowns. $\mathbf{b}$ can be fixed to be the solution that results in a product $\begin{bmatrix} 1 & 0 & \cdots \end{bmatrix}^T$. The product of $\mathbf{U}_{N1}$ and $\mathbf{b}$ is then a set of coefficients that are determined.

Adopting this approach $\mathbf{b}$ is obtained by

$$\mathbf{b} = \mathbf{U}_{N2}^{-1}\begin{bmatrix} 1 & 0 & \cdots & 0 \end{bmatrix}_{1\times(M-q)}^T \tag{3.15}$$

And $\mathbf{c} = \begin{bmatrix} c_1 & \cdots & c_q \end{bmatrix}$ is determined easily as

$$\mathbf{c} = \mathbf{U}_{N1}\mathbf{b} = \mathbf{U}_{N1}\mathbf{U}_{N2}^{-1}\begin{bmatrix} 1 & 0 & \cdots & 0 \end{bmatrix}_{1\times(M-q)}^T \tag{3.16}$$

Now that $\mathbf{c}$ has been determined, the polynomial $f(z)$ is formed by

$$f(z) = \sum_{i=1}^{q+1} c_i z^{i-1}, \qquad c_{M+1} = 1 \tag{3.17}$$

Eq.(3.17) has q roots which are correspond to the DOAs of q sources. After obtaining q roots of Eq.(3.13), $\{z_i\}_{i=1}^{q}$, the DOAs of the sources are obtained by Eq.(3.12).

From the well known conventional Root-MUSIC polynomial of Eq.(3.7), we can conclude that it is a function of z, namely

$$f_{\text{Root-MUSIC}}(z) = z^{M-1}\mathbf{a}^T(1/z)\mathbf{U}_N\mathbf{U}_N^H\mathbf{a}(z) = z^{M-1}\mathbf{a}^T(1/z)\left\{1-\mathbf{U}_S\mathbf{U}_S^H\right\}\mathbf{a}(z) \tag{3.18}$$

Here the orthogonal property of the signal and noise subspace is used.

3.3 Root-MUSIC with real-valued eigendecomposition

The matrix $\mathbf{R}$ is the centro-Hermitian if

$$\mathbf{R} = \mathbf{J}\mathbf{R}^*\mathbf{J} \tag{3.19}$$

where $\mathbf{J}$ is the exchange matrix with ones on its antidiagonal and zeros elsewhere, and $(\cdot)^*$ stands for complex conjugate. The matrix (3.3)is known to be centro-Hermitian if and only if $\mathbf{S}$ is a diagonal matrix, i.e., when the signal source are uncorrelated. However, to 'double' the number of snapshots and decorrelate possibly correlated source pairs in the case of an arbitrary matrix $\mathbf{S}$, the centro-Hermitian property is sometimes forced by means of the so-called forward-backward (FB) averaging:

$$\mathbf{R}_{FB} = \frac{1}{2}\left(\mathbf{R} + \mathbf{J}\mathbf{R}^*\mathbf{J}\right) = \mathbf{A}\tilde{\mathbf{S}}\mathbf{A}^H + \sigma^2\mathbf{I} \tag{3.20}$$

where

$$\tilde{\mathbf{S}} = \frac{1}{2}\left(\mathbf{S} + \mathbf{D}\mathbf{S}^*\mathbf{D}\right) \tag{3.21}$$

$$\mathbf{D} = diag\left\{e^{-j(2\pi/\lambda)d(M-1)\sin\theta_1}, \quad \cdots, \quad e^{-j(2\pi/\lambda)d(M-1)\sin\theta_q},\right\} \tag{3.22}$$

Let us define the matrix as:

$$\mathbf{C} = \mathbf{Q}^{\mathbf{H}}\mathbf{R}_{\mathbf{FB}}\mathbf{Q} \tag{3.23}$$

therefore, the $\mathbf{C}$ is a real-valued covariance matrix, where $\mathbf{Q}$ is any unitary,column conjugate symmetric $M \times M$ matrix. Any matrix $\mathbf{Q}$ is column conjugate symmetric if

$$\mathbf{J}\mathbf{Q}^* = \mathbf{Q} \tag{3.24}$$

For example, the following sparse matrices

$$\mathbf{Q}_{2n} = \frac{1}{\sqrt{2}}\begin{bmatrix}\mathbf{I} & j\mathbf{I} \\ \mathbf{J} & -j\mathbf{J}\end{bmatrix} \tag{3.25}$$

$$\mathbf{Q}_{2n+1} = \frac{1}{\sqrt{2}}\begin{bmatrix}\mathbf{I} & \mathbf{0} & j\mathbf{I} \\ \mathbf{0}^T & \sqrt{2} & \mathbf{0}^T \\ \mathbf{J} & \mathbf{0} & -j\mathbf{J}\end{bmatrix} \tag{3.26}$$

can be chosen for arrays with an even and odd number of sensors,respectively, where the vector $\mathbf{0} = (0, \quad 0, \quad \cdots, \quad 0)^T$

From (3.23), and insert (3.20) to it, it follows that

$$\mathbf{C} = \mathbf{Q^H R_{FB} Q} = \mathbf{Q^H}\left[\frac{1}{2}\left(\mathbf{R} + \mathbf{J R^* J}\right)\right]\mathbf{Q} = \frac{1}{2}\left[\mathbf{Q^H R Q} + \mathbf{Q^H}\left(\mathbf{J R^* J}\right)\mathbf{Q}\right] \tag{3.27}$$

using $\mathbf{JQ^*} = \mathbf{Q}$, $\mathbf{Q^*} = \mathbf{JQ}$ and $\mathbf{J}^H = \mathbf{J}$, we obtain that

$$\begin{aligned} \mathbf{C} &= \frac{1}{2}\left[\mathbf{Q^H R Q} + \mathbf{Q^H J R^* J Q}\right] = \frac{1}{2}\left[\mathbf{Q^H R Q} + (\mathbf{JQ})^{\mathbf{H}}\mathbf{R}^*(\mathbf{JQ})\right] \\ &= \frac{1}{2}\left[\mathbf{Q^H R Q} + \left(\mathbf{Q^*}\right)^{\mathbf{H}}\mathbf{R}^*\left(\mathbf{Q^*}\right)\right] = \frac{1}{2}\left[\mathbf{Q^H R Q} + \left(\mathbf{Q^H R Q}\right)^*\right] \\ &= \mathrm{Re}\left[\mathbf{Q^H R Q}\right] \end{aligned} \tag{3.28}$$

therefore, we prove that $\mathbf{C}$ is a real-valued covariance matrix.

Let the eigendecompositions of the matrices $\mathbf{R}$, $\mathbf{R_{FB}}$ and $\mathbf{C}$ be defined in a standard way

$$\mathbf{R} = \mathbf{V}\,\mathbf{\Pi}\,\mathbf{V}^H = \mathbf{V}_S\mathbf{\Pi}_S\mathbf{V}_S^H + \sigma^2\mathbf{V}_N\mathbf{V}_N^H \tag{3.29}$$

$$\mathbf{R}_{FB} = \mathbf{U}\,\mathbf{\Lambda}\,\mathbf{U}^H = \mathbf{U}_S\mathbf{\Lambda}_S\mathbf{U}_S^H + \sigma^2\mathbf{U}_N\mathbf{U}_N^H \tag{3.30}$$

$$C = \mathbf{E}\,\mathbf{\Gamma}\,\mathbf{E}^H = \mathbf{E}_S\mathbf{\Gamma}_S\mathbf{E}_S^H + \sigma^2\mathbf{E}_N\mathbf{E}_N^H \tag{3.31}$$

where

$\mathbf{V}_S = \left[\mathbf{v}_1, \quad \cdots, \quad \mathbf{v}_q\right]$, $\mathbf{V}_N = \left[\mathbf{v}_{q+1}, \quad \cdots, \quad \mathbf{v}_M\right]$, $\mathbf{\Pi}_S = diag\left\{\pi_1, \quad \cdots, \quad \pi_q\right\}$

$\mathbf{U}_S = \left[\mathbf{u}_1, \quad \cdots, \quad \mathbf{u}_q\right]$, $\mathbf{U}_N = \left[\mathbf{u}_{q+1}, \quad \cdots, \quad \mathbf{u}_M\right]$, $\mathbf{\Lambda}_S = diag\left\{\lambda_1, \quad \cdots, \quad \lambda_q\right\}$

$\mathbf{E}_S = \left[\mathbf{e}_1, \quad \cdots, \quad \mathbf{e}_q\right]$, $\mathbf{E}_N = \left[\mathbf{e}_{q+1}, \quad \cdots, \quad \mathbf{e}_M\right]$, $\mathbf{\Gamma}_S = diag\left\{\gamma_1, \quad \cdots, \quad \gamma_q\right\}$

and the subscripts S and N stand for signal- and noise-subspace,respectively.

Assume the Characteristic equation for the matrix $\mathbf{R_{FB}}$ as

$$\mathbf{R_{FB}} \cdot \mathbf{u} = \lambda \cdot \mathbf{u} \tag{3.32}$$

we can obtain that

$$\mathbf{Q}^H \cdot \mathbf{R_{FB}}\mathbf{u} = \mathbf{Q}^H \cdot \lambda\mathbf{u} = \lambda \cdot \mathbf{Q}^H\mathbf{u} \tag{3.33}$$

with the use of equation: $\mathbf{QQ^H} = \mathbf{I}$ and the definition of $\mathbf{C}$,we obtain that

$$\mathbf{Q}^H \cdot \mathbf{R_{FB}}\mathbf{u} = \mathbf{Q}^H \cdot \mathbf{R_{FB}} \cdot \mathbf{QQ^H} \cdot \mathbf{u} = \mathbf{C} \cdot \mathbf{Q^H}\mathbf{u} = \lambda \cdot \mathbf{Q}^H\mathbf{u} \tag{3.34}$$

Equation $\mathbf{C} \cdot \mathbf{Q^H}\mathbf{u} = \lambda \cdot \mathbf{Q}^H\mathbf{u}$ can be identified as the characteristic one for the real-valued covariance matrix $\mathbf{C}$.

Hence, using (3.30), (3.31), (3.32) and (3.34), the eigenvectors and eigenvalues of the matrices $\mathbf{R_{FB}}$ and $\mathbf{C}$ are related as

$$\mathbf{E} = \mathbf{Q}^H \mathbf{U} \tag{3.35}$$

$$\mathbf{\Gamma} = \mathbf{\Lambda} \tag{3.36}$$

It is well known that the conventional Root-MUSIC polynomial is given by

$$f_{MUSIC}(z) = \mathbf{a}^T(1/z)\mathbf{V}_N\mathbf{V}_N^H\mathbf{a}(z) \tag{3.37}$$

$$= \mathbf{a}^T(1/z)\left\{1 - \mathbf{V}_S\mathbf{V}_S^H\right\}\mathbf{a}(z) \tag{3.38}$$

where

$$\mathbf{a}(z) = \left[1, \quad z, \quad \cdots, \quad z^{M-1}\right]^T \tag{3.39}$$

$z = e^{j\omega}$, and $\omega = (2\pi/\lambda)d\sin\theta$. Similarly to(3.37) and (3.38), the FB root-MUSIC polynomial can be used:

$$f_{FB-MUSIC}(z) = z^{M-1}\mathbf{a}^T(1/z)\mathbf{U}_N\mathbf{U}_N^H\mathbf{a}(z) \tag{3.40}$$

$$= z^{M-1}\mathbf{a}^T(1/z)\left\{1 - \mathbf{U}_S\mathbf{U}_S^H\right\}\mathbf{a}(z) \tag{3.41}$$

A simple manipulation with the use of (3.35) and $\mathbf{QQ^H} = \mathbf{I}$, we can obtain that:

$$f_{FB-MUSIC}(z) = z^{M-1}\mathbf{a}^T(1/z)\cdot\mathbf{QQ^H}\cdot\mathbf{U}_N\mathbf{U}_N^H\cdot\mathbf{QQ^H}\cdot\mathbf{a}(z) \tag{3.42}$$

$$= z^{M-1}\mathbf{a}^T(1/z)\cdot\mathbf{Q}\cdot\left(\mathbf{Q^H}\mathbf{U}_N\right)\cdot\left(\mathbf{Q^H}\mathbf{U}_N\right)^{\mathbf{H}}\mathbf{Q^H}\cdot\mathbf{a}(z) \tag{3.43}$$

$$= z^{M-1}\mathbf{a}^T(1/z)\cdot\mathbf{Q}\cdot\mathbf{E}_N\cdot\mathbf{E}_N^H\cdot\mathbf{Q^H}\cdot\mathbf{a}(z) \tag{3.44}$$

$$= z^{M-1}\tilde{\mathbf{a}}^T(1/z)\cdot\mathbf{E}_N\cdot\mathbf{E}_N^H\cdot\tilde{\mathbf{a}}(z) \tag{3.45}$$

$$= f_{C-MUSIC}(z) \tag{3.46}$$

where the manifold

$$\tilde{\mathbf{a}}(z) = \mathbf{Q^H}\cdot\mathbf{a}(z) \tag{3.47}$$

should be exploited for the polynomial rooting in (3.45). The relationship between the former and the new manifolds follows from the expression for the real-valued covariance matrix (3.23). From (3.23)and (3.20), we have

$$\mathbf{C} = \mathbf{Q}^{\mathbf{H}}\mathbf{R}_{\mathbf{FB}}\mathbf{Q} = \mathbf{Q}^{\mathbf{H}}\left(\mathbf{A}\tilde{\mathbf{S}}\mathbf{A}^{H} + \sigma^2\mathbf{I}\right)\mathbf{Q} = \mathbf{Q}^{\mathbf{H}}\mathbf{A}\tilde{\mathbf{S}}\mathbf{A}^{H}\mathbf{Q} + \sigma^2\mathbf{Q}^{\mathbf{H}}\mathbf{Q} \tag{3.48}$$

$$= \tilde{\mathbf{A}}\tilde{\mathbf{S}}\tilde{\mathbf{A}}^{H} + \sigma^2\mathbf{Q}^{\mathbf{H}}\mathbf{Q} \tag{3.49}$$

where

$$\tilde{\mathbf{A}} = \mathbf{A}^{H}\mathbf{Q} \tag{3.50}$$

Let us term the polynomial (3.46) as the polynomial of Root-MUSIC with real-valued eigendecomposition (RVED-Root-MUSIC), since it exploits the eigendecomposition of the real-valued matrix (3.24) instead of that of the complex matrices (3.18) or (3.20). But from (3.42) to (3.44), it is clear that the FB and RVED-Root-MUSIC polynomials are identical. Hence, the performance of RVED-ROOT-MUSIC does not depend on a particular choice of the unitary column conjugate symmetric matrix $\mathbf{Q}$.

3.4 Polynomial coefficient finding

From (3.44) and (3.45), we obtain the polynomial of RVED-Root-MUSIC, which is a function of z. The next thing is finding the coefficient of the polynomial[56]..

Using (3.44), we have:

$$\begin{aligned} f_{C-MUSIC}(z) &= z^{M-1}\mathbf{a}^{T}(1/z)\cdot\mathbf{Q}\cdot\mathbf{E}_N\cdot\mathbf{E}_N^{H}\cdot\mathbf{Q}^{\mathbf{H}}\cdot\mathbf{a}(z) \\ &= z^{M-1}\mathbf{a}^{T}(1/z)\cdot\mathbf{G}\cdot\mathbf{a}(z) \end{aligned} \tag{3.51}$$

where

$$\mathbf{G} = \mathbf{Q}\cdot\mathbf{E}_N\cdot\mathbf{E}_N^{H}\cdot\mathbf{Q}^{\mathbf{H}} = \left(g_{i,j}\right)_{M\times M} \tag{3.52}$$

Inserting (3.39) into (3.52), and with simple manipulation, we obtain that

$$\begin{aligned} f_{C-MUSIC}(z) &= z^{M-1}\left[1,\ z^{-1},\ \cdots,\ z^{-(M-1)}\right]\cdot\mathbf{G}\cdot\left[1,\ z^{1},\ \cdots,\ z^{(M-1)}\right]^{T} \\ &= \left[z^{M-1},\ z^{M-2},\ \cdots,\ 1\right]\cdot\begin{bmatrix} g_{1,1} & \cdots & g_{1,M} \\ \vdots & \cdots & \vdots \\ g_{M,1} & \cdots & g_{M,M} \end{bmatrix}\cdot\left[1,\ z^{1},\ \cdots,\ z^{(M-1)}\right]^{T} \\ &= \left[\sum_{i=1}^{M} g_{i,1}z^{M-i},\ \sum_{i=1}^{M} g_{i,2}z^{M-i},\ \cdots,\ \sum_{i=1}^{M} g_{i,M}z^{M-i}\right]\cdot\begin{bmatrix} 1 \\ z^{1} \\ \vdots \\ z^{(M-1)} \end{bmatrix} \\ &= 1\cdot\left(\sum_{i=1}^{M} g_{,i1}z^{M-i}\right) + z^{1}\cdot\left(\sum_{i=1}^{M} g_{i,2}z^{M-i}\right) + \cdots + z^{(M-1)}\cdot\left(\sum_{i=1}^{M} g_{i,M}z^{M-i}\right) \end{aligned}$$

the polynomial of RVED-Root-MUSIC is given by

$$\begin{aligned}
f_{C-MUSIC}(z) = & \left(g_{1,M}\right)\cdot z^{2M-2-0} \\
& +\left(g_{2,M}+g_{2,M-1}\right)\cdot z^{2M-2-1} \\
& +\left(g_{3,M}+g_{2,M-1}+g_{1,M-2}\right)\cdot z^{2M-2-2} \\
& +\cdots \\
& +\left(g_{M,M}+g_{M-1,M-1}+\cdots+g_{2,2}+g_{1,1}\right)\cdot z^{2M-2-(M-1)} \\
& +\left(g_{M,M-1}+g_{M-1,M-2}+\cdots+g_{3,2}+g_{2,1}\right)\cdot z^{2M-2-M} \\
& +\left(g_{M,M-1}+g_{M-1,M-2}+\cdots+g_{3,2}+g_{2,1}\right)\cdot z^{2M-2-(M+1)} \\
& +\cdots \\
& +\left(g_{M,2}+g_{M-1,1}\right)\cdot z^{2M-2-(M+M-3)} \\
& +\left(g_{M,1}\right)\cdot z^{2M-2-(M+M-2)}
\end{aligned}$$

So the number of coefficient of the polynomial is $2M-1$, and the computation of the coefficient is given as follows

$$a_k = \begin{cases} \sum_{i=1}^{k} g_{i,M-k+i} & k=1,\quad 2,\quad \cdots,\quad L \\ \sum_{i=1}^{(2M-1)-k+1} g_{k-M+i,i} & k=L+1,\quad L+2,\quad \cdots,\quad 2L-1 \end{cases} \tag{3.53}$$

where a_k denotes the kth coefficient of the polynomial.

Based upon our analysis, using (3.4), (3.20), (3.23), (3.35), (3.26), (3.31), (3.35), (3.44), (3.51), (3.52) and (3.53), the fast algorithm for RVED-Root-MUSIC can be formulated as the following seven-step procedure:

Step 1. Compute $\mathbf{R}$ and $\mathbf{R_{FB}}$ with the use of (3.4) and (3.6).and the estimate is given by $\hat{\mathbf{R}} = \frac{1}{N}\sum_{k=1}^{N}\mathbf{x}(k)\mathbf{x}^{H}(k)$ then $\hat{\mathbf{R}}_{FB} = \frac{1}{2}\left(\hat{\mathbf{R}} + \mathbf{J}\hat{\mathbf{R}}^{*}\mathbf{J}\right)$.

Step 2. Compute $\mathbf{C}$, and the $\mathbf{Q}$ is dependent on the number of array sensors. The estimate of the real-valued covariance matrix is given by $\hat{\mathbf{C}} = \mathbf{Q}^{\mathbf{H}}\hat{\mathbf{R}}_{\mathbf{FB}}\mathbf{Q}$

Step 3. Obtain $\mathbf{E}_N$ from the eigendecomposition of $\mathbf{C}$.and the estimate of $\mathbf{E}_N$, $\hat{\mathbf{E}}$ is given by the eigendecomposition of $\hat{\mathbf{C}}$

Step 4. Compute $\mathbf{G}$ with the use of (3.52). And the estimate of $\mathbf{G}$, $\hat{\mathbf{G}}$ is given by $\mathbf{G} = \mathbf{Q}\cdot\hat{\mathbf{E}}_N\cdot\hat{\mathbf{E}}_N^{H}\cdot\mathbf{Q}^{\mathbf{H}}$

Step 5. Compute the coefficient of the polynomial by (3.53).
Step 6. Find the root of the polynomial (3.51), and select the q roots that are nearest to the unit circle as being the roots corresponding to the DOA estimates.
Step 7. DOA estimate, using:

$$\theta_k = \arcsin\left(\frac{\lambda}{2\pi d}\arg(z_k)\right) \qquad k = 1, \quad \cdots, \quad q$$

where z_k represents one of the q roots selected for DOA estimation.

From the above analysis, we can conclude that the RVED-Root-MUSIC has a lower computational complexity than the conventional root-MUSIC technique thanks to the eigendecomposition of the real-valued matrix instead of that of the complex matrices, and the asymptotic performance of it is better than of conventional root-MUSIC due to the FB averaging effect..

3.5 Simulations

In this section, we present some simulation results to illustrate the performance of RVED-Root-MUSIC. We consider a ULA with M=8 elements and the inter-element space is equal to a half of wavelength. There are three signals with SNRs of 30 dB impinges on the array from $\theta_1 = -80$, $\theta_2 = -20$, $\theta_3 = 40$. The detailed simulation results are shown as Fig. 22. ~ Fig. 25.

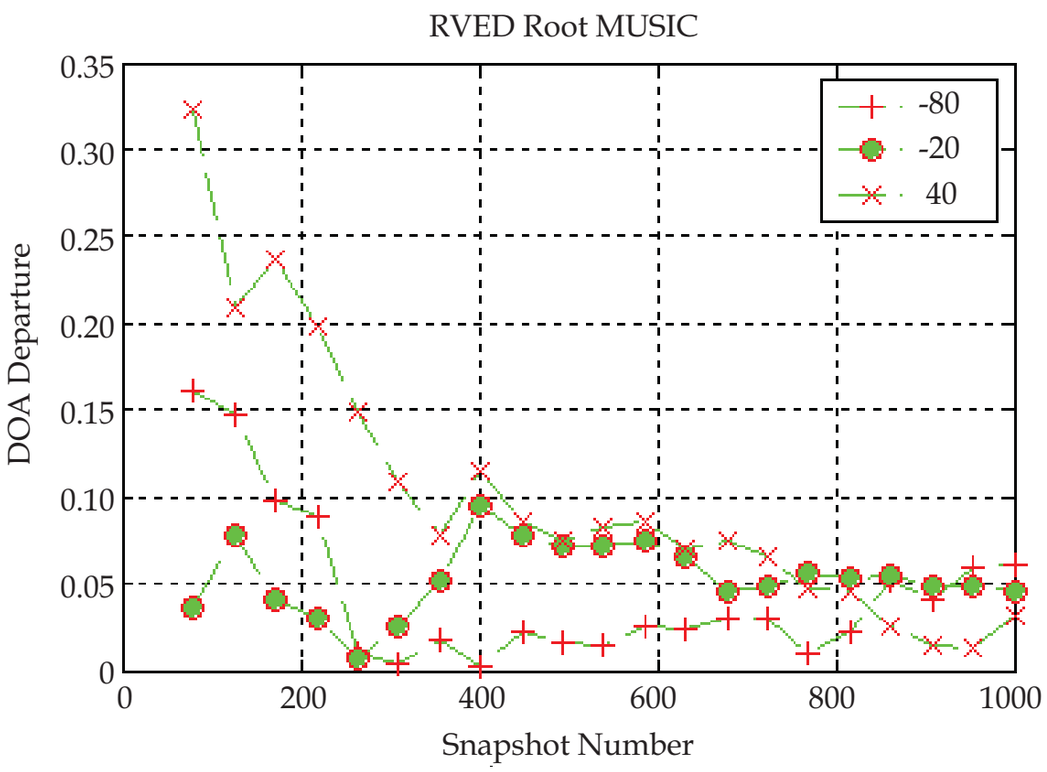

Fig. 22. DOA departure vs dnapshot number. Signal DOA=[-80 -20 40], SNR=5dB

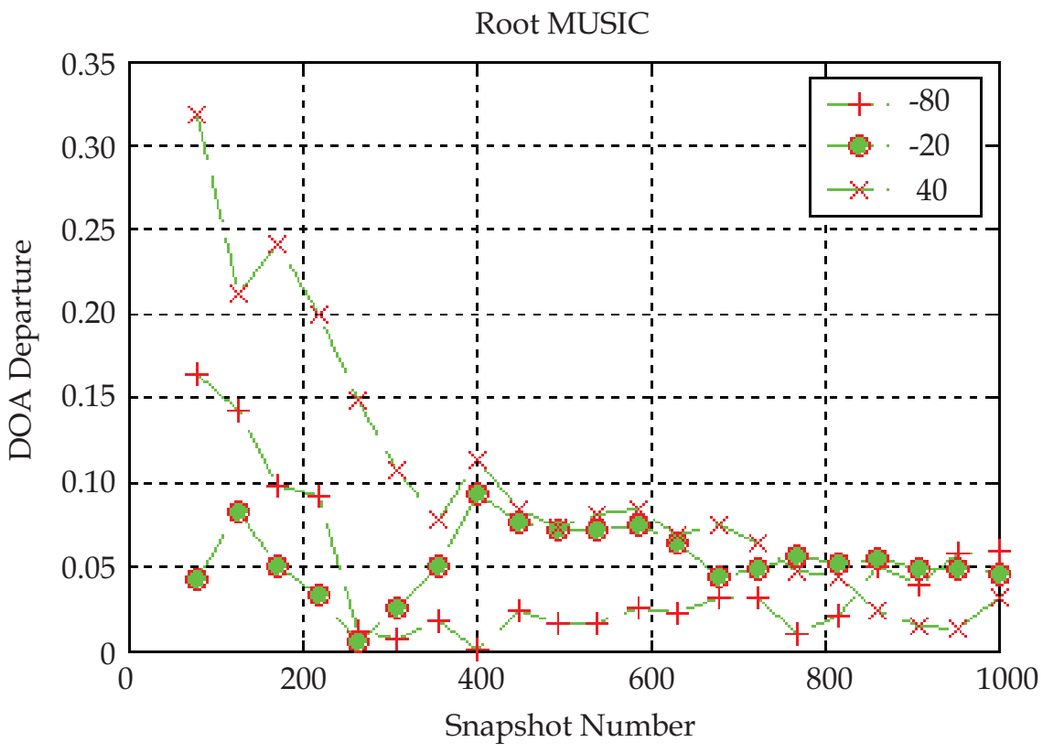

Fig. 23. DOA departure vs snapshot number. Signal DOA=[-80 -20 40], SNR=5dB

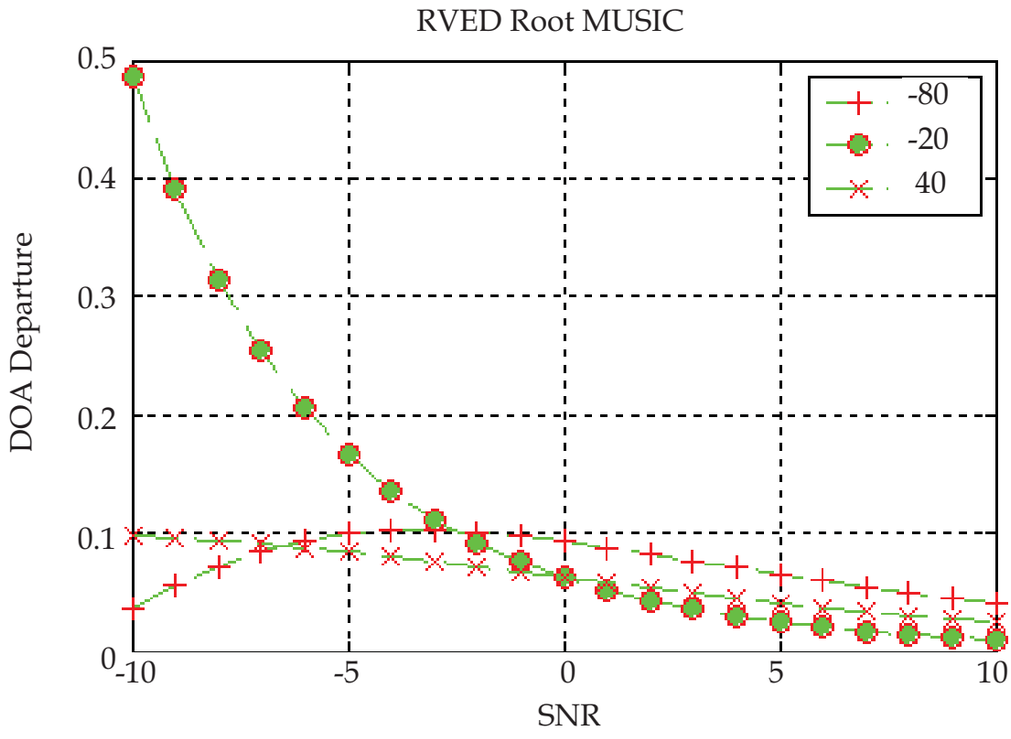

Fig. 24. DOA departure vs SNR. Signal DOA=[-80 -20 40], Snapshot number =1000

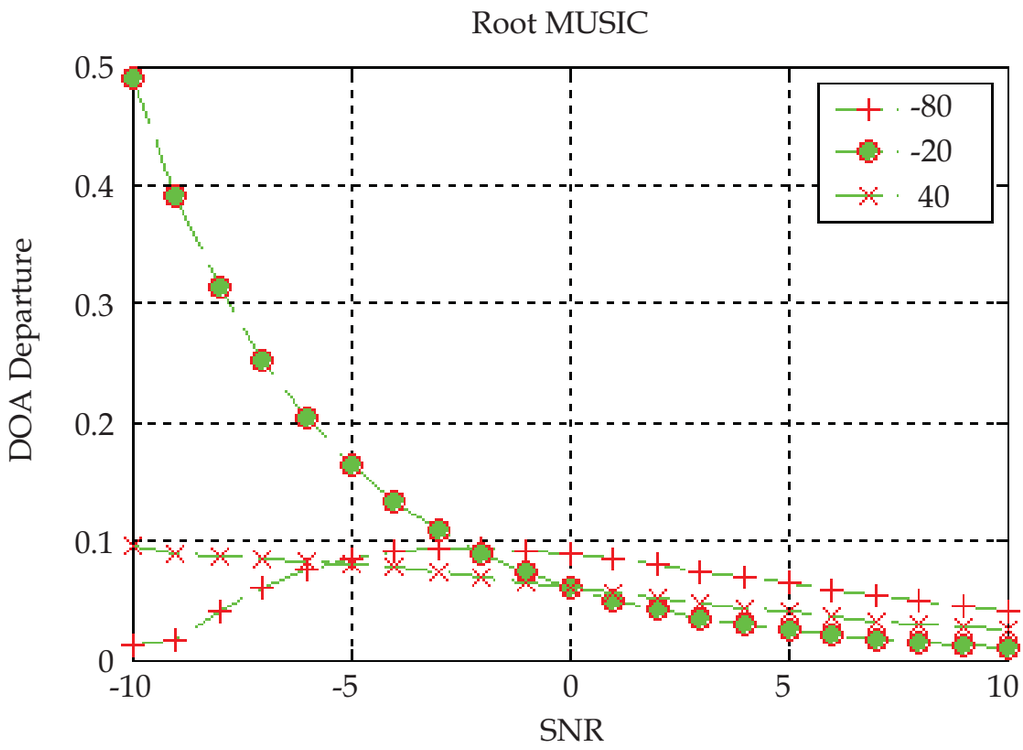

Fig. 25. DOA departure vs SNR. Signal DOA=[-80 -20 40], Snapshot number =1000

Fig. 22. and Fig. 23. depict DOA departure versus snapshot number results of RVED-Root-MUSIC and Root-MUSIC respectively, where the SNR=5dB. In figure 22. and 23., the x-axis denotes the snapshot number, and y-axis denotes the departure of signal DOA.

Fig. 24. and Fig. 25. depict DOA departure versus SNR results of RVED-Root-MUSIC and Root-MUSIC respectively, where the snapshot number =1000. In figure 24. and 25., the x-axis denotes the SNR, and y-axis denotes the departure of signal DOA .

From the detecting results and the comparison between RVED-Root-MUSIC and Root-MUSIC, we can conclude that RVED-Root-MUSIC can detect DOA of signal quickly and effectively. At the same time, the results validate the correctness and effective of this algorithm.

3.6 Conclusion

An improved version of the Root-MUSIC algorithm, called Root-MUSIC with real-valued eigendecomposition (RVED-Root-MUSIC), has been presented in this chapter. The computational complexity is reduced significantly by exploiting the one-to-one correspondence between centro-Hermitian and real matrices, allowing a transformation to real matrices, which can be maintained for all steps of the algorithm. Due to the inherent forward-backward averaging effect, RVED-Root-MUSIC can separate two completely coherent sources and provide improved estimates for correlated signals.

4. Real-value space ESPRIT algorithm and its implement

The recovery of signal parameters from noisy observations is a fundamental problem in (real-time) array signal processing. Due to their simplicity and high-resolution capability,the subspace estimation schemes have been attracting considerable attention. Among them the most representative are MUSIC and ESPRIT methods. MUSIC utilizes the orthogonal characteristic of noisy subspace of data covariance matrix,but ESPRIT exploits the rotational invariance structure of the signal subspace[57,58]. The virtue of ESPRIT is the low computational burden,and not requiring spectrum peak searching by contrast with MUSIC. Comparing with Root-MUSIC, ESPRIT obtains the information of signal direction of arriving (DOA) via exploiting the rotational invariance of every subarray (every subarray 's signal subspace), but Root-MUSIC estimates the signal DOA by solving the polynomial, which is constructed by using the orthogonal between the steering vector and noise subspace.

Unitary ESPRIT achieves even more accurate results than previous ESPRIT techniques by taking advantage of the unit magnitude property of the phase factors that represent the phase delays between the two subarrays [59]. It has been shown in [63] that constraining the phase factors to the unit circle can also give some improvement for correlated sources. For centro-symmetric sensor arrays with a translational invariance structure, Unitary ESPRIT provides a very simple and efficient solution to this task.

Although Unitary ESPRIT effectively doubles the number of data samples, the computational complexity is reduced by transforming the required rank-revealing factorizations of complex matrices into decompositions of real-valued matrices of the same size. Thus, we obtain increased estimation accuracy with a reduced computational load. This reduction can be achieved by constructing invertible transformations that map centro-Hermitian matrices to real matrices.

The real-value ESPRIT algorithm is proposed by [62] and [63], which is on the foundation of the Unitary ESPRIT, by constructing a transformation matrix, transforms the complex data of original array into real-value data. Thus lowered the computational burden. Moreover this algorithm is also applicable to centro-symmetric sensor arrays.

This chapter bases on the foundation of the algorithm that above references proposes and reference [64], analyzes the rotational invariance principle of RVS-ESPRIT algorithm, and the relationship of RVS-ESPRIT and complex space ESPRIT(CS-ESPRIT), definitely give:

1. The rotational invariance relationship of the real-value space array steering,
2. The rotational invariance relationship of the real-value space signal subspace,
3. The rotational invariance relationship between the array steering and the signal subspace of the real-value space,
4. The rotational invariance relationship between the real-value space signal subspace and the complex value space signal space,
5. The rotational invariance relationship between the real-value space array steering and the complex value space array steering.

And give the implementing algorithm of REV-ESPRIT. At last compares its performance with other algorithm by simulation.

This chapter is organized as follows[65]. It starts with a review of the signal model and the rotational invariance subspace principle. Next the RVS-ESPRIT algorithm is analyzed, among which includes the transformation from the complex space to real-value space, the rotational invariance principle of real-value space, and its implementing algorithm. Finally, the computer simulations with the comparison the performance of RVS-ESPRIT and the well-known LS- ESPRIT algorithm are given.

4.1 Signal model

Assume that there are two completely same subarray, their space Δ is already known, and every subarray consists of m elements. Consider N $(N<m)$ narrowband plane waves from far-field of the array, these plane waves are assumed to be impinging on the array from directions θ_1, θ_2, $\cdots$, θ_N, among them, θ_i, $i=1,\ 2,\ \cdots,\ N$ is angle between the array normal and the direction of the ith signal of the N narrowband planes waves imping. Because the structure of two arrays is completely same, therefore, for a signal, the difference of the two subarray outputs is only one phase difference φ_i, $i=1,\ 2,\ \cdots,\ N$. Suppose the first subarray receives the data for $\mathbf{X}_1$, the second receives the data for $\mathbf{X}_2$, then:

$$\mathbf{X}_1=\left[\mathbf{a}(\theta_1)\ \ \cdots\ \ \mathbf{a}(\theta_N)\right]\mathbf{S}+\mathbf{N}_1=\mathbf{A}\cdot\mathbf{S}+\mathbf{N}_1 \tag{4.1}$$

$$\mathbf{X}_2=\left[\mathbf{a}(\theta_1)e^{j\varphi_1}\ \ \cdots\ \ \mathbf{a}(\theta_N)e^{j\varphi_N}\right]\mathbf{S}+\mathbf{N}_2=\mathbf{A}\mathbf{\Phi}\cdot\mathbf{S}+\mathbf{N}_2 \tag{4.2}$$

Where, the direction matrix of subarray 1 is $\mathbf{A}_1=\mathbf{A}=\left[\mathbf{a}(\theta_1)\ \ \cdots\ \ \mathbf{a}(\theta_N)\right]$, the direction matrix of subarray 2 is $\mathbf{A}_2=\mathbf{A}\mathbf{\Phi}$, $\mathbf{S}$ is the space signal vector, $\mathbf{N}_1$ and $\mathbf{N}_2$ are the noise vectors of the subarray 1 and 2, respectively,and are assumed to be white Gaussian, and among the formula:

$$\mathbf{\Phi}=diag\left[e^{j\varphi_1}\ \ \cdots\ \ e^{j\varphi_N}\right] \tag{4.3}$$

4.2 The rotational invariance subspace principle

From the above mathematics model, we can know that the signal direction information is included in $\mathbf{A}$ and $\mathbf{\Phi}$, because $\mathbf{\Phi}$ is a diagonal matrix, so that we can obtain the DOA of signal through solving $\mathbf{\Phi}$, that is:

$$\varphi_k=\frac{2\cdot\pi\left|\Delta\right|\sin\theta_k}{\lambda} \tag{4.4}$$

where λ is the center wave-length of Arriving the wave. So if we obtain the rotational invariance relationship $\mathbf{\Phi}$ of the two subarray, we can get the signal DOA information. First uniting the two subarray models, namely:

$$\mathbf{X}=\begin{bmatrix}\mathbf{X}_1\\ \mathbf{X}_2\end{bmatrix}=\begin{bmatrix}\mathbf{A}\\ \mathbf{A}\cdot\mathbf{\Phi}\end{bmatrix}\mathbf{S}+\begin{bmatrix}\mathbf{N}_1\\ \mathbf{N}_2\end{bmatrix}=\overline{\mathbf{A}}\cdot\mathbf{S}+\mathbf{N} \tag{4.5}$$

Under the ideal condition, the covariance matrix is estimated as fellows:

$$\mathbf{R} = E\left\{\mathbf{X}\cdot\mathbf{X}^H\right\} = \overline{\mathbf{A}}\cdot\mathbf{R}_S\cdot\overline{\mathbf{A}}^H + \mathbf{R}_N \tag{4.6}$$

where $\mathbf{R}_S = E\left\{\mathbf{S}\cdot\mathbf{S}^H\right\}$, $\mathbf{R}_N = E\left\{\mathbf{N}\cdot\mathbf{N}^H\right\}$.

Let the eigendecompositions of the covariance matrix, there is:

$$\mathbf{R} = \sum_{i=1}^{2m}\lambda_i e_i e_i^H = \mathbf{U}_S\cdot\mathbf{\Sigma}_S\cdot\mathbf{U}_S{}^H + \mathbf{U}_N\cdot\mathbf{\Sigma}_N\cdot\mathbf{U}_N{}^H \tag{4.7}$$

Very obviously, the eigenvalue that gets from the top have the relationship as follows: $\lambda_1 \geq \cdots \geq \lambda_N > \lambda_{N+1} = \cdots = \lambda_{2m}$. where $\mathbf{U}_S$ is signal subspace that spanned by eigenvectors which are corresponding to large eigenvalues, $\mathbf{U}_N$ is noise subspace that spanned by eigenvectors which are corresponding to small eigenvalues.

We know that the signal subspace is spanned by large eigenvector is equal to that is spanned by array direction matrix in the above eigendecomposition, that is:

$$span\left\{\mathbf{U}_S\right\} = span\left\{\overline{\mathbf{A}}(\theta)\right\} \tag{4.8}$$

At this time, existing a nonsingular matrix $\mathbf{T}$, which can make:

$$\mathbf{U}_S = \overline{\mathbf{A}}(\theta)\cdot\mathbf{T} \tag{4.9}$$

Obviously above-mentioned structure is coming into existence to the two subarrays, so have:

$$\mathbf{U}_S = \begin{bmatrix}\mathbf{U}_{S1}\\ \mathbf{U}_{S2}\end{bmatrix} = \begin{bmatrix}\mathbf{A}\cdot\mathbf{T}\\ \mathbf{A}\mathbf{\Phi}\cdot\mathbf{T}\end{bmatrix} \tag{4.10}$$

Very obvious, the subspace spanned by array direction matrix $\mathbf{A}$ is equal to $\mathbf{U}_{S1}$ and $\mathbf{U}_{S2}$ which are spanned by the large eigenvectors of subarray 1 and 2 respectively.

$$span\left\{\mathbf{U}_{S1}\right\} = span\left\{\mathbf{A}(\theta)\right\} = span\left\{\mathbf{U}_{S2}\right\} \tag{4.11}$$

Moreover, from the relationship of the two subarrays with regard to signal direction matrix, we can know:

$$\mathbf{A}_2 = \mathbf{A}_1\mathbf{\Phi} \tag{4.12}$$

Again from (4.10),we can know:

$$\begin{cases}\mathbf{U}_{S1} = \mathbf{A}\cdot\mathbf{T}\\ \mathbf{U}_{S2} = \mathbf{A}\mathbf{\Phi}\cdot\mathbf{T}\end{cases} \Rightarrow \begin{cases}\mathbf{A} = \mathbf{U}_{S1}\cdot\mathbf{T}^{-1}\\ \mathbf{U}_{S2} = \mathbf{A}\mathbf{\Phi}\cdot\mathbf{T} = \mathbf{U}_{S1}\cdot\mathbf{T}^{-1}\cdot\mathbf{\Phi}\cdot\mathbf{T}\end{cases} \tag{4.13}$$

$$\mathbf{U}_{S2} = \mathbf{U}_{S1}\cdot\mathbf{T}^{-1}\cdot\mathbf{\Phi}\cdot\mathbf{T} = \mathbf{U}_{S1}\cdot\mathbf{\Psi} \tag{4.14}$$

where $\mathbf{\Psi} = \mathbf{T}^{-1}\cdot\mathbf{\Phi}\cdot\mathbf{T}$. (4.12) reflects the rotational invariance characteristic of the signal direction matrix of the two subarrays, but (4.14) reflects the rotational invariance characteristic of the received signal data subspace of the two subarrays.

If the signal direction matrix $\mathbf{A}$ is full rank, we can obtain form (4.14) as fellows:

$$\mathbf{\Phi} = \mathbf{T} \cdot \mathbf{\Psi} \cdot \mathbf{T}^{-1} \tag{4.15}$$

So that,the diagonal matrix which is consisted of the eigenvalues of $\mathbf{\Psi}$ certainly be equal to $\mathbf{\Phi}$, but the every column of $\mathbf{T}$ is the eigenvectors of $\mathbf{\Psi}$. Therefore, once we get the rotational invariance matrix $\mathbf{\Psi}$, we can obtain the signal DOA from (4.4) directly.

4.3 Real-value space ESPRIT algorithm

4.3.1 The transformation from complex space into realvalue space

We know that the uniform linear array is centro-symmetric, and its signal direction matrix satisfy the nether formula:

$$\mathbf{J}_M \cdot \mathbf{A}^* = \mathbf{A} \cdot \mathbf{\Delta} \tag{4.16}$$

where, $\mathbf{J}_M$ is the $M \times M$ exchange matrix with ones on its antidiagonal and zeros elsewhere, and the signal direction matrix makes reference to the first element of the array, the diagonal matrix $\mathbf{\Delta} = \mathbf{\Phi}^{-(M-1)}$, and the $\mathbf{\Phi}$ is expressed as (4.3). If the reference point is selected as the central point of the array, so we have:

$$\mathbf{A}_C = \mathbf{A} \cdot \mathbf{\Delta}^{1/2} = \left[\mathbf{a}_C(\beta_1) \quad \cdots \quad \mathbf{a}_C(\beta_N) \right] \tag{4.17}$$

where

$$\mathbf{a}_C(\beta_i) = e^{-j\left(\frac{M-1}{2}\right)\beta_i} \left[1 \quad e^{-j\beta_i} \quad \cdots \quad e^{-j(M-1)\beta_i} \right]^T = e^{-j\left(\frac{M-1}{2}\right)\beta_i} \mathbf{a}(\beta_i) \tag{4.18}$$

If matrix $\mathbf{Q}$ satisfying:

$$\mathbf{J}_M \cdot \mathbf{Q}^* = \mathbf{Q} \tag{4.19}$$

we call it as the left real transformation matrix.

For example, $\mathbf{Q}$ can be chosen for arrays with an even and odd number of sensors respectively as the following sparse matrices:

$$\mathbf{Q}_{2n} = \frac{1}{\sqrt{2}} \begin{bmatrix} \mathbf{I}_n & j\mathbf{I}_n \\ \mathbf{J}_n & -j\mathbf{J}_n \end{bmatrix} \tag{4.20}$$

$$\mathbf{Q}_{2n+1} = \frac{1}{\sqrt{2}} \begin{bmatrix} \mathbf{I}_n & \mathbf{0} & j\mathbf{I}_n \\ \mathbf{0}^T & \sqrt{2} & \mathbf{0}^T \\ \mathbf{J}_n & \mathbf{0} & -j\mathbf{J}_n \end{bmatrix} \tag{4.21}$$

Moreover, from the bidirectional averaging algorithm, we can process the array data by once bidirectional averaging, and insert (4.16) into it, we can obtain:

$$\mathbf{R}_{FB} = \frac{1}{2}\left(\mathbf{R} + \mathbf{J}_M \cdot \mathbf{R}^* \cdot \mathbf{J}_M \right) \tag{4.22}$$

Insert $\mathbf{R} = \mathbf{A} \cdot \mathbf{R}_S \cdot \mathbf{A}^H + \mathbf{R}_N$ into(4.13), we can obtain:

$$\begin{aligned} \mathbf{R}_{FB} &= \frac{1}{2}\left(\mathbf{A} \cdot \mathbf{R}_S \cdot \mathbf{A}^H + \mathbf{R}_N + \mathbf{J}_M \cdot \left(\mathbf{A} \cdot \mathbf{R}_S \cdot \mathbf{A}^H + \mathbf{R}_N \right)^* \cdot \mathbf{J}_M \right) \\ &= \frac{1}{2}\left(\mathbf{A} \cdot \mathbf{R}_S \cdot \mathbf{A}^H + \mathbf{R}_N + \mathbf{J}_M \cdot \mathbf{A}^* \cdot \mathbf{R}_S^* \cdot \mathbf{A}^T \cdot \mathbf{J}_M + \mathbf{J}_M \cdot \mathbf{R}_N^* \cdot \mathbf{J}_M \right) \end{aligned} \tag{4.23}$$

because of $\mathbf{J}_M \cdot \mathbf{A}^* = \mathbf{A} \cdot \mathbf{\Delta} \Rightarrow \left(\mathbf{J}_M \cdot \mathbf{A}^* \right)^H = \left(\mathbf{A} \cdot \mathbf{\Delta} \right)^H \Rightarrow \mathbf{A}^T \cdot \mathbf{J}_M = \mathbf{\Delta}^H \cdot \mathbf{A}^H$, and insert it into (4.23), get the result:

$$\begin{aligned} \mathbf{R}_{FB} &= \mathbf{A} \cdot \frac{1}{2}\left(\mathbf{R}_S + \mathbf{\Delta} \cdot \mathbf{R}_S^* \cdot \mathbf{\Delta}^H \right) \cdot \mathbf{A}^H + \frac{1}{2}\left(\mathbf{R}_N + \mathbf{J}_M \cdot \mathbf{R}_N^* \cdot \mathbf{J}_M \right) \\ &= \mathbf{A} \cdot \frac{1}{2}\left(\mathbf{R}_S + \mathbf{\Delta} \cdot \mathbf{R}_S^* \cdot \mathbf{\Delta}^H \right) \cdot \mathbf{A}^H + \mathbf{R}_N^{'} \qquad (4.24) \\ &= \frac{1}{2L} \mathbf{Z} \cdot \mathbf{Z}^H \qquad (4.25) \end{aligned}$$

where

$$\mathbf{Z} = \begin{bmatrix} \mathbf{X} & \mathbf{J}_M \cdot \mathbf{X}^* \cdot \mathbf{J}_L \end{bmatrix} \tag{4.26}$$

Since:

$$\begin{aligned} \frac{1}{2L} \mathbf{Z} \cdot \mathbf{Z}^H &= \frac{1}{2L} \begin{bmatrix} \mathbf{X} & \mathbf{J}_M \cdot \mathbf{X}^* \cdot \mathbf{J}_L \end{bmatrix} \cdot \begin{bmatrix} \mathbf{X} & \mathbf{J}_M \cdot \mathbf{X}^* \cdot \mathbf{J}_L \end{bmatrix}^H \\ &= \frac{1}{2L}\left(\mathbf{X}\mathbf{X}^H + \mathbf{J}_M \cdot \mathbf{X}^* \cdot \mathbf{J}_L \cdot \mathbf{J}_L^H \cdot \mathbf{X}^T \cdot \mathbf{J}_M^H \right) \\ &= \frac{1}{2L}\left(\mathbf{X}\mathbf{X}^H + \mathbf{J}_M \cdot \mathbf{X}^* \cdot \mathbf{X}^T \cdot \mathbf{J}_M^H \right) \\ &= \frac{1}{2L}\left(\mathbf{X}\mathbf{X}^H + \mathbf{J}_M \cdot \left(\mathbf{X}\mathbf{X}^H \right)^* \cdot \mathbf{J}_M^H \right) \\ &= \frac{1}{2}\left[\frac{1}{L}\left(\mathbf{X} \cdot \mathbf{X}^H \right) + \mathbf{J}_M \cdot \left(\frac{1}{L}\left(\mathbf{X} \cdot \mathbf{X}^H \right) \right)^* \cdot \mathbf{J}_M^H \right] \end{aligned} \tag{4.27}$$

Because $\hat{\mathbf{R}} = \frac{1}{L}\left(\mathbf{X} \cdot \mathbf{X}^H \right)$ is the estimating formula of $\mathbf{R}$. Thus (4.25) is established. When the row number of data vector $\mathbf{X}$ is odd, we can definite:

$$\mathbf{X} = \begin{bmatrix} \mathbf{X}_1 \\ \mathbf{x}^T \\ \mathbf{X}_2 \end{bmatrix}_{M \times L} \tag{4.28}$$

If we process $\mathbf{Z}$ which is defined by (4.26) By means of matrix $\mathbf{Q}$ which is defined by (4.20) or (4.21) as fellows:

$$\mathbf{T}(\mathbf{X}) = \mathbf{Q}_M^H \cdot \mathbf{Z} \cdot \mathbf{Q}_{2L}$$

$$\begin{aligned}\mathbf{T}(\mathbf{X}) &= \mathbf{Q}_M^H \cdot \mathbf{Z} \cdot \mathbf{Q}_{2L} \\ &= \begin{bmatrix} \mathrm{Re}\{\mathbf{X}_1 + \mathbf{J}\mathbf{X}_2^*\} & -\mathrm{Im}\{\mathbf{X}_1 - \mathbf{J}\mathbf{X}_2^*\} \\ \sqrt{2}\,\mathrm{Re}\{\mathbf{x}^T\} & -\sqrt{2}\,\mathrm{Im}\{\mathbf{x}^T\} \\ \mathrm{Im}\{\mathbf{X}_1 + \mathbf{J}\mathbf{X}_2^*\} & \mathrm{Re}\{\mathbf{X}_1 - \mathbf{J}\mathbf{X}_2^*\} \end{bmatrix}\end{aligned} \tag{4.29}$$

If the row dimension of the data vector is even, the transformation matrix is:

$$\begin{aligned}\mathbf{T}(\mathbf{X}) &= \mathbf{Q}_M^H \cdot \mathbf{Z} \cdot \mathbf{Q}_{2L} \\ &= \begin{bmatrix} \mathrm{Re}\{\mathbf{X}_1 + \mathbf{J}\mathbf{X}_2^*\} & -\mathrm{Im}\{\mathbf{X}_1 - \mathbf{J}\mathbf{X}_2^*\} \\ \mathrm{Im}\{\mathbf{X}_1 + \mathbf{J}\mathbf{X}_2^*\} & \mathrm{Re}\{\mathbf{X}_1 - \mathbf{J}\mathbf{X}_2^*\} \end{bmatrix}\end{aligned} \tag{4.30}$$

What to need to be noticed here is, the matrix $\mathbf{Q}$ which defined by (4.20) and (4.21) satisfies

$$\mathbf{Q} \cdot \mathbf{Q}^H = \mathbf{I} \tag{4.31}$$

From the transformation relationship of (4.28) and (4.29), we can see that $\mathbf{T}(\mathbf{X})$ transforms complex data into real data, so that the computational burden is lowered greatly, and we can obtain:

$$\begin{aligned}\mathbf{R}_T &= \frac{1}{2L}\mathbf{T}(\mathbf{X}) \cdot \mathbf{T}^H(\mathbf{X}) \\ &= \frac{1}{2L}\mathbf{Q}_M^H \cdot \mathbf{Z} \cdot \mathbf{Q}_{2L} \cdot \left(\mathbf{Q}_M^H \cdot \mathbf{Z} \cdot \mathbf{Q}_{2L}\right)^H = \frac{1}{2L}\mathbf{Q}_M^H \cdot \mathbf{Z} \cdot \mathbf{Q}_{2L} \cdot \mathbf{Q}_{2L}^H \cdot \mathbf{Z}^H \cdot \mathbf{Q}_M \\ &= \frac{1}{2L}\mathbf{Q}_M^H \cdot \mathbf{Z} \cdot \mathbf{Z}^H \cdot \mathbf{Q}_M = \mathbf{Q}_M^H \cdot \left[\frac{1}{2L}\left(\mathbf{Z} \cdot \mathbf{Z}^H\right)\right] \cdot \mathbf{Q}_M \\ &= \mathbf{Q}_M^H \cdot \mathbf{R}_{FB} \cdot \mathbf{Q}_M\end{aligned} \tag{4.32}$$

If the eigendecompositions of $\mathbf{R}_{FB}$ as follows:

$$\mathbf{R}_{FB} = \begin{bmatrix}\mathbf{U}_S & \mathbf{U}_N\end{bmatrix} \cdot \mathbf{\Sigma} \cdot \begin{bmatrix}\mathbf{U}_S^H \\ \mathbf{U}_N^H\end{bmatrix} \tag{4.33}$$

Insert (4.33) into (4.32), we can obtain:

$$\mathbf{R}_T = \mathbf{Q}_M^H \cdot \begin{bmatrix}\mathbf{U}_S & \mathbf{U}_N\end{bmatrix} \cdot \mathbf{\Sigma} \cdot \begin{bmatrix}\mathbf{U}_S^H \\ \mathbf{U}_N^H\end{bmatrix} \cdot \mathbf{Q}_M \tag{4.34}$$

(4.34) shows that the signal subspace of the transformation matrix $\mathbf{R}_T$ is:

$$\mathbf{E}_S = \mathbf{Q}_M^H \cdot \mathbf{U}_S \tag{4.35}$$

Insert (4.24) into (4.32), we can obtain:

$$\begin{aligned}\mathbf{R}_T &= \mathbf{Q}_M^H \cdot \mathbf{R}_{FB} \cdot \mathbf{Q}_M = \mathbf{Q}_M^H \cdot \left[\mathbf{A} \cdot \frac{1}{2}\left(\mathbf{R}_S + \mathbf{\Delta} \cdot \mathbf{R}_S^* \cdot \mathbf{\Delta}^H\right) \cdot \mathbf{A}^H + \mathbf{R}_N^{'} \right] \cdot \mathbf{Q}_M \\ &= \mathbf{Q}_M^H \cdot \mathbf{A} \cdot \frac{1}{2}\left(\mathbf{R}_S + \mathbf{\Delta} \cdot \mathbf{R}_S^* \cdot \mathbf{\Delta}^H\right) \cdot \mathbf{A}^H \cdot \mathbf{Q}_M + \mathbf{Q}_M^H \cdot \mathbf{R}_N^{'} \cdot \mathbf{Q}_M \\ &= \left(\mathbf{Q}_M^H \cdot \mathbf{A}\right) \cdot \frac{1}{2}\left(\mathbf{R}_S + \mathbf{\Delta} \cdot \mathbf{R}_S^* \cdot \mathbf{\Delta}^H\right) \cdot \left(\mathbf{Q}_M^H \cdot \mathbf{A}\right)^H + \mathbf{Q}_M^H \cdot \mathbf{R}_N^{'} \cdot \mathbf{Q}_M \\ &= \mathbf{A}_T \cdot \frac{1}{2}\left(\mathbf{R}_S + \mathbf{\Delta} \cdot \mathbf{R}_S^* \cdot \mathbf{\Delta}^H\right) \cdot \mathbf{A}_T^H + \mathbf{Q}_M^H \cdot \mathbf{R}_N^{'} \cdot \mathbf{Q}_M\end{aligned} \tag{4.36}$$

Therefore, the relationship between the real-value transformed signal direction matrix $\mathbf{A}_T$ and the original complex signal direction matrix $\mathbf{A}$ is given by:

$$\mathbf{A}_T = \mathbf{Q}_M^H \cdot \mathbf{A} \tag{4.37}$$

4.3.2 The real-value space rotational invariance principle

We analyze the signal subspace relationship of the two subarray data in the rotational invariance subspace algorithm theory, which is given by (4.14) $\mathbf{U}_{S2} = \mathbf{U}_{S1} \cdot \mathbf{\Psi}$. If the array is uniform linear array, and the overlap element of the two subarrays is maximum, namely, $m = M - 1$, so the signal subspace rotational invariance of the two subarray data can be expressed as:

$$\mathbf{K}_2 \cdot \mathbf{U}_S = \mathbf{K}_1 \cdot \mathbf{U}_S \cdot \mathbf{\Psi} \tag{4.38}$$

where $\mathbf{U}_S$ is the signal subspace of the received data of the whole uniform linear array, and:

$$\mathbf{K}_1 = \left[\mathbf{I}_{M-1} \quad 0\right]_{(M-1)\times M} \tag{4.39}$$

$$\mathbf{K}_2 = \left[0 \quad \mathbf{I}_{M-1}\right]_{(M-1)\times M} \tag{4.40}$$

In the same way, the rotational invariance of the two subarray signal direction matrix can be given as follows:

$$\mathbf{K}_2 \cdot \mathbf{A} = \mathbf{K}_1 \cdot \mathbf{A} \cdot \mathbf{\Phi} \tag{4.41}$$

where $\mathbf{A}$ is the signal direction matrix of the whole array.

From the definition of (4.39) and (4.40), we can see that $\mathbf{K}_1$ and $\mathbf{K}_2$ satisfies:

$$\mathbf{K}_1 = \mathbf{J}_m \cdot \mathbf{K}_2 \cdot \mathbf{J}_M \tag{4.42}$$

Utilize the relationship of the definition (4.19): $\mathbf{J}_M \cdot \mathbf{Q}^* = \mathbf{Q} \Rightarrow \mathbf{J}_M \cdot \mathbf{Q} = \mathbf{Q}^*$ again, we can obtain:

$$\begin{aligned}\mathbf{Q}_m^H \cdot \mathbf{K}_2 \cdot \mathbf{Q}_M &= \mathbf{Q}_m^H \cdot \mathbf{J}_m \cdot \mathbf{J}_m \cdot \mathbf{K}_2 \cdot \mathbf{J}_M \cdot \mathbf{J}_M \cdot \mathbf{Q}_M = \left(\mathbf{J}_m^H \cdot \mathbf{Q}_m\right)^H \cdot \mathbf{J}_m \cdot \mathbf{K}_2 \cdot \mathbf{J}_M \cdot \left(\mathbf{J}_M \cdot \mathbf{Q}_M\right) \\ &= \left(\mathbf{J}_m \cdot \mathbf{Q}_m\right)^H \cdot \mathbf{K}_1 \cdot \left(\mathbf{J}_M \cdot \mathbf{Q}_M\right) = \left(\mathbf{Q}_m^*\right)^H \cdot \mathbf{K}_1 \cdot \mathbf{Q}_M^* = \left(\mathbf{Q}_m^H\right)^* \cdot \mathbf{K}_1 \cdot \mathbf{Q}_M^* \\ &= \left(\mathbf{Q}_m^H \cdot \mathbf{K}_1 \cdot \mathbf{Q}_M\right)^*\end{aligned} \tag{4.43}$$

therefore, define:

$$\mathbf{H}_1 \overset{\Delta}{=} \mathbf{Q}_m^H \cdot \mathbf{K}_1 \cdot \mathbf{Q}_M + \mathbf{Q}_m^H \cdot \mathbf{K}_2 \cdot \mathbf{Q}_M = \mathbf{Q}_m^H \cdot (\mathbf{K}_1 + \mathbf{K}_2) \cdot \mathbf{Q}_M = 2\,\mathrm{Re}\left\{\mathbf{Q}_m^H \cdot \mathbf{K}_2 \cdot \mathbf{Q}_M\right\} \quad (4.44a)$$

$$\mathbf{H}_2 \overset{\Delta}{=} j \cdot \mathbf{Q}_m^H \cdot \mathbf{K}_1 \cdot \mathbf{Q}_M - j \cdot \mathbf{Q}_m^H \cdot \mathbf{K}_1 \cdot \mathbf{Q}_M = \mathbf{Q}_m^H \cdot j \cdot (\mathbf{K}_1 - \mathbf{K}_2) \cdot \mathbf{Q}_M = 2\,\mathrm{Im}\left\{\mathbf{Q}_m^H \cdot \mathbf{K}_2 \cdot \mathbf{Q}_M\right\} \quad (4.44b)$$

so that:

$$\mathbf{Q}_m^H \cdot \mathbf{K}_1 \cdot \mathbf{Q}_M = \frac{1}{2}(\mathbf{H}_1 - j\mathbf{H}_2) \quad (4.45a)$$

$$\mathbf{Q}_m^H \cdot \mathbf{K}_2 \cdot \mathbf{Q}_M = \frac{1}{2}(\mathbf{H}_1 + j\mathbf{H}_2) \quad (4.45b)$$

From the result given by (4.37): $\mathbf{A}_T = \mathbf{Q}_M^H \cdot \mathbf{A} \Rightarrow \mathbf{A} = \mathbf{Q}_M \cdot \mathbf{A}_T$, and insert it into the formula defined by (4.41): $\mathbf{K}_2 \cdot \mathbf{A} = \mathbf{K}_1 \cdot \mathbf{A} \cdot \mathbf{\Phi}$,we can obtain the results as follows:

$$\mathbf{K}_2 \cdot \mathbf{Q}_M \cdot \mathbf{A}_T = \mathbf{K}_1 \cdot \mathbf{Q}_M \cdot \mathbf{A}_T \cdot \mathbf{\Phi} \quad (4.46)$$

The both side of the upper formula multiplies by the $\mathbf{Q}_m^H$ together, we can obtain:

$$\mathbf{Q}_m^H \cdot \mathbf{K}_2 \cdot \mathbf{Q}_M \cdot \mathbf{A}_T = \mathbf{Q}_m^H \cdot \mathbf{K}_1 \cdot \mathbf{Q}_M \cdot \mathbf{A}_T \cdot \mathbf{\Phi} \quad (4.47)$$

Using (4.45), and removing the constant factor $1/2$, we can obtain that:

$$(\mathbf{H}_1 + j\mathbf{H}_2) \cdot \mathbf{A}_T = (\mathbf{H}_1 - j\mathbf{H}_2) \cdot \mathbf{A}_T \cdot \mathbf{\Phi} \quad (4.48)$$

Via moving item, combination and so on simplifications, we will have:

$$\mathbf{H}_1 \cdot \mathbf{A}_T \cdot (\mathbf{\Phi} - \mathbf{I}) = \mathbf{H}_2 \cdot \mathbf{A}_T \cdot j \cdot (\mathbf{\Phi} + \mathbf{I}) \quad (4.49)$$

From the definition of (4.3) $\mathbf{\Phi} = diag\left[\, e^{j\varphi_1} \quad \cdots \quad e^{j\varphi_N} \,\right]$ again, (4.49) can be simplified as :

$$\mathbf{H}_2 \cdot \mathbf{A}_T = \mathbf{H}_1 \cdot \mathbf{A}_T \cdot \frac{1}{j}(\mathbf{\Phi} - \mathbf{I}) \cdot (\mathbf{\Phi} + \mathbf{I})^{-1} = \mathbf{H}_1 \cdot \mathbf{A}_T \cdot \mathbf{\Phi}_T \quad (4.50)$$

where

$$\begin{aligned} \mathbf{\Phi}_T &= \frac{1}{j}(\mathbf{\Phi} - \mathbf{I}) \cdot (\mathbf{\Phi} + \mathbf{I})^{-1} \qquad (4.51) \\ &= \frac{1}{j} \cdot diag\left\{e^{j\varphi_1} - 1 \quad \cdots \quad e^{j\varphi_N} - 1\right\} \cdot diag\left\{\frac{1}{e^{j\varphi_1} + 1} \quad \cdots \quad \frac{1}{e^{j\varphi_N} + 1}\right\} \\ &= \frac{1}{j} \cdot diag\left\{\frac{e^{j\varphi_1} - 1}{e^{j\varphi_1} + 1} \quad \cdots \quad \frac{e^{j\varphi_N} - 1}{e^{j\varphi_N} + 1}\right\} \\ &= diag\left\{\tan\left(\frac{\varphi_1}{2}\right) \quad \cdots \quad \tan\left(\frac{\varphi_N}{2}\right)\right\} \qquad (4.52) \end{aligned}$$

So that, (4.50) reflects the rotational invariance relationship of the real-value space array steering, but (4.51) reflects the rotational invariance relationship between the real-value space array steering and the complex value space array steering.

Resembling the derivation of (4.50), from $\mathbf{E}_S = \mathbf{Q}_M^H \cdot \mathbf{U}_S \Rightarrow \mathbf{U}_S = \mathbf{Q}_M \cdot \mathbf{E}_S$, and insert it into the formula given by (4.38): $\mathbf{K}_2 \cdot \mathbf{U}_S = \mathbf{K}_1 \cdot \mathbf{U}_S \cdot \mathbf{\Psi}$, we can obtain:

$$\mathbf{K}_2 \cdot \mathbf{Q}_M \cdot \mathbf{E}_S = \mathbf{K}_1 \cdot \mathbf{Q}_M \cdot \mathbf{E}_S \cdot \mathbf{\Psi} \tag{4.53}$$

The both side of the upper formula multiplies by the $\mathbf{Q}_m^H$ together, we can obtain:

$$\mathbf{Q}_M^H \cdot \mathbf{K}_2 \cdot \mathbf{Q}_M \cdot \mathbf{E}_S = \mathbf{Q}_M^H \cdot \mathbf{K}_1 \cdot \mathbf{Q}_M \cdot \mathbf{E}_S \cdot \mathbf{\Psi} \tag{4.54}$$

Using (4.45), and removing the constant factor $1/2$, we can obtain that:

$$\left(\mathbf{H}_1 + j\mathbf{H}_2\right) \cdot \mathbf{E}_S = \left(\mathbf{H}_1 - j\mathbf{H}_2\right) \cdot \mathbf{E}_S \cdot \mathbf{\Psi} \tag{4.55}$$

Via moving item, combination and so on simplifications, we will have:

$$\mathbf{H}_2 \cdot \mathbf{E}_S \cdot \left(j\mathbf{\Psi} + \mathbf{I}\right) = \mathbf{H}_1 \cdot \mathbf{E}_S \cdot \left(\mathbf{\Psi} - \mathbf{I}\right) \tag{4.56}$$

$$\mathbf{H}_2 \cdot \mathbf{E}_S = \mathbf{H}_1 \cdot \mathbf{E}_S \cdot \left(\mathbf{\Psi} - \mathbf{I}\right) \cdot \left(j\mathbf{\Psi} + \mathbf{I}\right)^{-1} = \mathbf{H}_1 \cdot \mathbf{E}_S \cdot \mathbf{\Psi}_T \tag{4.57}$$

where

$$\mathbf{\Psi}_T = \left(\mathbf{\Psi} - \mathbf{I}\right) \cdot \left(j\mathbf{\Psi} + \mathbf{I}\right)^{-1} \tag{4.58}$$

So that, (4.57) reflects the rotational invariance relationship of the real-value space signal subspace, but (4.58) reflects the rotational invariance relationship between the real-value space signal subspace and the complex value space signal space.

Utilizing the character that the space spanned by array direction matrix is equal to which is spanned by the signal subspace, so a nonsingular matrix $\mathbf{T}_T$ exists, and satisfying $\mathbf{A}_T = \mathbf{E}_S \cdot \mathbf{T}_T$, thus using (4.50): $\mathbf{H}_2 \cdot \mathbf{A}_T = \mathbf{H}_1 \cdot \mathbf{A}_T \cdot \mathbf{\Phi}_T$, we can obtain that:

$$\mathbf{H}_2 \cdot \mathbf{E}_S \cdot \mathbf{T}_T = \mathbf{H}_1 \cdot \mathbf{E}_S \cdot \mathbf{T}_T \cdot \mathbf{\Phi}_T \Rightarrow \mathbf{H}_2 \cdot \mathbf{E}_S = \mathbf{H}_1 \cdot \mathbf{E}_S \cdot \mathbf{T}_T \cdot \mathbf{\Phi}_T \cdot \mathbf{T}_T^{-1} \tag{4.59}$$

Comparing with (4.57), we can obtain that:

$$\mathbf{\Psi}_T = \mathbf{T}_T \cdot \mathbf{\Phi}_T \cdot \mathbf{T}_T^{-1} \tag{4.60}$$

This formula reflects the rotational invariance relationship between the array steering and the signal subspace of the real-value space.

4.3.3 The real-value space ESPRIT algorithm

The observational data of M elements are given as:

$$x_1(t), \quad \cdots, \quad x_M(t), \; t = 1, \quad \cdots \quad L$$

Step 1. Construct the $M \times L$ observational data matrix $\mathbf{X} = \left[\mathbf{x}(1), \cdots, \mathbf{x}(L)\right]$, where $\mathbf{x}(t) = \left[x_1(t), \cdots, x_M(t)\right]^T$ is the observational data vector which is consists of M elements observational signals.

Step 2. Get the estimating formula of $\mathbf{R}$ by $\hat{\mathbf{R}} = \frac{1}{L}\left(\mathbf{X} \cdot \mathbf{X}^H\right)$, and transform the received array data into real-value space $\hat{\mathbf{R}}_T$ via (4.32).

Step 3. Compute the eigendecompositions of the real-value space $\hat{\mathbf{R}}_T$, and get the signal subspace $\hat{\mathbf{E}}_S$, and the source number $\hat{N}$.

Step 4. Solve the rotational invariance of (4.57) by least square method (or total least square method), and gain $\hat{\mathbf{\Psi}}_T$.

Step 5. Compute the eigendecompositions of $\hat{\mathbf{\Psi}}_T$, where $\hat{\mathbf{\Psi}}_T = \hat{\mathbf{T}}_T \cdot \hat{\mathbf{\Phi}}_T \cdot \hat{\mathbf{T}}_T^{-1}$, get $\hat{\mathbf{\Phi}}_T = diag\left\{\Omega_1, \cdots, \Omega_{\hat{N}}\right\}$.

Step 6. If $\hat{\mathbf{\Phi}}_T$ is the real diagonal matrix, according as (4.3) and (4.52), compute the DOA of imping signal as fellows:

$$\begin{cases} \varphi_k = 2 \cdot \arctan\left(\Omega_k\right) \\ \theta_k = \arcsin\left(\dfrac{\lambda}{2 \cdot \pi \left|\Delta\right|} \cdot \varphi_k\right) \end{cases} \qquad \left(k = 1, \cdots, \hat{N}\right) \tag{4.61}$$

If $\Omega_k \left(k = 1, \cdots, \hat{N}\right)$ is complex, compute the DOA by (4.61) with the real part of Ω_k.

4.4 Simulations

In order to validating the correctness and the effective of the proposed algorithm, we present some simulation results to illustrate the performance of RVS-ESPRIT. We consider a ULA with M=8 element and the interelement space is equal to a half of wavelength. There are three signals impinge on the array from $\theta_1 = -80$, $\theta_2 = -20$, $\theta_3 = 40$. The detailed simulation results are shown as Fig. 26. ~ Fig. 29.

Fig. 26. and Fig. 27. depicts DOA departure versus snapshot number results of RVS-ESPRIT and TLS-ESPRIT respectively, where the SNR=5dB. In figure 26. and 27., the x-axis denotes the snapshot number, and y-axis denotes the departure of signal DOA.

Fig. 28. and Fig. 29. depicts DOA departure versus SNR results of RVS-ESPRIT and TLS-ESPRIT respectively, where the snapshot number =1000. In figure 28. and 29., the x-axis denotes the SNR, and y-axis denotes the departure of signal DOA.

From the detecting results and comparison between RVS-ESPRIT and TLS-ESPRIT, we can conclude that RVS-ESPRIT can detect DOA of signal quickly and effectively. At the same time, the results validate the correctness and effective of this algorithm.

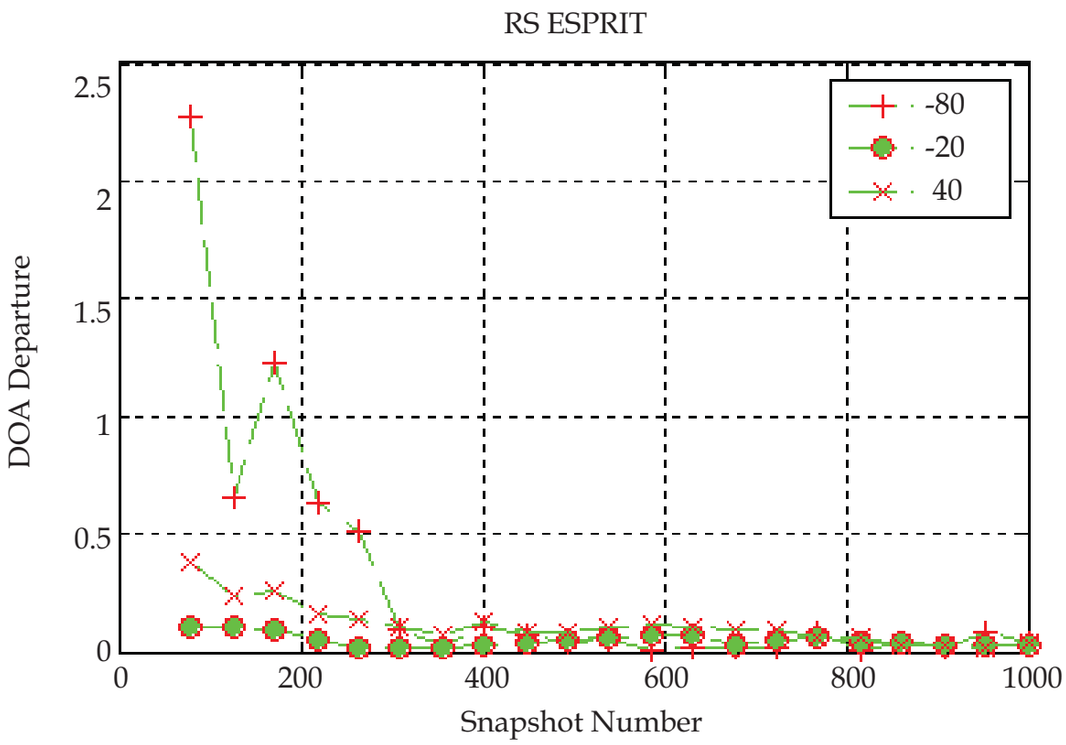

Fig. 26. DOA departure vs snapshot number. Signal DOA=[-80 -20 40], SNR=5dB

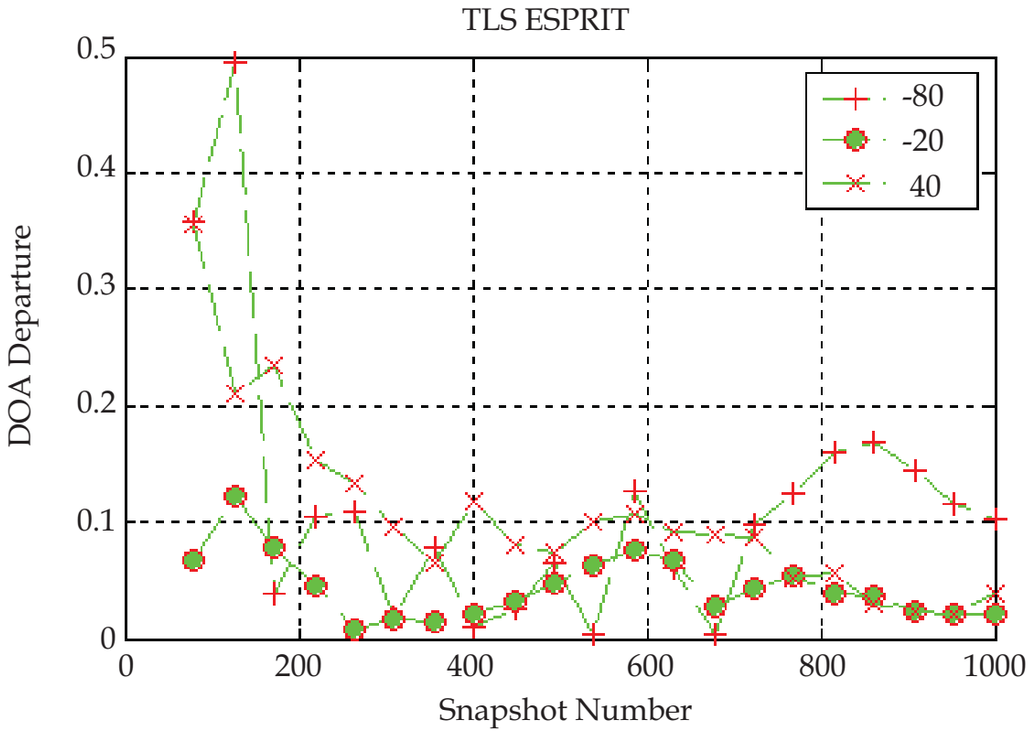

Fig. 27. DOA departure vs snapshot number. Signal DOA=[-80 -20 40], SNR=5dB

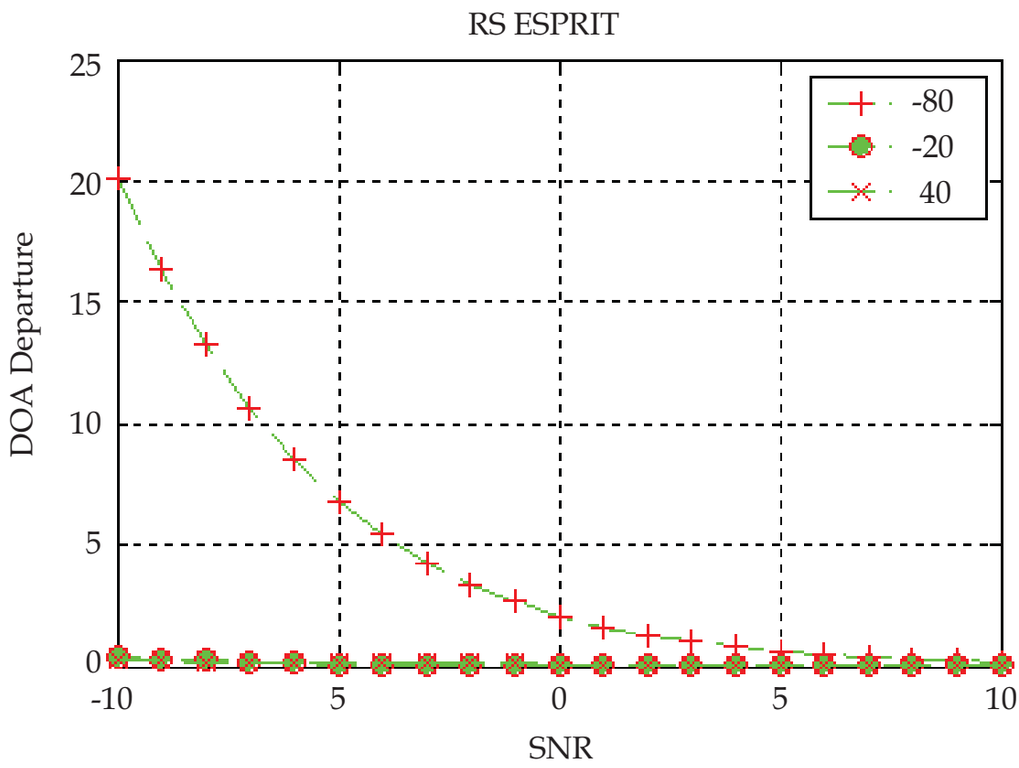

Fig. 28. DOA departure versus SNR. Signal DOA=[-80 -20 40], Snapshot number =1000

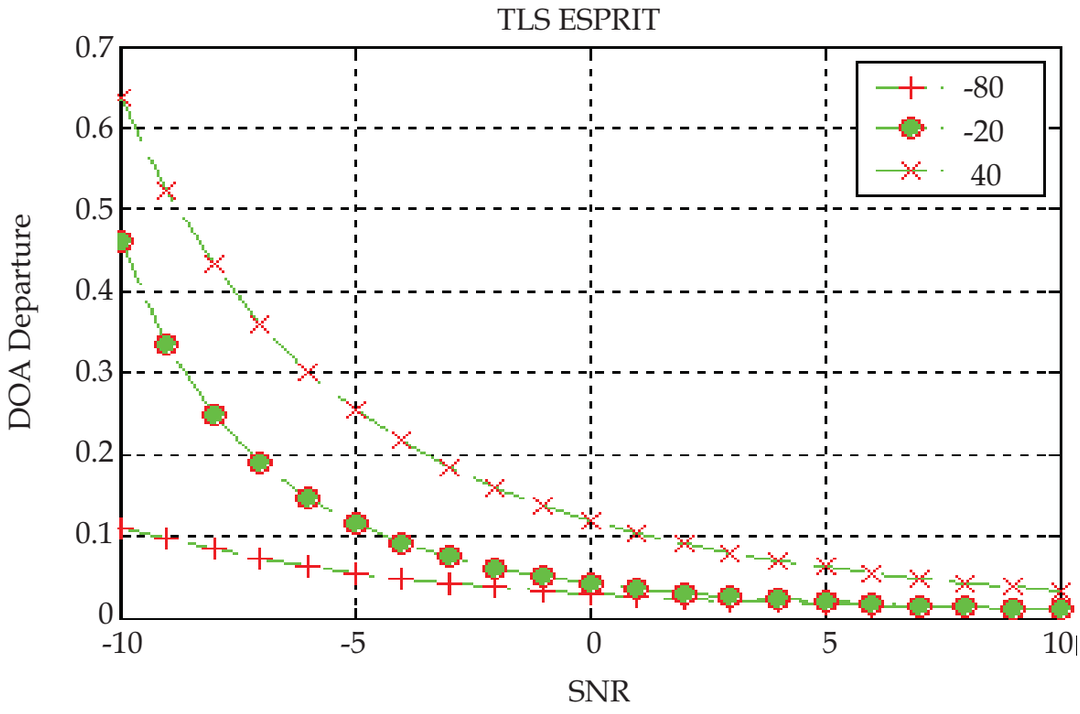

Fig. 29. DOA departure versus SNR. Signal DOA=[-80 -20 40], Snapshot number =1000

4.5 Conclusion

This chapter carrys on the detailed theories analysis of RVS-ESPRIT based on the theory of CS-ESPRIT, and gives the concrete implementing algorithm. Because the eigendecompositions of RVS-ESPRIT is in real domain, so the calculation speed is raised consumedly, then the speed of DOA estimating is improved largely also. Due to the inherent forward-backward averaging effect, RVS-ESPRIT can separate two completely coherent sources and provides improved estimates for correlated signals.

5. References

[1] J. Capon. High resolution frequency-wavenumber spectrum analysis. Proc. IEEE, Vol.57, pp: 1408-1418, Aug.1969.
[2] J. S. Reed, J. D. Mallet, L. E. Brennan. Rapid convergence rate in adaptive arrays. IEEE Trans. Aerosp. Electron. Syst., Vol. AES-10, No.6, pp: 853-863, Nov.1974.
[3] D. H. Johnson, D. E. Dudgeon. Array signal processing: Concepts and Techniques. Englewood Cliffs, NJ: Prentice-Hall, 1993.
[4] H. Krim, M. Viberg. Two decades of array signal processing research. IEEE Signal Process. Mag., Vol.13, No.4, pp: 67-94, Jul.1996.
[5] L. C. Godara. Application of antenna arrays to mobile communications, Part II: Beamforming and direction-of-arrival considerations. Proc. IEEE, Vol.85, No.8, pp: 1195-1245, Aug.1997.
[6] H. L. Van Trees. Detection, estimation, and modulation theory, Part IV, Optimum array processing. New York: Wiley, 2002.
[7] P. S. Naidu. Sensor array signal processing. Boca Raton, FL: CRC, 2001.
[8] J. R. Guerci. Space-time adaptive processing. Norwood, MA: Artech House, 2003.
[9] Jian Li, Petre Stotica. Robust adaptive beamforming. New York: Wiley, 2006.
[10] H. Cox. Resolving power and sensitivity to mismatch of optimum array processors. J. Acoust. Soc. Amer., Vol.54, No.3, pp: 771-785, Mar.1973.
[11] D. D. Feldman, L. J. Griffiths. A projection approach to robust adaptive beamforming. IEEE Trans. Signal Processing, Vol.42, pp: 867-876, Apr.1994.
[12] M. Wax, Y. Anu. Performance analysis of the minimum variance beamformer in the presence of steering vector errors. IEEE Trans. Signal Processing, Vol.44, pp: 938-947, Apr.1996.
[13] E. K. Hung, R. M. Turner. A fast beamforming algorithm for large arrays. IEEE Trans. Aerosp. Electron. Syst., Vol.AES-19, pp: 598-607, Jul.1983.
[14] B. D. Carlson. Covariance matrix estimation errors and diagonal loading in adaptive arrays. IEEE Trans. Aerosp. Electron. Syst., Vol.24, pp: 397-401, Jul.1988.
[15] M. Wax, Y. Anu. Performance analysis of the minimum variance beamformer. IEEE Trans. Signal Processing, Vol.44, pp: 928-937, Apr.1996.
[16] H. Cox, R. M. Zeskind, M. H. Owen. Robust adaptive beamforming. IEEE Trans. Acoust., Speech, Signal Processing, Vol.ASSP-35, pp:1365-1376, Oct.1987.
[17] A. B. Gershman. Robust adaptive beamforming in sensor arrays. Int. J. Electron. Commun., Vol.53, pp: 305-314, Dec.1999.
[18] A. B. Gershman. Robust adaptive beamforming: an overview of recent trends and advances in the field. International Conference on Antenna Theory and Technique, 9-12 September, 2003, Sewstopol, Ukraine, pp: 30-35.

[19] Sergiy A. Vorobyov, A. B. Gershman, Zhi-Quan Luo. Robust adaptive beamforming using worst-case performance optimization: a solution to the signal mismatch problem. IEEE Trans. Signal Processing. Vol.51, No.2, pp: 313-324, Feb.2003.
[20] Jian Li, Petre Stotica, Zhisong Wang.On robust capon beamformer and diagonal loading. IEEE Trans. Signal Processing. Vol.51, No.7, pp: 1702-1715, Jul.2003.
[21] S. Shahram, A. B. Gershman, Zhiquan Luo, et al. Robust adaptive beamforming for general-rank signal models. IEEE Trans. Signal Processing, Vol.51, No.9, pp: 2257-2269, Sep.2003.
[22] Jian Li, Petre Stotica, Zhisong Wang, Doubly constrained robust capon beamformer. IEEE Trans. Signal Processing. Vol.52, No.9, pp: 2407-2423, Sep.2004.
[23] G.L. Robert, P.B. Stephen. Robust minimum variance beamforming. IEEE Trans. Signal Processing, Vol.53, No.5, pp: 1684-1696, May.2005.
[24] Ayman Elnashar, Said M. Elnoubi, Hamdi A. El-Mikati. Further study on robust adaptive beamforming with optimum diagonal loading. IEEE Trans. Antennas Propagation, Vol.AP-54, No.12, pp: 3647-3658, Dec.2006.
[25] C.Y.Chen, P.P.Vaidyanathan. Quadratically constrained beamforming robust against direction-of- arrival mismatch. IEEE Trans. Signal Processing, Vol.55, No.8, pp: 4139-4150, Aug.2007.
[26] R. A. Monzingo, T. W. Miller. Introduction to adaptive arrays. New York: Wiley, 1980.
[27] Z. Tian, K. L. Bell, H. L. Van Trees. A recursive least squares implementation for LCMP beamforming under quadratic constraint. IEEE Trans. Signal Processing, Vol.49, No.6, pp: 1365-1376, Jun.2001.
[28] L. C. Godara. Error analysis of the optimal antenna array processors. IEEE Trans. Aerosp. Electron. Syst., Vol. AES-22, pp: 395-409, Jul.1986.
[29] K. L. Bell, Y. Ephraim, H. L. Van Trees, A Bayesian approach to robust adaptive beamforming. IEEE Trans. Signal Processing, Vol.48, pp: 386-398, Feb.2000.
[30] L. Chang, C. C. Yeh. Performance of DMI and eigenspace-based beamformers. IEEE Trans. Antennas Propagation, Vol.40, pp: 1336-1347, Nov.1992.
[31] Cheng-Chou Lee, Ju-Hong Lee. Eigenspace-based adaptive array beamforming with robust capabilities. IEEE Trans. Antennas Propagation, Vol.45, pp: 1711-1716, Dec.1997.
[32] J. Riba, J. Goldberg, G. Vazquez. Robust beamforming for interference rejection in mobile communications. IEEE Trans. Signal Processing, Vol.45, pp: 271-275, Jan.1997.
[33] J. R. Guerci. Theory and application of covariance matrix tapers for robust adaptive beamforming. IEEE Trans. Signal Processing, Vol.47, pp: 997-985, Apr.1999.
[34] J. R. Guerci, J.S.Bergin. Principal components,covariance matrix tapers,and the subspace leakage problem. IEEE Trans. Aerosp. Electron. Syst, Vol.38, pp: 152-162, Jan.2002.
[35] F. Vincent, O. Besson. Steering vector errors and diagonal loading, IEE Proceedings.-Radar Sonar Navig., Vol.151, No.6, pp: 337-343, Dec.2004.
[36] O. Besson, F. Vincent. Performance analysis of beamformers using generalized loading of the covariance matrix in the presence of random steering vector errors. IEEE Trans. Signal Processing, Vol.53, pp: 452-459, Feb.2005.
[37] Almir Mutapcic, Seung-Jean Kim, Stephen Boyd. Beamforming with uncertain weights. IEEE Signal Processing Letter, Vol.14, No.5, pp: 348-351, May.2007.

[38] Liu Congfeng, Liao Guisheng, Robust capon beamformer under norm constraint, Signal Processing, May.2010, Vol.90, Issue.5, pp: 1573-1581.
[39] Dolph C L. A current distribution for broadside arrays which optimizes the relationship between beam width and sidelobe level. Proc IRE, June.1946, Vol.34, pp:335–348.
[40] Zhou P, Ingram M. Pattern synthesis for arbitrary arrays using an adaptive array method. IEEE Transactions on Antennas And Propagation. May.1999, Vol.47, No.5, pp:862-869.
[41] Wang F, Balakrishnan V, Zhou P Y, et al. Optimal array pattern synthesis using semidefinite programming. IEEE Transactions on Signal Processing, May.2003, Vol.51, No.5, pp:1172-1183.
[42] Guo Q, Liao G., Wu Y, et al. Pattern synthesis method for arbitrary arrays based on LCMV criterion. Electronics Letters. May.2003, Vol.39, No.23, pp:1628-1630.
[43] Xie Yao, Jian Li, Zheng Xiayu, et al. Optimal array pattern synthesis via matrix weighting, ICASSP, IEEE International Conference on Acoustics, Speech and Signal Processing – Proceedings, Apr 15-20 2007, Honolulu, HI, United States, IEEE Inc., Piscataway, NJ 08855-1331, United States, Vol.2, pp: 885-888.
[44] Kurup D G., Himdi M, Rydberg A. Synthesis of uniform amplitude unequally spaced antenna arrays using the differential evolution algorithm, IEEE Transactions on Antennas And Propagation. Sep.2003, Vol.51, No.9, pp:2210-2217.
[45] Boeringer D W, Werner D H. Particle swarm optimization versus genetic algorithms for phased array synthesis, IEEE Transactions on Antennas And Propagation. Mar.2004, Vol.52, No.3, pp:771-779.
[46] Liu Xiaojun, Liu Congfeng, Liao Guisheng, Improved pattern synthesis method with linearly constraint minimum variance criterion, 2010 IEEE Internation Conference on Wireless Communications, Networking and Information Security (WCNIS2010), 2010.6,25-27, Vol.2, Beijing China。
[47] Barabell A.J, Improving the resolution performance of eigenstructure-based direction-finding algorithms.Proc,ICASSP 83,1983,pp.336-339.
[48] Kumaresan R. and Tufts D.W., Estimating the angles of arrival of multiple plane wave,IEEE Trans,1983,AES-19,pp.134-138.
[49] Bao B and Hari.K, Performance analysis of root-MUSIC, IEEE Trans, 1989, ASSP-37,pp.1939-1949.
[50] Li F and Vaccaro.R.J,Analytical performance prediction of subspace-based algorithms for DOA estimation: SVD and Signal Processing II Algorithms,Analysis and Applications (Elsevier,New York,1991)
[51] Xu X.L and Buckley K.M, Reduced dimension beamspace broad-band localization, preprocessor design and evaluation.Proc.IEEE Forth Workshop on Spectrum Estimation and Modeling, 1988,pp22-26.
[52] Ta sung Lee, Fast implementation of root-form eigen-based methods for detecting closely spaced sources IEE Proceedings-F Vol.139.No.4,August 1992.
[53] Marius P, Alex B.G and Martin H, Unitary root-MUSIC with a real-valued eigendecomposition: a theoretical and experimental performacce study, IEEE Transactions on SP,Vol.48,No.5,May 2000,pp:1306-1314.
[54] Liu Congfeng, Liao Guisheng, Fast algorithm for root-MUSIC with real-valued eigendecomposition, Radar-2006: 2006 CIE International Conference on Radar 2006.10 ShangHai China.

[55] Q. S Ren and A. J. Willis, Extending MUSIC to single snapshot and on line direction finding applications, International Radar Conference, IEE, Stevenage, United Kingdom, Oct.1997: 783-787.

[56] Liu Xiaojun, Liu Congfeng, Liao Guisheng, Polynomial coefficient finding for root-MUSIC, Journal of Electronic (China), 2009.8, Vol.26(4).

[57] R. Roy and T. Kailath, "ESPRIT-Estimation of signal parameters via rotational invariance techniques," in Signal Processing Part 11: Control Theory and Applications (L. Auslander, F. A. Griinbaum, J. W. Helton, T. Kailath, P. Khargonekar, and S. Mitter, Eds.). Berlin, Vienna, New York Springer-Verlag, 1990, pp. 36941 1.

[58] R. H. Roy, "ESPRIT-estimation of signal parameters via rRotational invariance techniques," Ph.D. thesis, Stanford Univ., Stanford, CA, Aug. 1987.

[59] M. Haardt and M. E. Ali-Hackl, "Unitary ESPRIT: How to exploit additional information inherent in the rotational invariance structure," in Proc. IEEE Int. ConJ Acoust., Speech, Signal Processing, Adelaide, Australia, Apr. 1994, pp. 229-232, vol. IV.

[60] S. U. Pillai and B. H. Kwon, "Forwardhackward spatial smoothing techniques for coherent signal identification," IEEE Trans. Acoust., Speech, Signal Processing, vol. 37, pp. 8-15, Jan. 1989.

[61] B. D. Rao and K. V. S. Hari, "Weighted subspace methods and spatial smoothing: Analysis and comparison," IEEE Trans. Signal Processing, vol. 41, pp. 788-803, Feb. 1993.

[62] Martin Haardt, Josef A. Nossek Unitary ESPRIT: how to obtain increased estimation accuracy with a reduced computational burden IEEE Trans. Signal Processing, Vol. 43, No. 5, pp.1232-1242. MAY 1995

[63] B. Ottersten, M. Viberg, and T. Kailath, "Performance analysis of the total least squares ESPRIT algorithm," IEEE Trans. Signal P mcessing, vol. 39, pp. 1122-1135, May 1991.

[64] Wang Yongliang, Chen Hui, Peng Yingning, Wan qun Spatial spectrum estimation techniques and algorithm Tsinghua university press Beijing China 2004.

[65] Liu Congfeng, Liao Guisheng, Real-value space ESPRIT algorithm and Its implement, WiCOM 2006: 2006 International Conference on Wireless Communications, Networking, and Mobile Computing 2006.09 WuHan China.

Fourier Transform Applications

Edited by Dr Salih Salih

ISBN 978-953-51-0518-3
Hard cover, 300 pages
Publisher InTech
Published online 25, April, 2012
Published in print edition April, 2012

The book focuses on Fourier transform applications in electromagnetic field and microwave, medical applications, error control coding, methods for option pricing, and Helbert transform application. It is hoped that this book will provide the background, reference and incentive to encourage further research and results in these fields as well as provide tools for practical applications. It provides an applications-oriented analysis written primarily for electrical engineers, control engineers, signal processing engineers, medical researchers, and the academic researchers. In addition the graduate students will also find it useful as a reference for their research activities.

How to reference

In order to correctly reference this scholarly work, feel free to copy and paste the following:

Liu Congfeng (2012). Robust Beamforming and DOA Estimation, Fourier Transform Applications, Dr Salih Salih (Ed.), ISBN: 978-953-51-0518-3, InTech, Available from: http://www.intechopen.com/books/fourier-transform-applications/robust-beamforming-and-doa-estimation

INTECH
open science | open minds

InTech Europe
University Campus STeP Ri
Slavka Krautzeka 83/A
51000 Rijeka, Croatia
Phone: +385 (51) 770 447
Fax: +385 (51) 686 166
www.intechopen.com

InTech China
Unit 405, Office Block, Hotel Equatorial Shanghai
No.65, Yan An Road (West), Shanghai, 200040, China
中国上海市延安西路65号上海国际贵都大饭店办公楼405单元
Phone: +86-21-62489820
Fax: +86-21-62489821

IntechOpen